7.3. Design of Experiments Analyses

One initial problem with the original test matrix was the instability of four specific test runs. These are run numbers 30, 31, 42, and 67 in Figure 5.3. Note that runs 67 and 42 are repeats of runs 30 and 31, respectively. These runs share the following factor settings: (1) radial depth = 0.625", (2) throat depth = 1.125", (3) fuel difference = +5.0, and (4) excess air = 30%. This specific combination of conditions were unattainable due to instability of the reaction. Therefore, two choices were made. The first was made in the actual testing process; this was to test these runs at its highest possible excess air and then to enter this actual value into the matrix. This resultant matrix is called a "botched", or incomplete, design. The second choice was made in the data analysis process; this was to block the experiment into two separate matrices, one at 30% excess air and the second at 10% excess air. These matrices could then be analyzed separately; the 30% excess air matrix remains a botched design, but the 10% excess air matrix would be full and complete. The 10% is symmetrically balanced and is thus more accurate, but the 30% matrix could still be analyzed.

In retrospect, this decision to block on excess air was quite useful for both analytical and practical reasons. First, since the matrices are at different excess air conditions, their data analysis results could be compared to check if trends at 10% would also occur at 30%. The practical benefit was that most boiler burner manufacturers desire to maintain excess air as a constant, not a variable. Because of these two benefits, the decision to block on excess air was deemed acceptable.

The first main task in the analysis of the results is to calculate the main effects for each response. This is automatically done in the program using Yates's algorithm. In order to best explain this procedure, the 10% excess air blocked matrix is given in standard form in Figure 7.8. The factors in this matrix are coded. The positive signs indicate the high level of the factor and the negative signs indicate the low level. Since replicates are incorporated into this test matrix, the first task is to average the response, NO_X in this case, for each of the two replicated runs. This is shown in the Run Average column. The run averages in Figure 7.8 are then treated as successive pairs. The first eight entries in column (1) are obtained by adding each pair together. Thus, 24.7 + 24.4 = 49.1, 29.2 + 29.05 = 58.25, and so on. The next eight numbers in column (1) are obtained by subtracting the top number from the bottom number in each of those pairs. Thus, the ninth number in column (1) is obtained by subtracting 24.4 - 24.7 = -0.3. In just the same way as column (1) is calculated from the Run Average column, column (2) is obtained from (1), column (3) is obtained from (2), and column (4) is obtained from (3). Finally, to obtain the effects, one must divide by a divisor, which is 2^4 for the first row and 2^3 for the remainder rows. The first estimated effect is the average NO_X response over all runs, which was verified through manual calculations. The remainder effects are attributed to the factor abbreviations in the final row of Figure 7.8. Notice that the throat depth (T) and fuel difference (F) have the largest effect on the NO_X response, 4.275 and -3.3, respectively.

Design Identification	Radial (R) Depth	Throat (T) Depth	Outer (O) Depth	Fuel (F) Diff.	Outer (OD) Direction	NOx Response	Run Average
1	-	-	-	-	+	25.3	24.7
1	-	-	-	-	+	24.1	
2	+	-	-	-	-	24.3	24.4
2	+	-	-	-	-	24.5	
3	-	+	-	-	-	27.2	29.2
3	-	+	-	-	-	31.2	
4	+	+	-	-	+	28.9	29.05
4	+	+	-	-	+	29.2	
5	-	-	+	-	-	24.9	25.2
5	-	-	+	-	-	25.5	
6	+	-	+	-	+	23.8	24.2
6	+	-	+	-	+	24.6	
7	-	+	+	-	+	29.6	29.85
7	-	+	+	-	+	30.1	
8	+	+	+	-	-	27.9	28.55
8	+	+	+	-	-	29.2	
9	-	-	-	+	-	22.8	22.55
9	-	-	-	+	-	22.3	
10	+	-	-	+	+	22.4	21.9
10	+	-	-	+	+	21.4	
11	-	+	-	+	+	25.4	25.8
11	-	+	-	+	+	26.2	
12	+	+	-	+	-	26.1	26.05
12	+	+	-	+	-	26	
13	-	-	+	+	+	22.5	21.8
13	-	-	+	+	+	21.1	
14	+	-	+	+	-	20	20.1
14	+	-	+	+	-	20.2	
15	-	+	+	+	-	26.1	25.95
15	-	+	+	+	-	25.8	
16	+	+	+	+	+	25.3	24.6
16	+	+	+	+	+	23.9	

Figure 7.7: Standard Form of 10% Blocked Matrix with Coded Factors

When the effects are generated using Yates's algorithm, the effects may also be plotted on a normal or half-normal probability graph. This is simply a graphical means of identifying which factors are of most importance. If the effects truly represent a sample from a normal population, the effects will form an approximate straight line on the probability plot. If some effects are significant in relation to the response output, they will appear as outliers from this straight line. These type of effect graphs will be shown later in this section.

Now that an understanding of how the effects are calculated is complete, the following paragraphs explain the last three steps in the analysis of the data: (1) analysis of variance, (2) model diagnostic checks, and (3) model interpretation.

After the effects are generated, the user must select which factors to include in the statistical model. Obviously, the selections are based on the magnitudes of the effects; the smaller the effect, the less likely to include it in the model. Therefore, in Figure 7.8 throat depth and fuel difference are definitely included in the model, and an argument could also be made to include radial depth, the third largest effect. After these are chosen, the next step is to compute the ANOVA (analysis of variance). These calculations

provide the bulk of the statistical data. These data are used as a check on the validity of the model and to develop a mathematical relationship between the chosen factors and the response.

Column (1)	Column (2)	Column (3)	Column (4)	Divisor	Estimated Effect	Factor(s) Identification
49.1	107.35	215.15	403.9	16	25.24375	average
58.25	107.8	188.75	-6.2	8	-0.775	R
49.4	96.3	-2.75	34.2	8	4.275	T
58.4	92.45	-3.45	1.1	8	0.1375	R,T
44.45	-0.45	18.15	-3.4	8	-0.425	O
51.85	-2.3	16.05	-4.5	8	-0.5625	R,O
41.9	-0.4	-0.15	1.1	8	0.1375	T,O
50.55	-3.05	1.25	-1	8	-0.125	F,OD
-0.3	9.15	0.45	-26.4	8	-3.3	F
-0.15	9	-3.85	-0.7	8	-0.0875	R,F
-1	7.4	-1.85	-2.1	8	-0.2625	T,F
-1.3	8.65	-2.65	1.4	8	0.175	R,OD
-0.65	0.15	-0.15	-4.3	8	-0.5375	O,F
0.25	-0.3	1.25	-0.8	8	-0.1	T,OD
-1.7	0.9	-0.45	1.4	8	0.175	R,OD
-1.35	0.35	-0.55	-0.1	8	-0.0125	OD

Figure 7.8: Yates's Algorithm Calculations for Effects on NO_X Response

An example ANOVA output from the 10% excess air blocked matrix on the NO_X response is given in Figure 7.9. The first check is on the F-value and p-value of the model. If the model is valid, the F-value will typically be greater than 10 and the p-value will be less than 0.05. In the example output shown, notice that the F-value is 105 and the p-value is less than 0.0001. The p-value actually gives the confidence level. Therefore, a p-value of 0.0001 gives a 99.98%

SOURCE	SUM OF SQUARES (SS)	DEGREES OF FREEDOM (DF)	MEAN SQUARE MS = SS/DF	F-VALUE	PROB > F P-VALUE
MODEL	238.13	3	79.37667	105.1906	< 0.0001
RESIDUAL	21.12875	28	0.754598		
- LACK OF FIT	7.89875	12	0.658229	0.796044	0.6503
- PURE ERROR	13.23	16	0.826875		
CORRECTED TOT.	259.2588	31			

ROOT MEAN SQUARE ERROR (RMSE)	0.8687	(standard deviation for experiment)
DEPENDENT MEAN (DM)	25.2438	(overall mean of all NOx response data)
COEFFICIENT OF VARIATION %	3.4412	(experimental error; RMSE/DM)

R-SQUARED	0.9185	(8.2% must be explained by other factors not included in model)
ADJUSTED R-SQUARED	0.9098	(adjusted for number of parameters in model)
PREDICTED R-SQUARED	0.8936	(measure of model's predictive capability)

Predicted Residual Sum of Squares (PRESS) = 27.597

FACTOR	COEFFICIENT ESTIMATE	DEGREES OF FREEDOM (DF)	STANDARD ERROR	t FOR H0 COEFFICIENT = 0	PROB > |t|
INTERCEPT	25.24375	1	0.153562		
A	-0.3875	1	0.153562	-2.52342	0.0176
B	2.1375	1	0.153562	13.91949	< 0.0001
D	-1.65	1	0.153562	-10.7449	< 0.0001

Final Model Equation in Terms of Factors

NOx = 10.66875
- 1.24 * radial depth
+ 11.4 * throat depth
- 0.33 * fuel diff. (units = ppm, corrected to 3.0% O2)

OBS ORDER	ACTUAL VALUE	PRED. VALUE	RESIDUAL	LEVER	STUDENT RESIDUAL	COOK'S DIST.	OUTLIER T-VALUE	RUN ORDER
1	25.3	25.144	0.156	0.125	0.192	0.001	0.189	28
2	24.1	25.144	-1.044	0.125	-1.285	0.059	-1.300	21
3	24.3	24.369	-0.069	0.125	-0.085	0.000	-0.083	24
4	24.5	24.369	0.131	0.125	0.162	0.001	0.159	15
5	27.2	29.419	-2.219	0.125	-2.731	0.266	-3.130	3
6	31.2	29.419	1.781	0.125	2.192	0.172	2.365	32
7	28.9	28.644	0.256	0.125	0.315	0.004	0.310	4
8	29.2	28.644	0.556	0.125	0.685	0.017	0.678	11
9	24.9	25.144	-0.244	0.125	-0.300	0.003	-0.295	16
10	25.5	25.144	0.356	0.125	0.438	0.007	0.432	25
11	23.8	24.369	-0.569	0.125	-0.700	0.017	-0.693	2
12	24.6	24.369	0.231	0.125	0.285	0.003	0.280	5
13	29.6	29.419	0.181	0.125	0.223	0.002	0.219	27
14	30.1	29.419	0.681	0.125	0.838	0.025	0.834	1
15	27.9	28.644	-0.744	0.125	-0.915	0.030	-0.913	30
16	29.2	28.644	0.556	0.125	0.685	0.017	0.678	10
17	22.8	21.844	0.956	0.125	1.177	0.049	1.185	22
18	22.3	21.844	0.456	0.125	0.561	0.011	0.555	19
19	22.4	21.069	1.331	0.125	1.638	0.096	1.692	23
20	21.4	21.069	0.331	0.125	0.408	0.006	0.402	20
21	25.4	26.119	-0.719	0.125	-0.885	0.028	-0.881	29
22	26.2	26.119	0.081	0.125	0.100	0.000	0.098	6
23	26.1	25.344	0.756	0.125	0.931	0.031	0.928	8
24	26	25.344	0.656	0.125	0.808	0.023	0.802	14
25	22.5	21.844	0.656	0.125	0.808	0.023	0.802	18
26	21.1	21.844	-0.744	0.125	-0.915	0.030	-0.913	17
27	20	21.069	-1.069	0.125	-1.315	0.062	-1.333	13
28	20.2	21.069	-0.869	0.125	-1.069	0.041	-1.072	31
29	26.1	26.119	-0.019	0.125	-0.023	0.000	-0.023	9
30	25.8	26.119	-0.319	0.125	-0.392	0.005	-0.386	7
31	25.3	25.344	-0.044	0.125	-0.054	0.000	-0.053	12
32	23.9	25.344	-1.444	0.125	-1.777	0.113	-1.852	26

Figure 7.9: ANOVA Output for NO_X Response in 10% Blocked Matrix

confidence level that the chosen model has an effect on NO_X. The second check is on the coefficient of variation. In the example output, the value is 3.44%. If this value approaches 100%, the user may want to consider transforming the response data before computing the effects. The last two checks are in the case statistics shown in columns at the bottom of Figure 7.9. The lever values are always between zero and one and indicate the weighting of each run in the model. It is desirable, but not necessary, for all these values to remain below 0.5. The fifth and final check is in the outlier t column. If a value in this column is greater than 3.5, than that run may be an outlier and the user must seriously consider whether to include it in the analysis. If the ANOVA results pass these checks, the user may proceed in developing the diagnostic graphs. These graphs are further means of checking the results and validating the model.

Two types of diagnostic graphs are very useful for the model analysis: (1) normal probability plot of residuals and (2) plot of residuals versus predicted response. The first graph is a plot which checks if those effects not selected in the model are indeed due to random noise. Therefore, it is similar to the effects graph, but in this case, all points should closely lie in a straight line. Some scatter will occur, but if some points are significantly off the line, the assumptions made for the ANOVA calculations must be reconsidered. The second graph is a plot of the residuals versus the predicted response. If the model is valid, the plot should be a random scatter; if trends are obvious, other variables not included in the design matrix were mistakenly neglected. Trends may also indicate that further blocking is necessary. Two acceptable plots of these two graphs are shown in Figure 7.10. Again, these results are for the NO_X response in the 10% excess air blocked matrix.

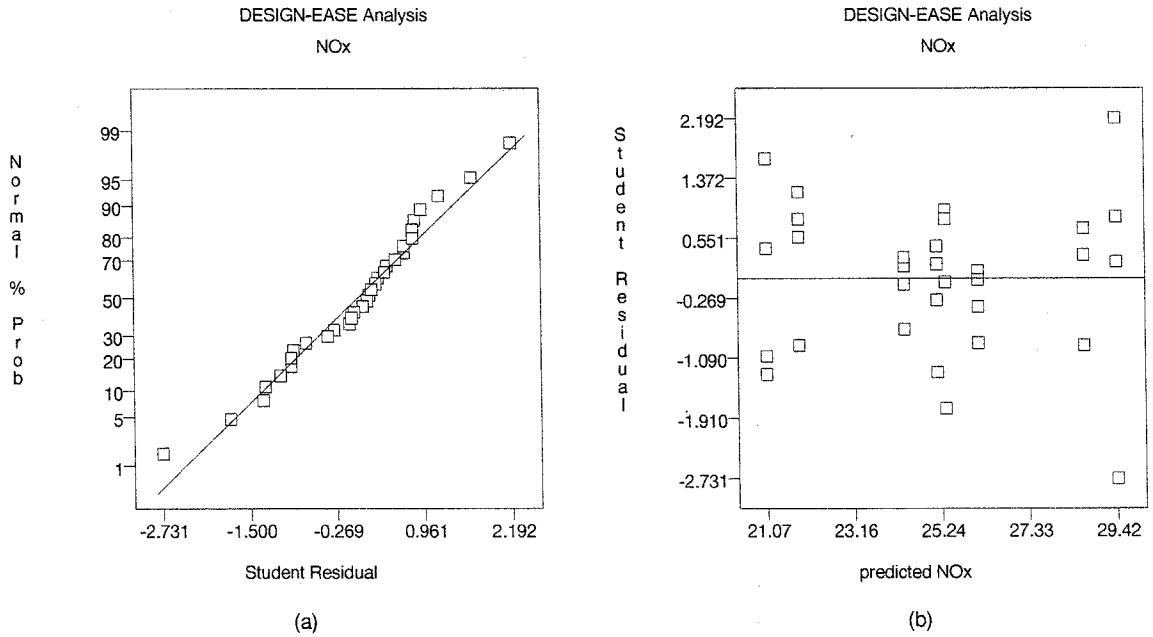

Figure 7.10: Diagnostic Graphs for NO_X Response in 10% Blocked Matrix

(a) Normal Probability Plot of Residuals

(b) Plot of Residuals versus Predicted Response

In summary, all response data were analyzed in this fashion. First, the main effects were calculated. Second, the effects which lie off the normal line were chosen for the model. Third, the ANOVA results were computed and the checks were made to ensure validity. Fourth, the two primary diagnostic graphs were plotted to ensure that the ANOVA assumptions were correct.

7.3.1. Interpretation of DoE Results

This section will discuss the response results from all three matrices: the full matrix of 69 runs, the 30% excess air blocked matrix, and the 10% excess air blocked matrix. Because of its completeness and higher accuracy, the 10% matrix will be analyzed in most detail and the full and 30% matrices will be used as secondary checks on the results.

The first response in the matrices is NO_X. The three factors with the largest effect on NO_X emissions were throat depth, fuel difference, and radial depth. These effects are shown on the half-normal probability plot in Figure 7.11. One means of showing their qualitative effects is through the use of cube plots. Figure 7.12 shows a cube plot of the NO_X response. This plot points out the optimum burner configuration for NO_X emissions, which is the lower right vertex, at 21.0 ppm. This is obtained with the shorter throat depth, the longer radial depth, and the larger fuel difference.

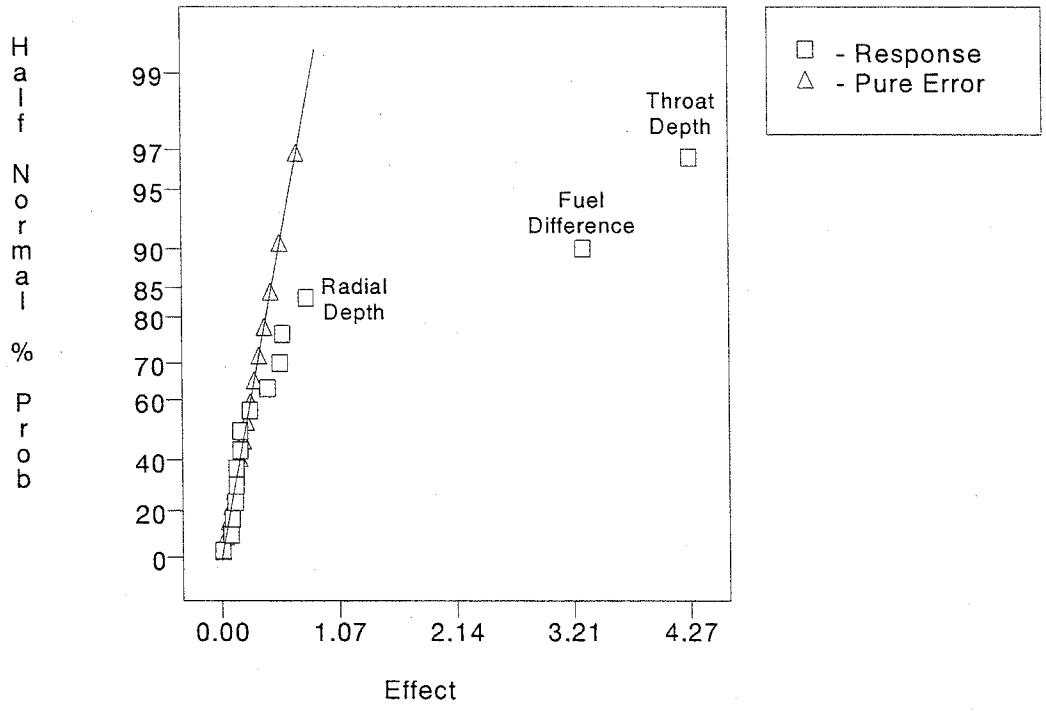

Figure 7.11: Half-Normal Probability Plot of NO_X Response
(10% Excess Air Blocked Matrix)

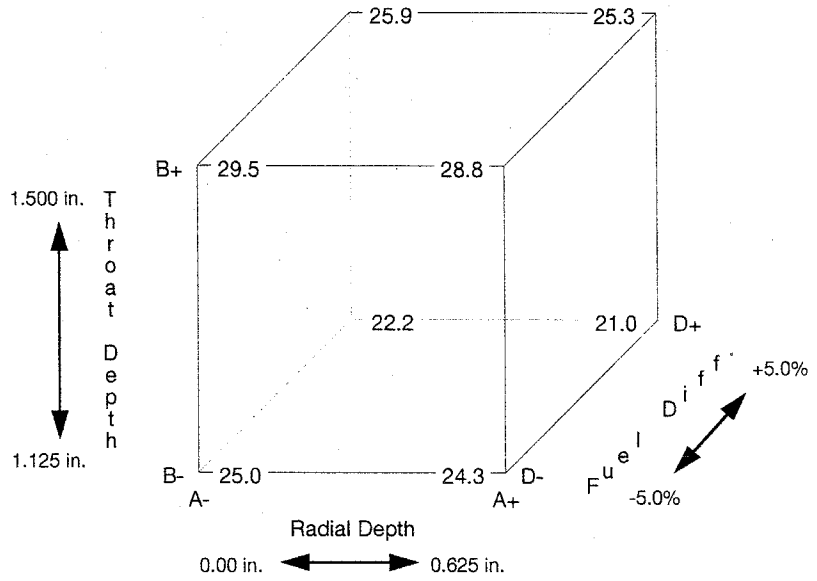

Figure 7.12: Cube Plot of NO_X (ppm) Response
(10% Excess Air Blocked Matrix)

The radial depth and fuel difference positions are consistent with combustion principles. The longer radial depth is actually a longer premixing distance. With this longer distance, more time is allowed for the fuel and air to mix, and lower stack NO_X emissions would be expected. The larger fuel difference is simply increasing the staging effect. Fuel staging has been shown to reduce peak temperatures, and thus NO_X, and these results are consistent with this effect.

The reasoning behind the effect of throat depth on NO_X emissions is not as straightforward. One hypothesis is that shortening the throat depth reduces the amount of reaction length in the throat and allows the reaction to radiate more to the walls of the enclosure. It has been noted that the average wall temperature for the shorter throat depth is greater than the average temperature at the longer throat depth. The shorter throat depth also reduces the timescale of the reaction in the throat section. This time reduction allows the reaction to enter the large enclosure more quickly. Reducing this time may also aid in suppressing thermal NO formation. Therefore, reducing the throat depth is thought to reduce the local temperature and reaction time within the throat section, both of which could reduce NO_X formation.

Similar NO_X response results were also shown to hold true in the full and 30% matrices, although both did not identify radial depth as an influential factor on NO_X. Square plots of these results are shown in Figure 7.13. Therefore, for lower NO_X emissions, this burner is optimized at a shorter throat length, a longer radial depth, and a greater fuel difference.

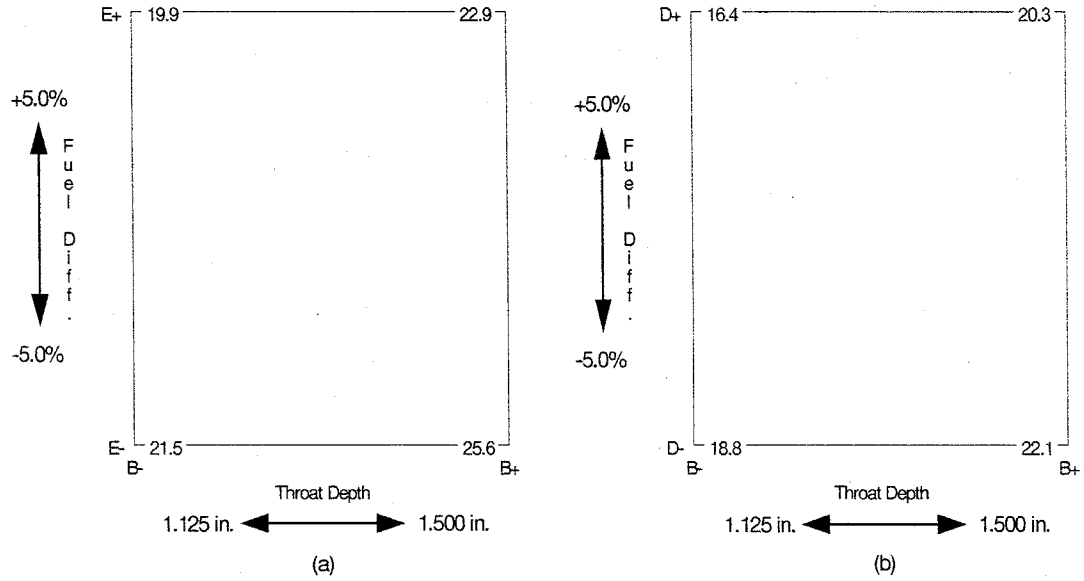

Figure 7.13: Square Plots of NO_X (ppm) Response

(a) Full DoE Matrix

(b) 30% Excess Air Blocked Matrix

The second response in the matrices is combustion efficiency. This response was not analyzed heavily because it remained virtually constant (99.99% and above) for all test runs. Figure 7.14 shows the effect graph of the combustion efficiency response for the 10% blocked matrix. It is immediately obvious that no strong effects exist and that no factors influence this response. The other two matrices display similar results.

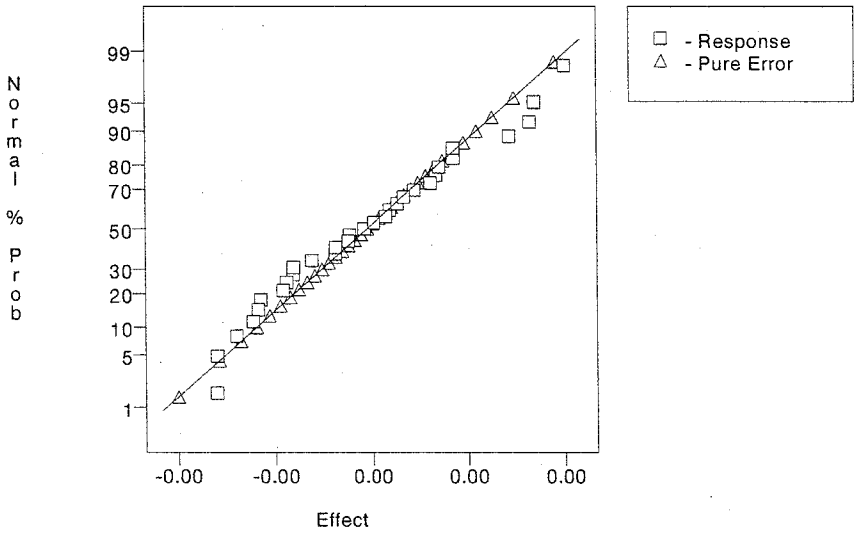

Figure 7.14: Normal Probability Plot of Combustion Efficiency Response
(10% Excess Air Blocked Matrix)

The third response in the matrices is the system efficiency, based on the heat extraction through the water panels. This response was the most difficult to interpret. The normal probability plot is given Figure 7.15. From the plot, it appears that points do indeed lie off the line. Several iterations were performed on

selecting alternate points to include in the model but the ANOVA checks in all iterations were borderline at best. Since the statistical checks were questionable, no strong statistical conclusions can be made in regards to this response. Similar results were identified in the other two matrices except that the full matrix indicated that excess air had a large impact on this efficiency. This was obviously expected since a higher excess air will cool the flame and thus reduce radiation to the enclosure. Figure 7.16 shows the system efficiency effect graph for the full matrix.

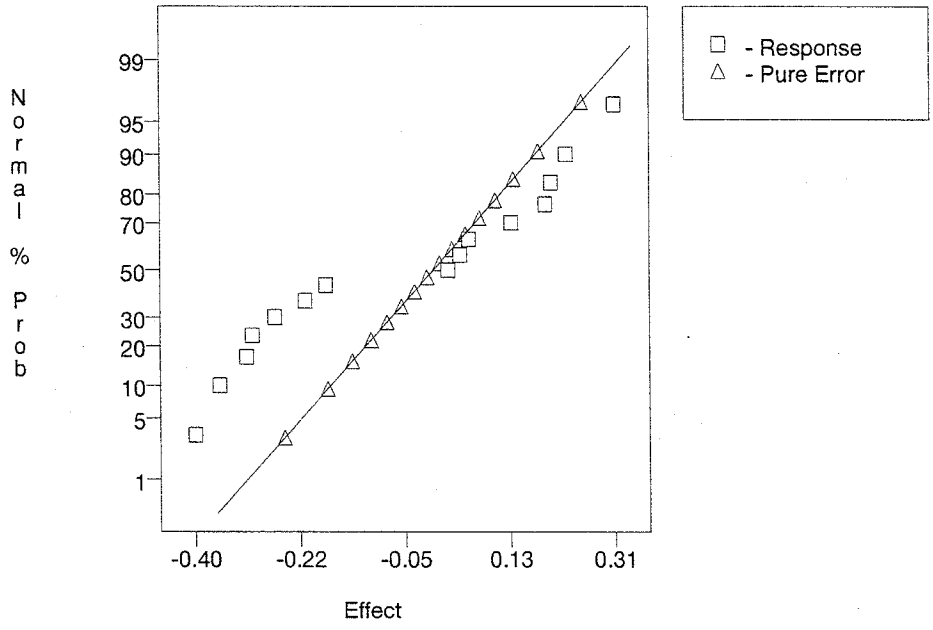

Figure 7.15: Normal Probability Plot of System Efficiency Response
(10% Excess Air Blocked Matrix)

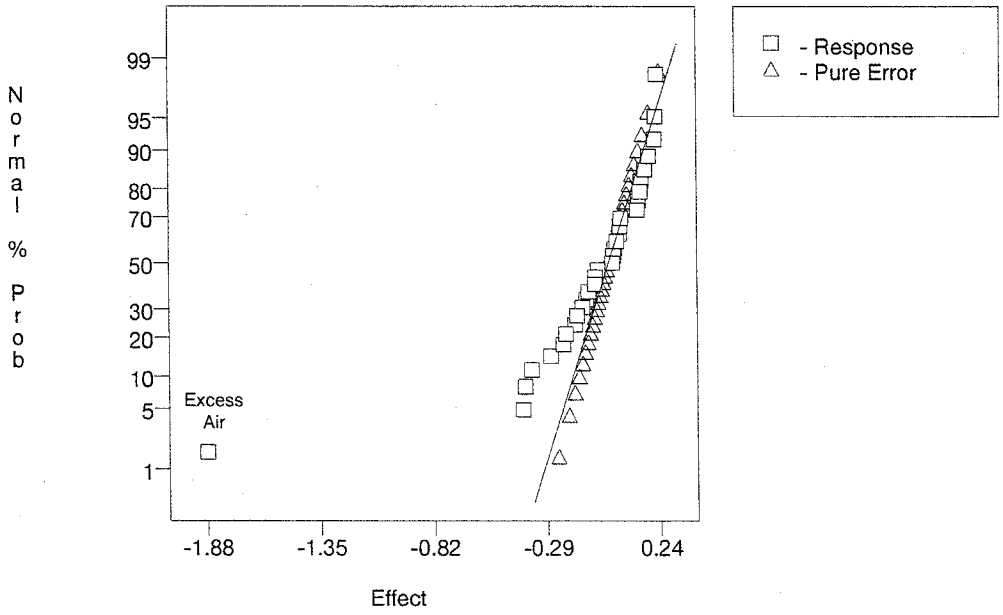

Figure 7.16: Normal Probability Plot of System Efficiency Response
(Full DoE Matrix)

7.3.2. Summary of Optimization Results

This section summarizes the design optimization results and identifies a high performance and low performance burner configuration. From the previous results, it has been identified that stack NO_X emissions are dependent on three input factors: (1) radial depth, (2) throat depth, and (3) fuel difference. In order to minimize NO_X, the radial depth should be 0.625 inches, the throat depth should be 1.125 inches, and the fuel difference should be +5.0%. Combustion efficiency was virtually constant (99.99% and above) throughout all runs and no factors had an influential impact on this response. The system efficiency based on the water heat extraction was relatively unaffected by all input factors except excess air; the higher the excess air input, the lower the system efficiency. Finally, the factors outer direction and outer depth did not effect any of the responses.

Therefore, in selecting high and low performance conditions, the effect on NO_X emissions was the primary consideration. The selected settings are shown in Figure 7.17. The outer depth and outer direction were set at 0.25" and 0°, respectively, for both high and low conditions since these factors did not affect NO_X. The radial depth was also selected to remain constant at 0.00" for both conditions since this factor only had a minor influence on NO_X emissions yet had a noticeable effect on stability, with 0.00" providing better stability. A common excess air condition of 15% was selected to approximate 3.0% O_2 out the stack. The detailed characterization measurements were taken using these two conditions for comparison.

	Low Performance	High Performance
Burner Load	400,000 Btu/hr	400,000 Btu/hr
Core Fuel Flow	1.64 scfm (25%)	1.64 scfm (25%)
Excess Air	15% (3.0% stack O_2)	15% (3.0% stack O_2)
Outer Depth	0.250 inches	0.250 inches
Outer Direction	0.0 degrees	0.0 degrees
Radial Depth	0.00 inches	0.00 inches
Throat Depth	1.500 inches	1.125 inches
Fuel Difference	-5.0%	+5.0%

Figure 7.17: High and Low Performance Burner Settings

7.4. Characterization Measurements

This section will explain the accomplishment of the fifth objective: to acquire detailed in-situ data of the velocity, temperature, and species fields at both high performance and low performance conditions.

The conditions of the burner for these two performances are given in Figure 7.17. The objective of these experiments were twofold. First, these measurements will aid in explaining the probable reaction scenarios which enable optimal performance. Second, these measurements will develop an experimental database for this burner which can be used as a comparison with expected future modeling efforts.

7.4.1. Temperature and Gas Sampling Measurements

All temperature and gas sampling measurements were taken at one quadrant of the burner at four different axial locations. Contour plots of these measurements replicate the single quadrant to give a complete

view of each axial plane. The four axial locations are 0.25" downstream of the distribution plate, the throat exit plane, 1.5" downstream of the throat exit, and 4.5" downstream of the throat exit.

Temperature contours for the low performance condition are shown in Figure 7.18. The gas sampling measurements are used for two plots. First, using the four main species of CO, CO_2, HC, and O_2, local equivalence ratios are calculated for each sampling location. Second, the gas sampling measurements quantify the local NO_X concentrations. Contour plots of the local equivalence ratio and NO_X concentrations for the low performance condition are given in Figure 7.19 and Figure 7.20, respectively. The temperature, local equivalence ratio, and NO_X concentration results for the high performance condition are shown in Figure 7.21, Figure 7.22, and Figure 7.23, respectively.

The purpose of taking characterization measurements at two burner configurations was to allow general comparisons between the high and low performances. There are seven key points that must be made from these plots. First, notice that the high performance temperature plots are approximately 100 degrees F lower than the low performance condition. Second, the high temperature areas in the high performance condition are smaller than the low performance high temperature areas. Third, the NO_X concentration profiles in both conditions at the first axial location (A) measured values ranging from 20 to 50 ppm, higher than expected. Fourth, the NO_X concentration values in the high performance condition are approximately 10 to 15 ppm less than the low performance condition for each axial plane. Fifth, as the equivalence ratio plots demonstrate, rich pockets exist near the core fuel injector in the first axial plane (A). Sixth, the high NO_X regions in the third and fourth planes (C and D) coincide with the high temperature regions. Seventh, the equivalence ratio plots of the third axial location (C) explicitly show the injection of fuel from the four outer injectors.

With these key points in mind, further deductive explanations of these results can be made. First, the high temperature regions in the low performance condition are higher and larger than the high performance. This is significant because this may lead to greater formation of thermal NO. This is reinforced by the NO_X concentration measurements, where the low performance condition shows greater NO_X than the high performance for nearly all locations. Second, the measurement of NO_X concentration values up to 50 ppm in the first axial plane is much greater than expected. Recall that this location is only 0.25" downstream of the distribution plate and is near the beginning of the flame. This result can be due to two effects. First, velocity measurements will show that a large recirculation zone exists directly above the core injector within the throat section. This recirculation zone may transport NO_X that is formed further downstream back upstream into this area. Second, the NO_X measured at this location could also be largely due to the formation of prompt NO from the core injector. Pure fuel from the core injector is radially injected into the crossflow of air and fuel passing through the slots. This would inevitably lead to rich pockets which are more prone to producing prompt NO. Evidence of these rich pockets are shown in the equivalence ratio plots of the first axial location. Notice the rich areas in the center of these two plots. Both of these effects may play a role in the observed high concentrations of NO_X at the first axial location. Finally, the coincidence of high NO_X with the high temperature regions in the third and fourth planes implies production of thermal NO at those localities.

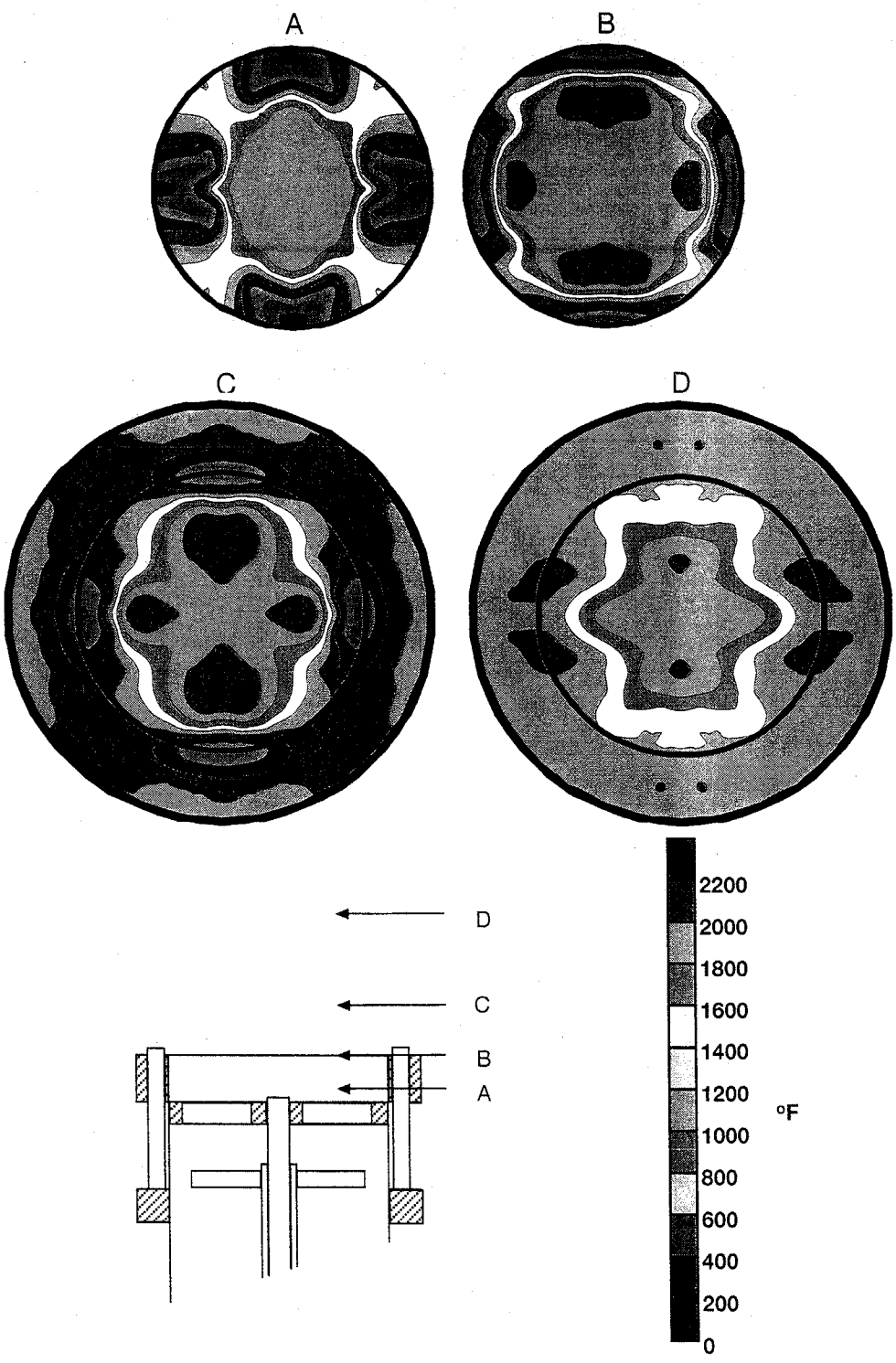

Figure 7.18: Temperatures for Low Performance Condition

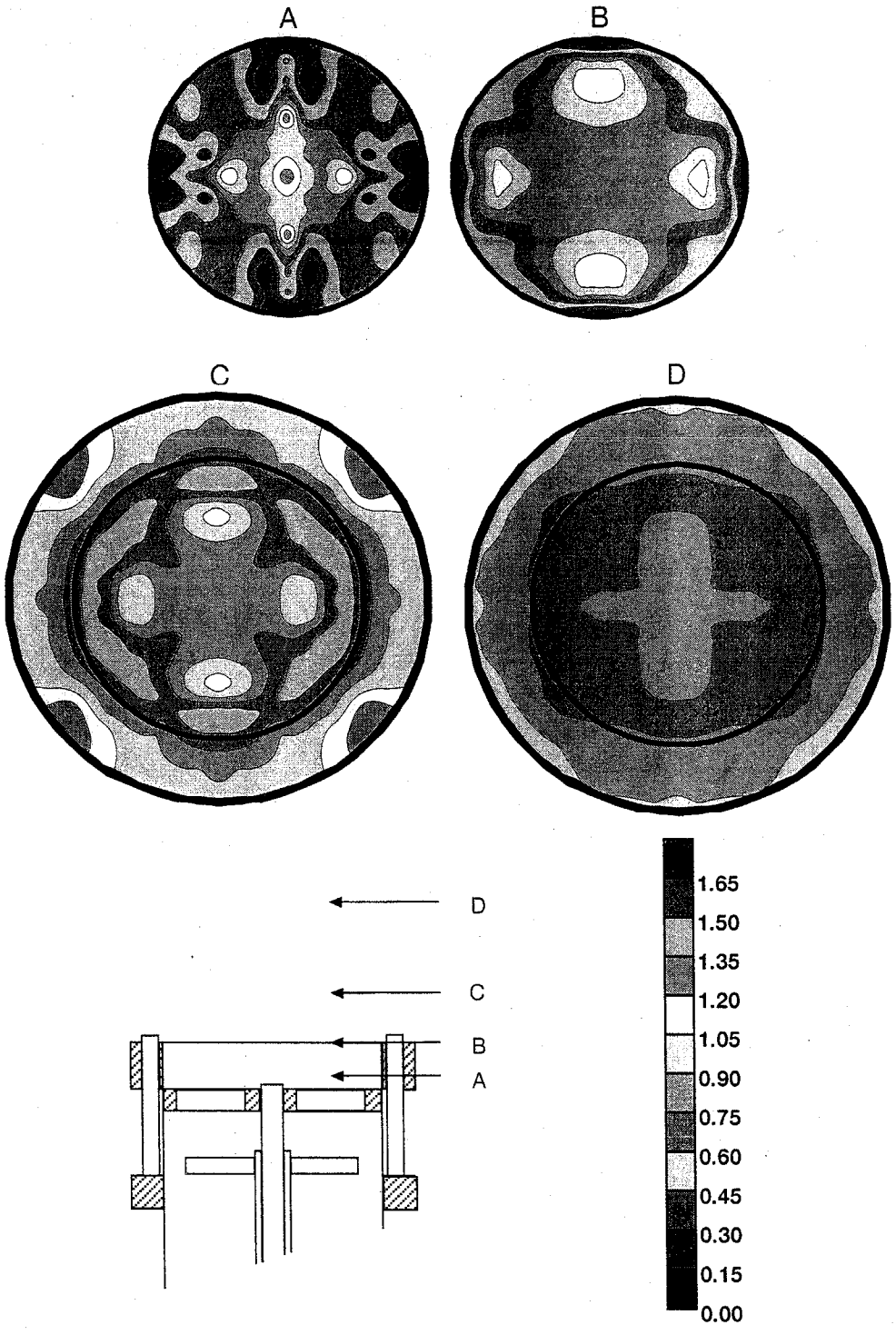

Figure 7.19: Equivalence Ratios for Low Performance Condition

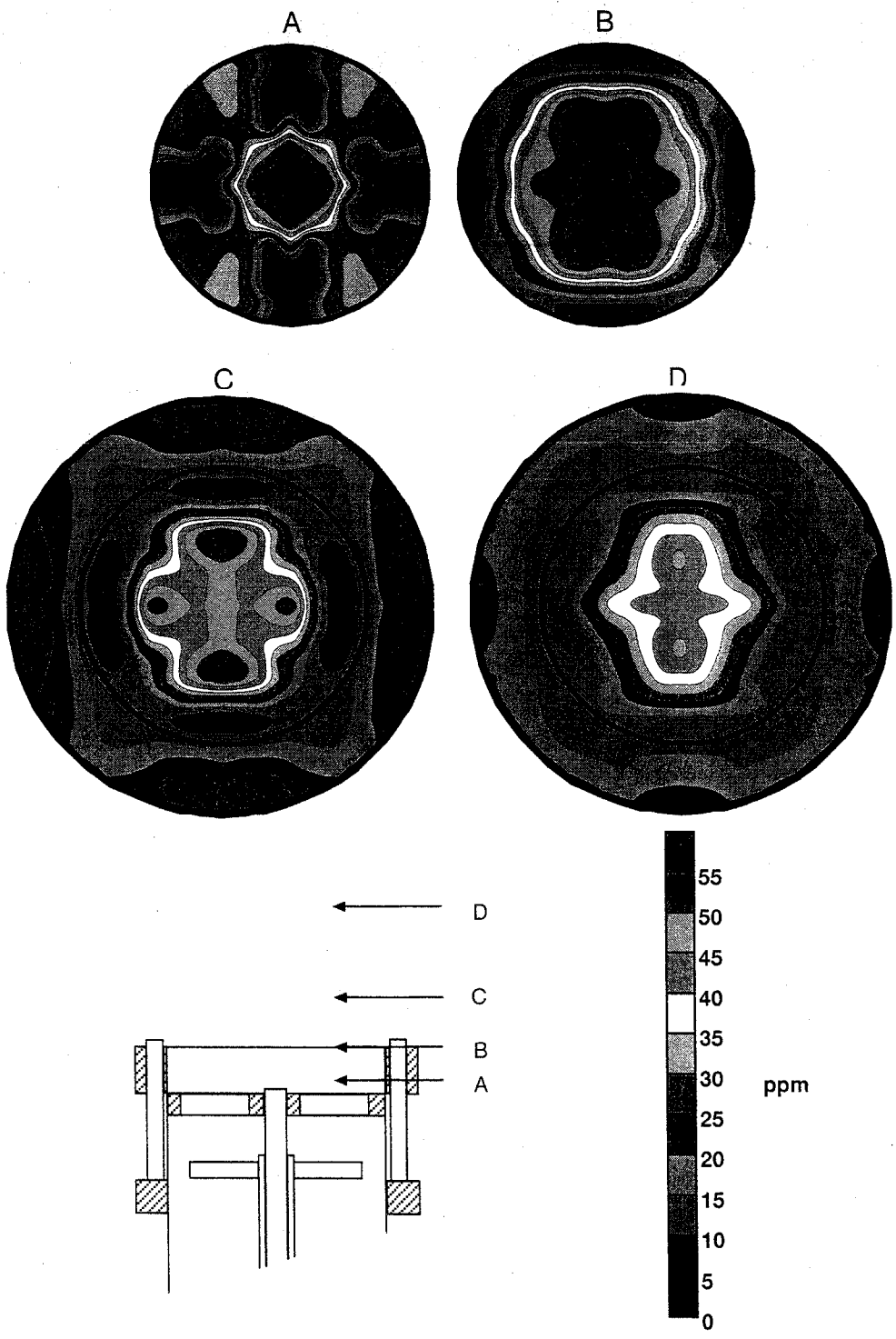

Figure 7.20: NO_X Concentrations for Low Performance Condition

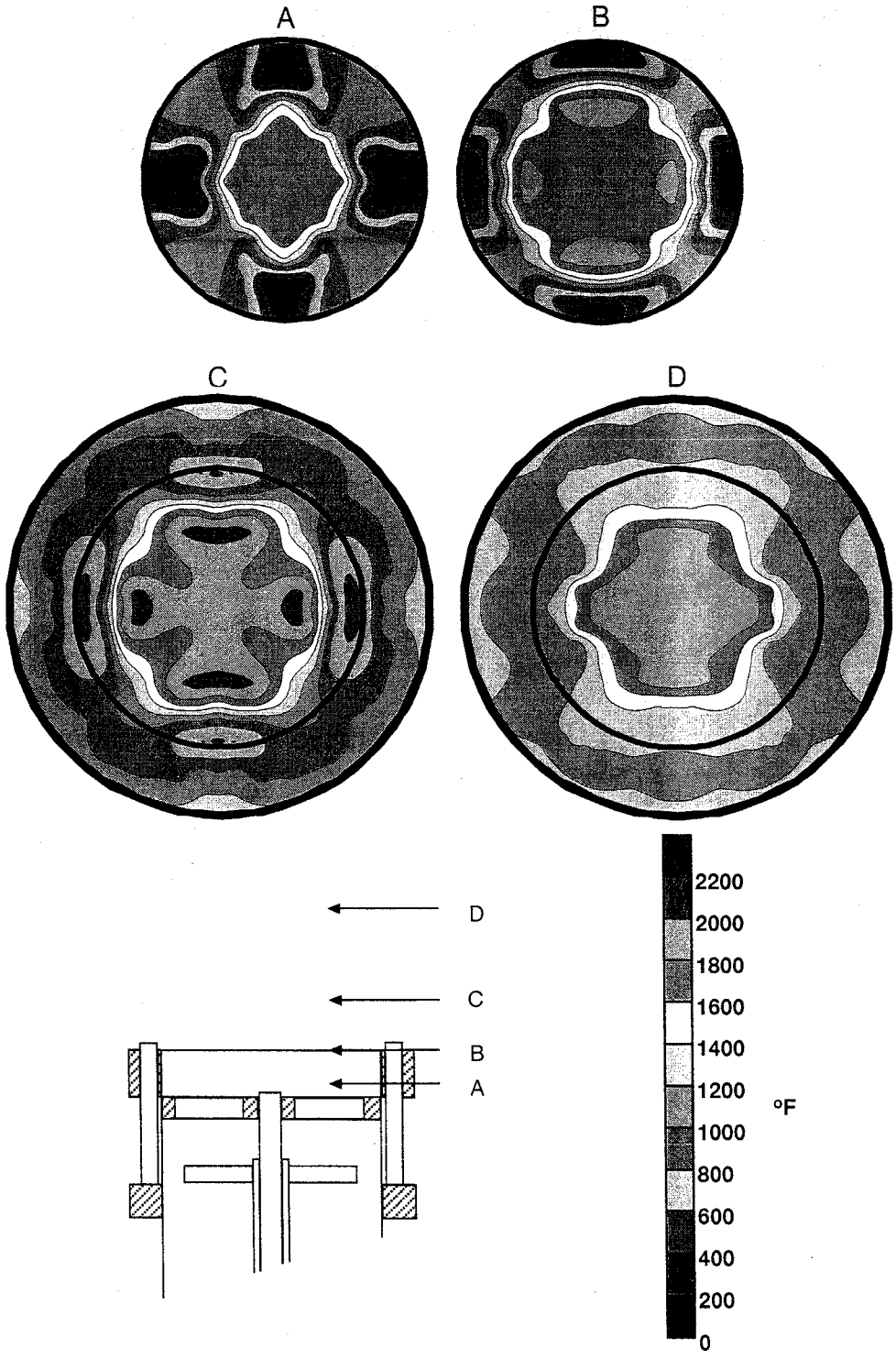

Figure 7.21: Temperatures for High Performance Condition

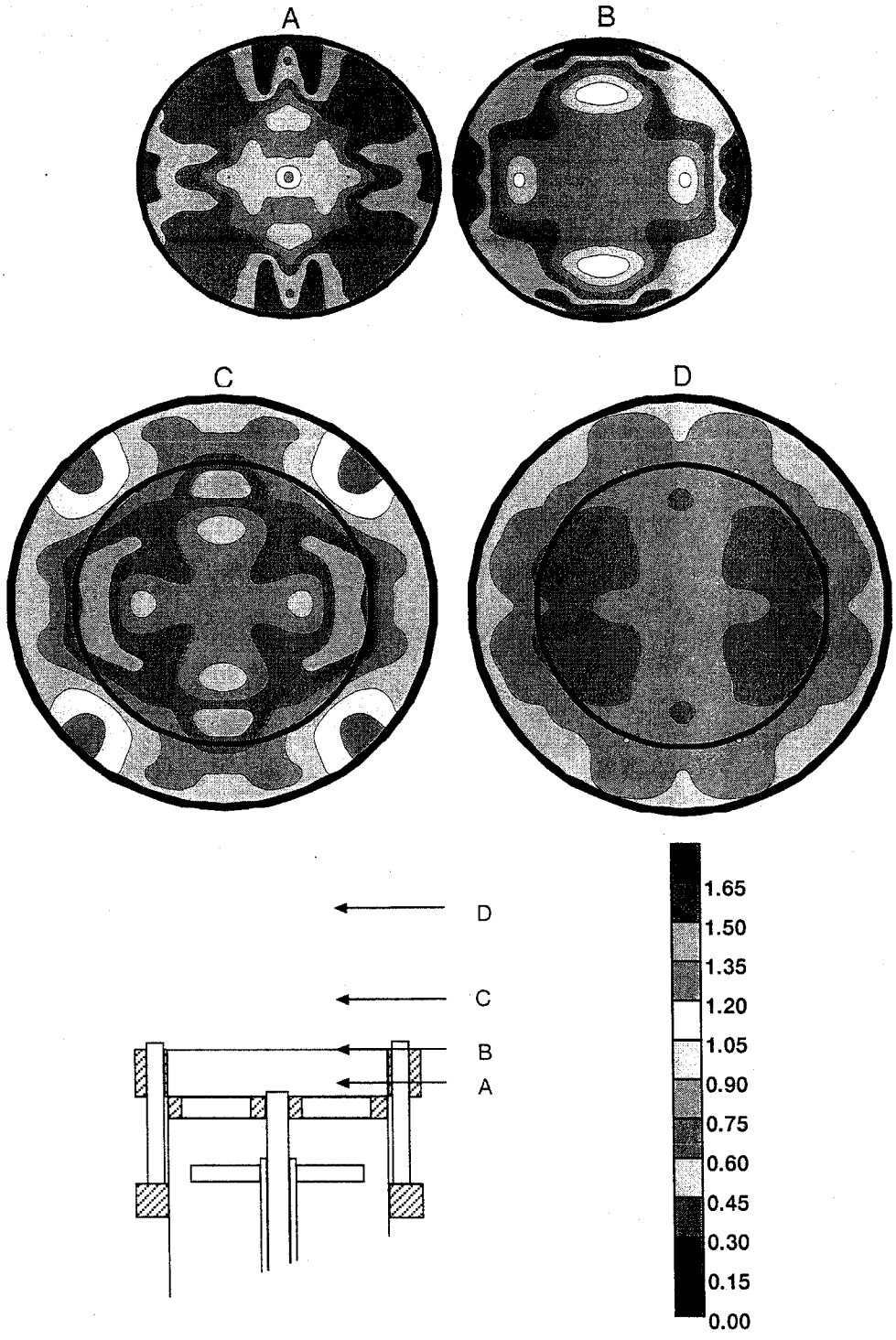

Figure 7.22: Equivalence Ratios for High Performance Condition

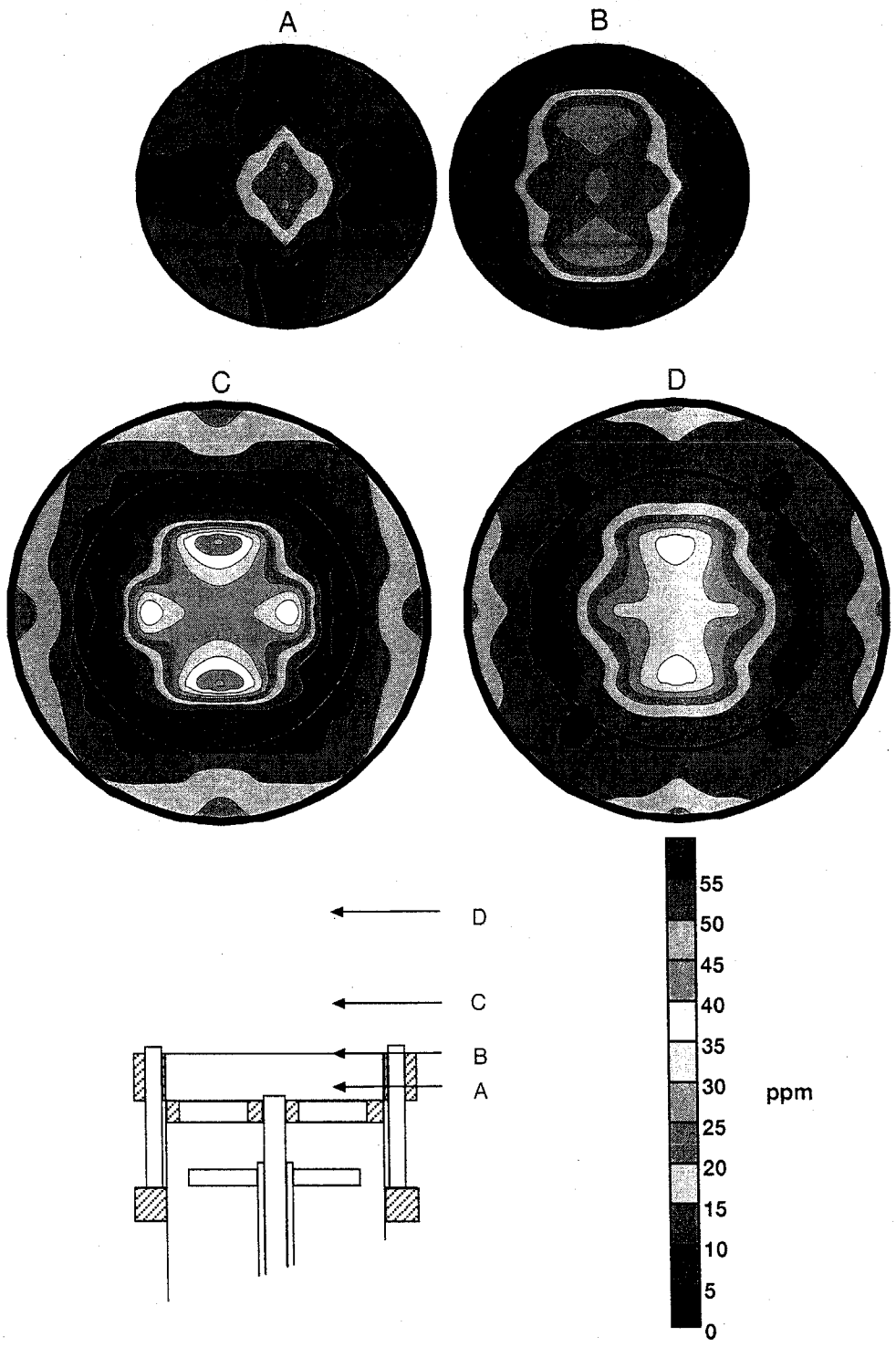

Figure 7.23: NO_x Concentrations for High Performance Condition

7.4.2. Velocity Measurements

The velocity measurements provide the third, crucial component to successfully analyze the reaction structure of the flame. Laser anemometry measurements were taken at two axial locations due to the physical limits of the burner, enclosure, and LA system. For the low performance condition, the two axial locations are 0.22" upstream and 1.50" downstream of the throat exit plane. For the high performance condition, the two axial locations are 0.15" and 1.50" downstream of the throat exit plane.

The axial velocity measurements for the low and high performance conditions are given in Figure 7.24 and Figure 7.25, respectively. The most important observation is the large recirculation zone in the center of the burner. This recirculation zone indicates a depressed pressure zone at the central core of the burner. In all probability, this recirculation zone is responsible for the continuous ignition or stability of the burner. As stated in the gas sampling results, it is believed this zone may also contribute to the high NO_X concentrations (up to 50 ppm) measured in the center of the burner at 0.25" above the distribution plate.

As expected, the highest axial velocities are above the slot locations. The measured velocities above the slots were between 23 to 26 m/s (75 to 85 ft/s). These values closely correspond with theoretical calculations based on the known throughput mass and cross-sectional area of the slots. These theoretical calculations gave a predicted velocity of 80 ft/s. As well, a pitot probe was used in non-reacting conditions to quantify the velocity through the slots. The pitot probe measurement gave a value of 75 ft/s.

It also appears that the slot flow entrains wakes above the solid parts of the distribution plate; this is deduced from the measurement of positive velocities above the solid plate, a location where no air or fuel flow is directly injected. The measured velocities at these locations are between 12 and 18 m/s (40 and 60 ft/s).

Since 2-D anemometry was utilized, radial velocity measurements were also taken. Radial velocities were not near as strong as the axial measurements because this burner does not incorporate swirl. In Figure 7.26 and Figure 7.27, radial and axial velocity measurements are given for both burner conditions at the 1.50" axial location. These plots show a velocity line profile across the center of the slots and a profile across the solid portion of the distribution plate.

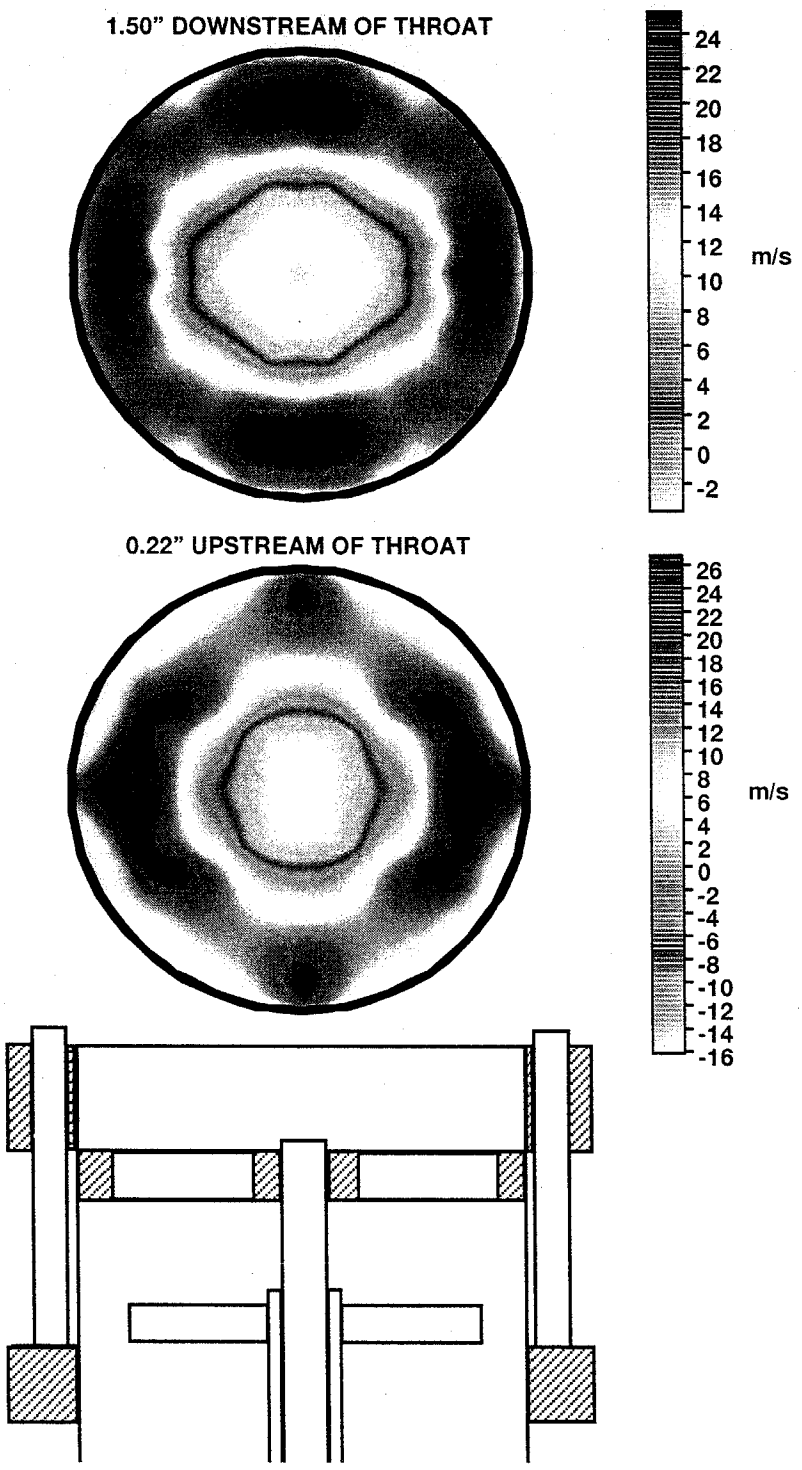

Figure 7.24: Axial Velocities for the Low Performance Condition

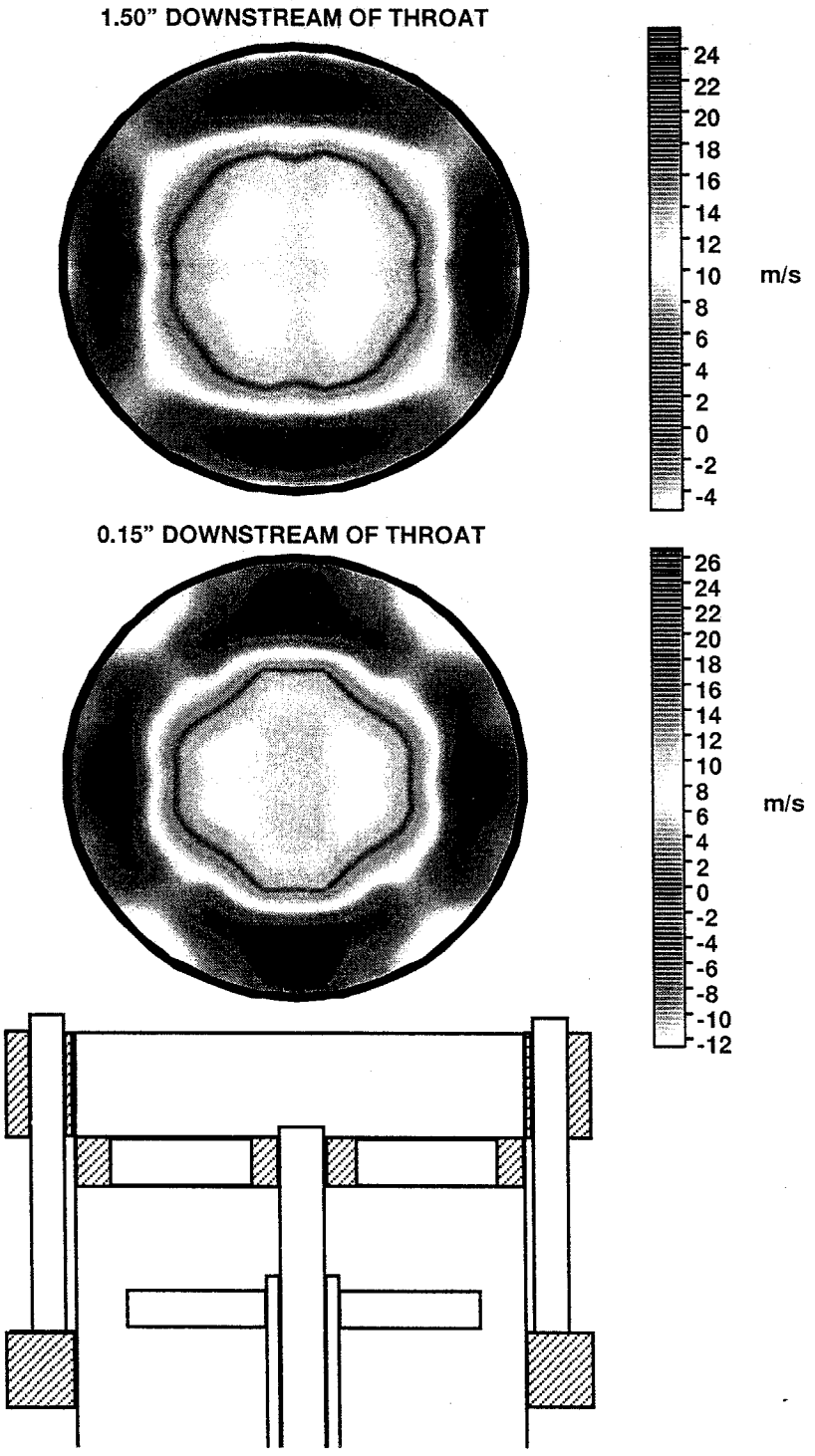

Figure 7.25: Axial Velocities for the High Performance Condition

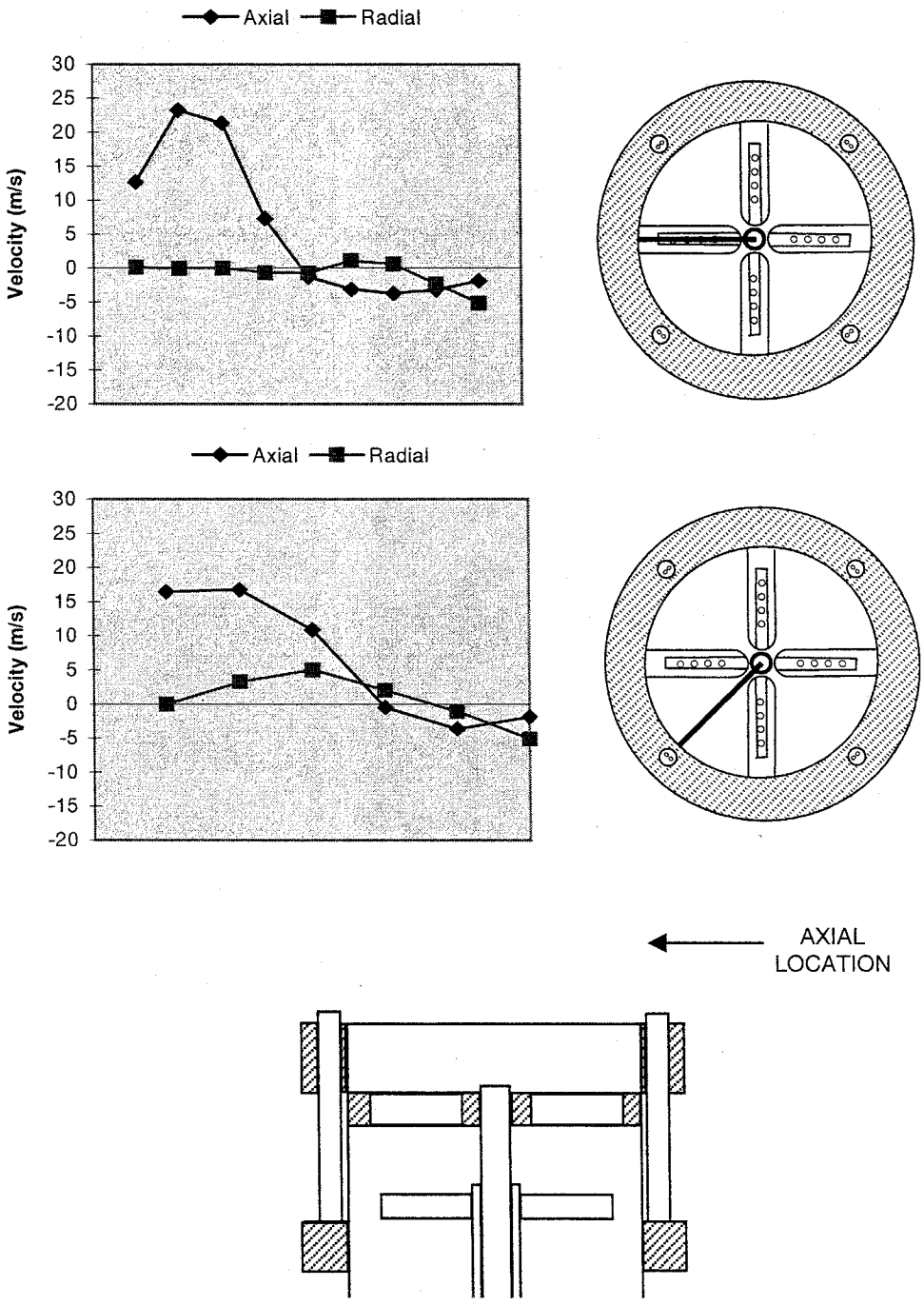

Figure 7.26: Axial and Radial Velocities for Low Performance Condition at 1.50" Downstream of Throat Exit

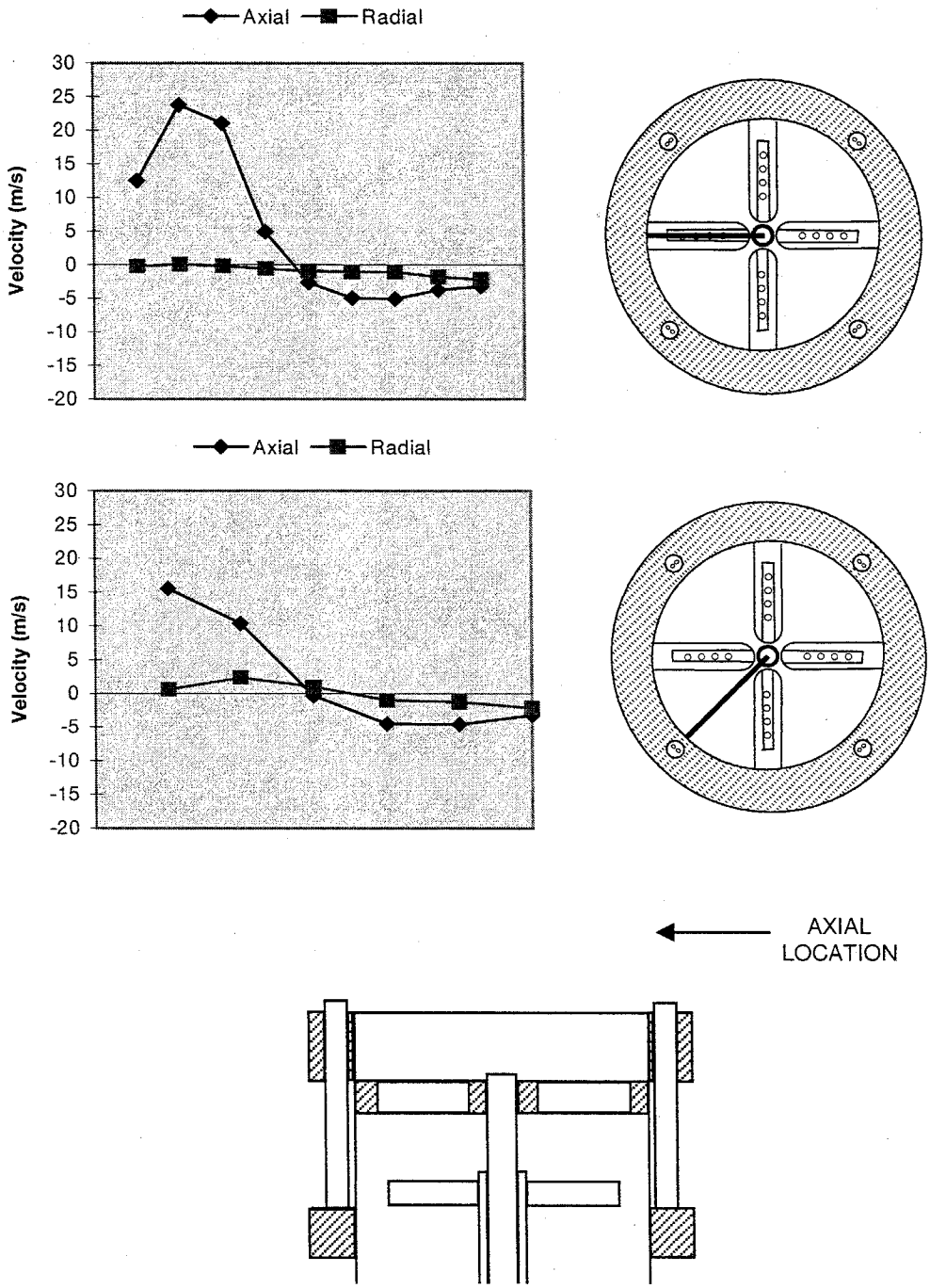

Figure 7.27: Axial and Radial Velocities for High Performance Conditions at 1.50" Downstream of Throat Exit

7.4.3. Photographic Structure

Photographs of the high and low performance condition were also taken as a visualization aid. Images of these photographs are given in Figure 7.28. Notice the increased intensity of the low performance condition over the high performance. This is thought to be due to the higher temperatures and lower fuel

staging in the low performance condition. In addition, it is interesting to note that the regions of highest intensity are directly above the slots.

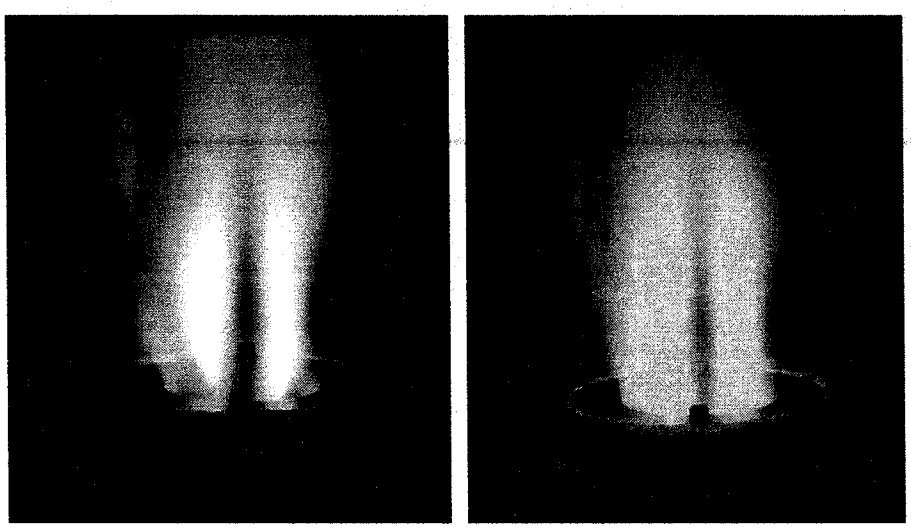

HIGH PERFORMANCE LOW PERFORMANCE

Figure 7.28: Images of the High and Low Performance Conditions

7.4.4. Summary of Characterization Measurements

The characterization measurements aided in properly understanding the reaction structure. These measurements have provided further insight into why one configuration performs "better" than another.

In comparing the two burner conditions, differences are noticeable. The low performance condition exhibited greater NO_X concentration values of 10 to 15 ppm. The low performance condition also showed higher temperature values than the high performance. Both of these results are due to the change in throat depth and the fuel staging effect. The shorter throat depth and greater fuel staging led to slightly lower temperatures within the primary zone.

The velocity measurements indicated a large recirculation zone within the center of the burner. This recirculation zone exhibited reverse axial velocities up to 16 m/s. It is probable that this recirculation zone may transport NO_X formed downstream back upstream near the beginning of the flame. The largest positive axial velocities were measured between 23 and 26 m/s above the four slotted regions. These high velocity slot flows also appear to entrain wakes above the solid portions of the distribution plate, where velocities were measured between 12 and 18 m/s. The radial velocities are relatively minor because this burner does not incorporate swirl.

7.5. Reproducibility and Modified QLN

The *QLN* burner design was modified by Coen in 1997 to more appropriately reflect the higher radial spud gas injection velocity. Stack emissions tests were conducted to

1. Verify the testing procedure and boundary conditions using the original *QLN* configuration ("QLN_O") and

2. Determine the effect on NO_X and efficiencies using the modified *QLN* ("QLN_r").

These two sets of emissions measurements are provided in the following sections.

7.5.1. Repeated DoE

Since the burner facility is shared for other experiments, the QLN_O burner was removed from the facility after the measurements described previously were completed. The burner was reinstalled over one year later to conduct the new radial spud tests (QLN_r). A reduced-matrix DoE was first performed using the *original* QLN_O burner to ensure the data quality; however, a different experimenter conducted these tests. These repeated results are described below.

The factors and limits are presented in Figure 4.2. The same responses were measured, i.e., NO_X, combustion efficiency, and system efficiency, at 10% excess air. The half-normal probability plot of NO_X response is compared to the original data in Figure 7.29.

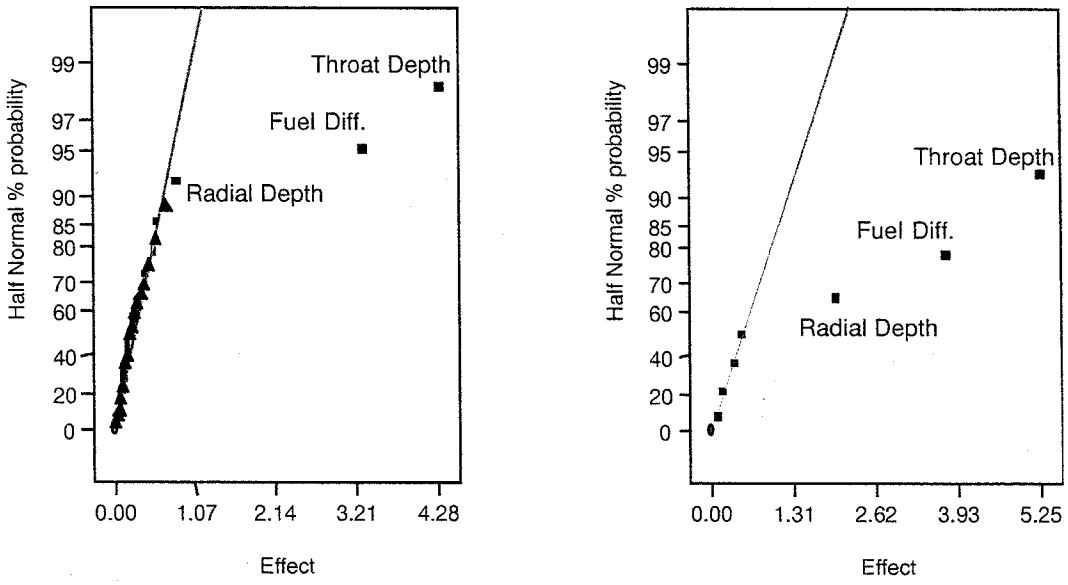

Figure 7.29: Repeated Half-Normal Probability of NO_X Response – QLN_O

The repeated data show the same results as the original data, i.e., the fuel difference and throat depth have the largest effect on the NO_X emissions. The repeated data also indicate a larger effect on NO_X due to the radial depth. However, due to the limited number of runs, no repeats, and small magnitude of the NO_X difference, this result should be treated with some scrutiny. The magnitude of the changes in NO_X is better illustrated in Figure 7.30, which shows the cube plots of NO_X response for the original and repeated data.

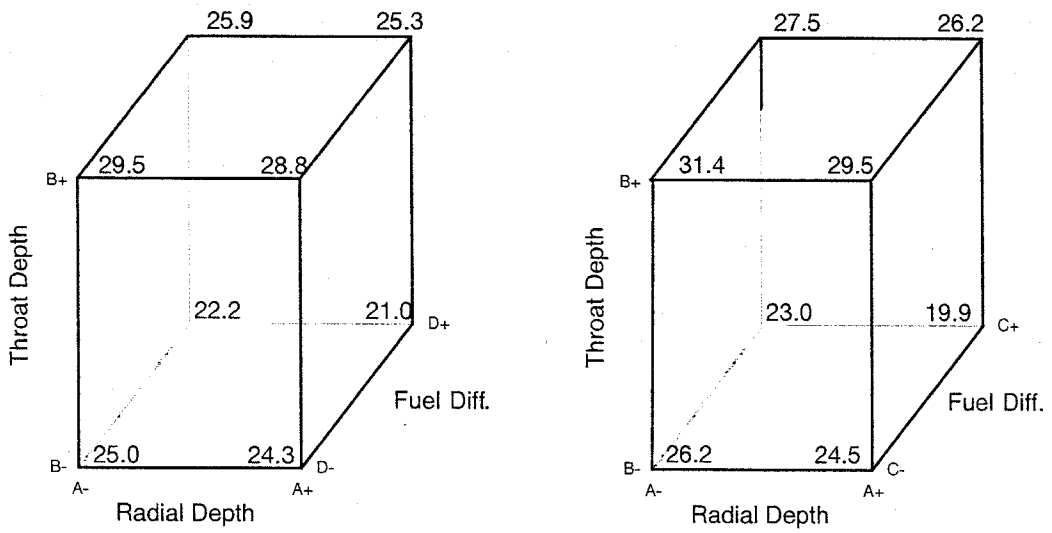

Figure 7.30: Cube Plot of NO_X Response – QLN_O

As with the original data, the combustion efficiency and system measurements for the repeated data were unaffected by changes in the input factors.

These repeated data match well with the original data, despite having the burner removed and reinstalled, the long time break, and a different researcher conducting the experiments. The results agree to within 2 ppm and identify the same trends and factors as effecting the NO_X emissions, namely the fuel difference and throat depth. These results indicate the *reproducibility* of the data and add confidence to the results and overall testing protocol. With this confidence established, the modified QLN_r was tested.

7.5.2. Modified Burner – QLN_r

The modified QLN_r consists of new radial spuds with smaller diameter fuel injection, approximately 0.05 inches compared to 0.12 inches for the original QLN_O. The same factors were tested (fuel difference, radial distance, throat depth, outer injection depth, and outer injection direction), and the same responses were measured (NO_X emissions, combustion efficiency, and system efficiency). All the measurements were conducted at 10% excess air to preclude any dilution effects.

The half-normal probability plot of NO_X response is shown in Figure 7.31. The fuel difference and throat depth are again identified as the major factors affecting the NO_X emissions in the QLN_r.

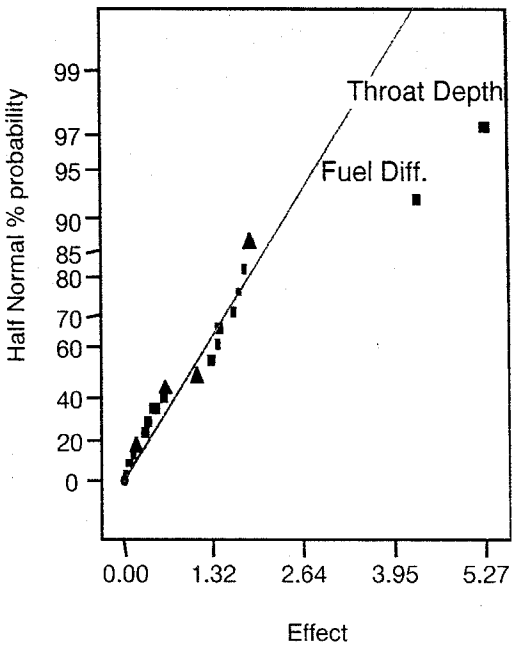

Figure 7.31: Half-Normal Probability Plot of NO_X Response – QLN_r

The magnitude of the changes due to these factors, however, are slightly larger than in the QLN_O. In addition, the overall NO_X values are approximately 2–7 ppm higher than the NO_X emissions from the QLN_O. These differences are shown in Figure 7.32, which compares the QLN_O and QLN_r NO_X cube plots.

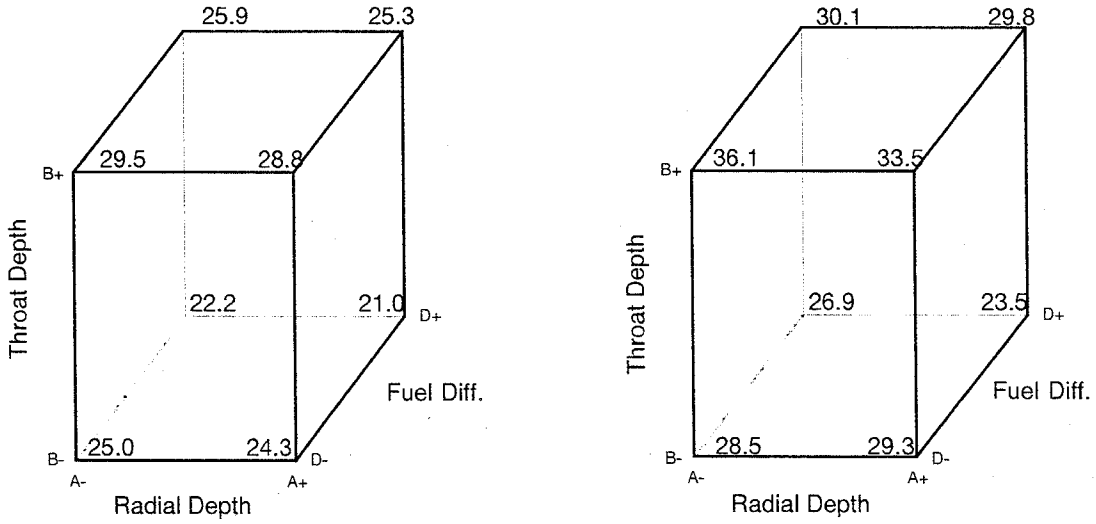

Figure 7.32: Cube Plot of NO_X Response – QLN_r

As with the reproduced data, the combustion efficiency and system efficiency were unaffected by changes in the input factors, i.e., all points are close to the random error line. The half-normal probability plots for these are shown in Figure 7.33.

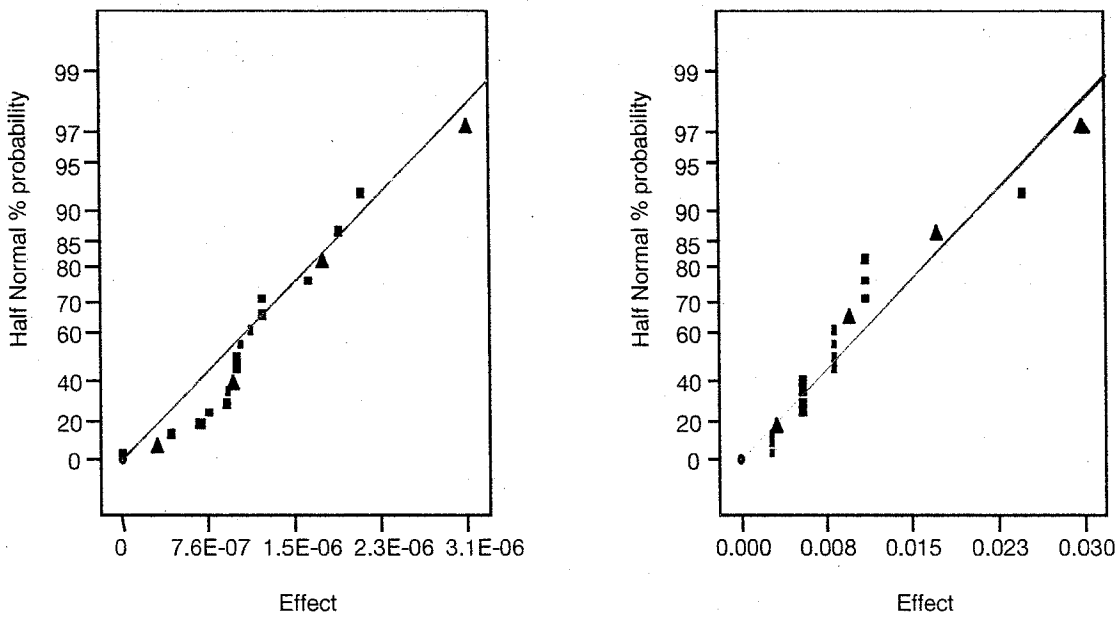

Figure 7.33: Half-Normal Probability Plot of Combustion Efficiency Response – QLN_r

7.5.3. Summary of Repeated and Modified *QLN* Burner Measurements

Repeated emissions measurements were conducted to verify the original data reported in section *4.2: Design of Experiments Analyses*; the *QLN* burner was reinstalled into the furnace facility after a long period of time and a reduced DoE was conducted by another researcher. These measurements provide the same trends and illustrate consistent sensitivity of NO_X to the radial depth, throat depth, and fuel split difference. These data also consistently illustrated that combustion efficiency and system efficiency were not greatly affected by any factor through the range investigated and that the outer spuds depth and direction did not contribute to changes in any response. These repeated measurements reproduced the conclusions originally stated in section *7.3.2 Summary of Optimization Results* and added confidence to the statistical protocol, thereby laying the foundation for the modified *QLN* tests.

Modified radial spuds with higher injection velocity were tested in a new DoE to determine the effects on NO_X, combustion efficiency, and system efficiency. This modified burner was dubbed the QLN_r to avoid confusion with the original radial spud design, QLN_O. The DoE measurements again identified the throat depth and fuel difference as the dominating factors for NO_X emissions, with little effect shown for combustion efficiency or system efficiency. The NO_x emissions overall for the QLN_r were approximately 5 ppm higher than the QLN_O.

7.6. Task 2A Summary

A specific geometric configuration was identified as the optimum for the *QLN* burner. This condition has a longer throat depth (1.50 inches) and 5% fuel staging at 15% excess air. Detailed measurements were conducted for this optimized condition and a poor performing configuration which had a slightly shorter throat depth (1.125 inches), less fuel staging, and the same excess air. Laser anemometry measurements determined that optimized configuration exhibited much greater central recirculation, inducing higher amounts of internal FGR and thereby providing better NO_x control. In-situ species measurements and

subsequent local equivalence ratio calculations also determined that the optimized configuration provided leaner local equivalence ratios further upstream than the poor condition, indicating faster fuel and air mixing.

A modification was done to the scaled *QLN* burner in order to more accurately reflect the commercial burner design. This model, QLN_r, was again tested using the DoE methodology. The results agreed with the initial tests, specifically that the throat depth and fuel difference are the dominating factors for NO_x emissions.

8. TASK 2B – MAXON, HIGH TEMPERATURE BURNER

Before formal tests could be run, a few system validation tests were run to make sure that the results gathered were not suspect. The first validation test was a system mass balance to eliminate, or at the least, correct for leakage into and out of the system. The following section describes the results from the various studies done on the high-temperature furnace and the modularized commercial burner.

8.1. Design of Experiments

Experimental error, or pure error, is the normal variation in the response which appears when an experiment is repeated. Repeated experiments rarely produce identical results. Pure error is the minimum variation expected in a series of experiments. It can be estimated by replicating points in the design. Pure error estimates are derived from replicated experiments. The more replicated points, the better will be the estimate of the pure error. Pure error is used to test the lack of fit terms for possible significance. Replication increases the precision of the response estimate by averaging results, but more importantly, provides an independent estimate of the experimental variability over the design space.

The first set of DoE shows no significant effects on NO_x emission. As can be seen in Figure 8.1, the normal probability plot shows that none of the four parameters (tip geometry, total effective area of the jets, location of the injection holes and the air swirl) produces an effect on bulk NO_x readings at the stack. After reviewing the data and inspecting the burner design, it was hypothesized that the tip geometry does not play an important role in NO_x emission due to the ratio between the throat diameter and the tip geometry diameter. Specifically the tip geometry may be so large in comparison to the throat diameter that its size, rather than its shape, is dominating the resulting stabilization behavior. Thus the tip geometry is eliminated from the *Kinedizer* burner test matrices. Another parameter that could be eliminated after studying these results is the location of the fuel injection holes, which sets the mixing length. The range of this parameter is 3 inches, which is the same as the burner diameter at the exit. The ratio between the mixing length and the exit diameter is too small to allow for the mixing length to play a large role in the resulting reaction. In other words, the mixing length is not large enough to effect NO_x. Figure 5-2 shows that the data also do not reflect any effects of burner geometry on combustion efficiency (η). This situation is anticipated since the operating conditions simulate a high-temperature, natural gas fired furnace application with long residence time (large volume and emissions measurements taken at the rear stack). Under these conditions, it is expected that there would be no HC emissions and that most of the CO would oxidize to CO_2. This is expected for all of the tests that were run under these operating conditions and this expectation is borne out by the resulting plots of data from all DoEs.

Once two of the four parameters have been eliminated, another parameter was added to the next set of tests. The second set of DoE also shows no significant effects on NO_x emission. As can be seen in Figure 8.3, the normal probability plot shows that none of the three parameters (number of jets, total effective area of the jets and the air swirl) produces an effect on bulk NO_x emissions. Figure 8.4 also shows that, as anticipated, the data also do not reflect any effects of burner geometry on η. The next step was to add another parameter without eliminating one, since there might be an interaction between these three parameters and jet swirl.

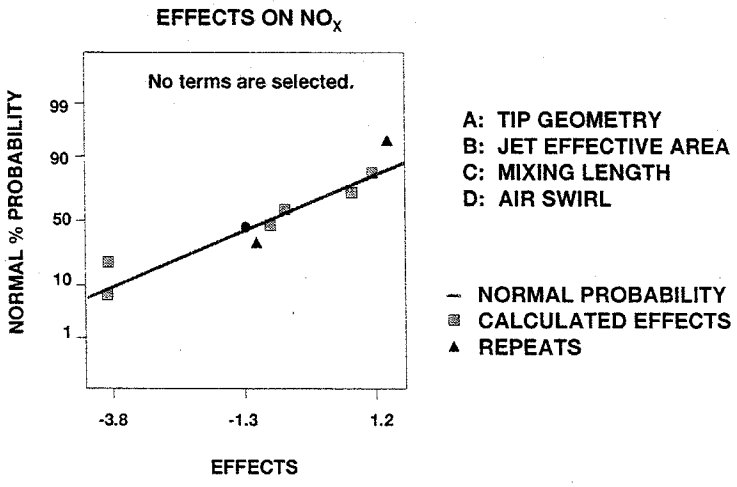

Figure 8.1: Results from test #1 of effects on NO_x

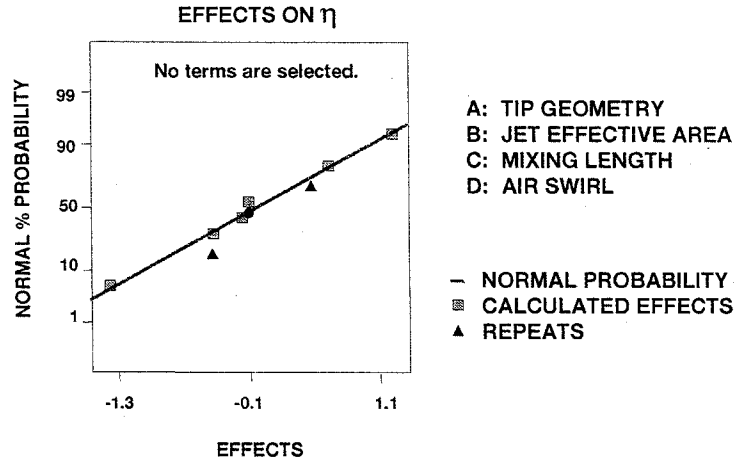

Figure 8.2: Results from test #1 of effects on η

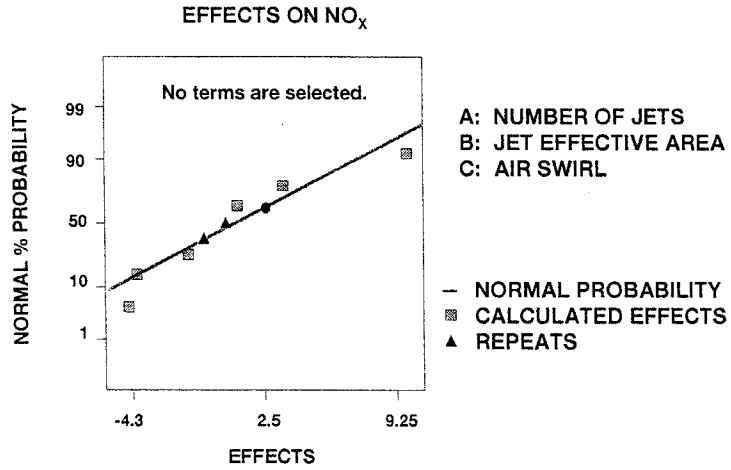

Figure 8.3: Results from test #2 of effects on NO_x

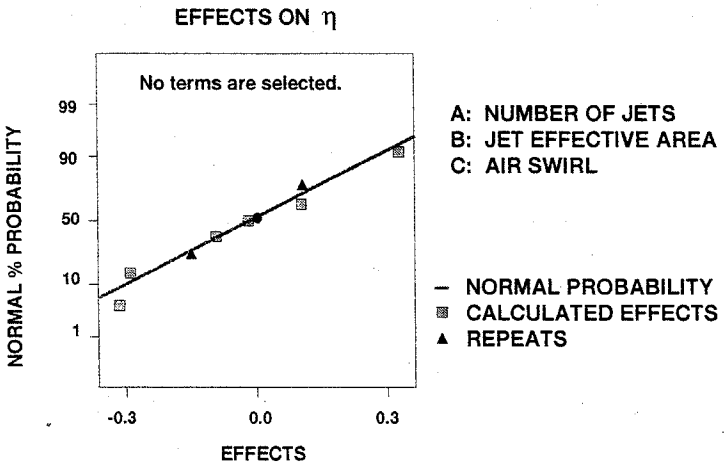

Figure 8.4: Results from test #2 of effects on η

The addition of jet swirl added something new to the factorial design since there were essentially three levels for this factor: co-swirl (jets swirl in the same direction as the air), radial (jets penetrate radially into annulus—no jet swirl) and counter-swirl (jets swirl in the opposite direction to the air). Since including a midpoint to only one of the factors would unduly complicate the matrix and make it impossible to have "day run" as a factor in blocking, a decision was made to divide the levels into different sets of DoEs. The first of these sets included only the radial and co-swirl jet injection levels and excluded the counter-swirl (CX) jet injection level. Figure 8.5 and Figure 8.6 plot the results of this experiment onto normal probability graphs and show that the four parameters under consideration do not give rise to any effects on NO_x or η. The second set of this experiment included only the counter-swirl and radial jet injection and not the co-swirl jet injection level. Once again, the results reveal no effects on either NO_x nor η. This can be seen in Figure 8.7 and Figure 8.8. The third set of plots combine the co-swirl and counter-swirl injection levels but excludes the radial injection and result in no effects on NO_x or η that falls outside experimental error (Figure 8.9 and Figure 8.10).

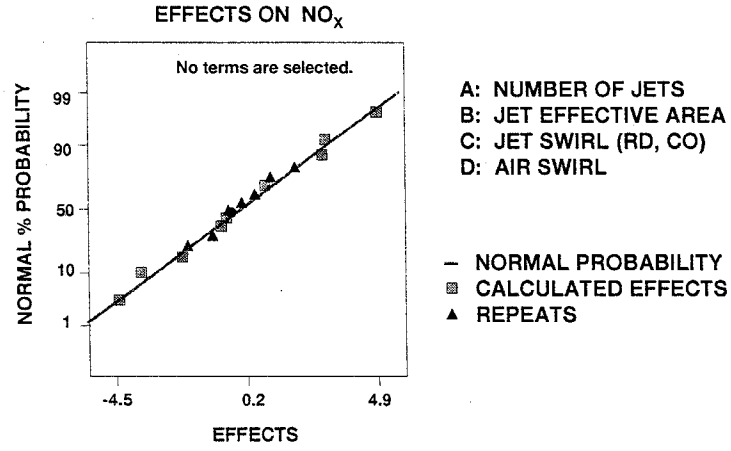

Figure 8.5: Results from test #3 of effects on NO_x

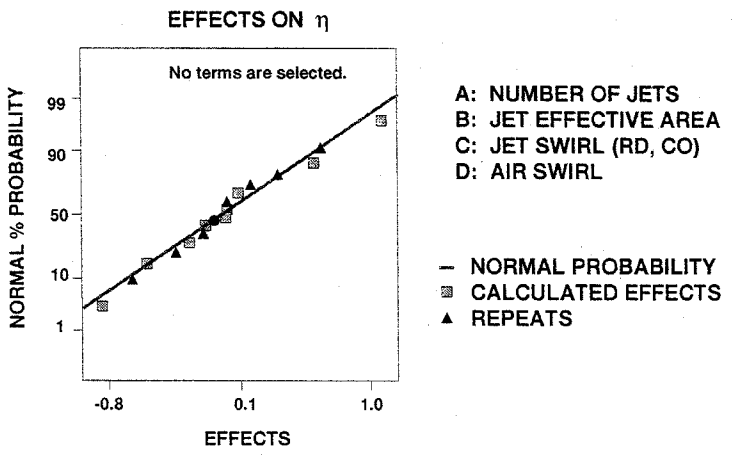

Figure 8.6: Results from test #3 of effects on η

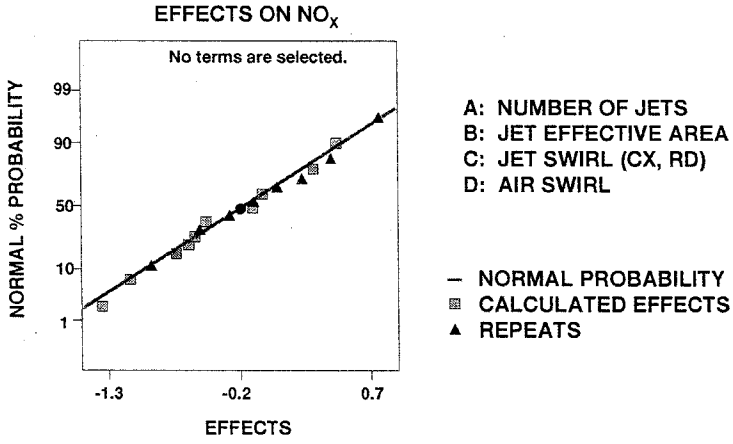

Figure 8.7: Results from test #4 of effects on NO_x

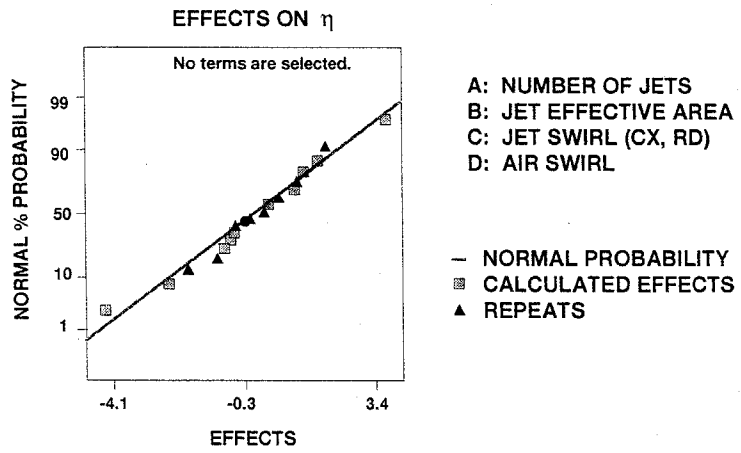

Figure 8.8: Results from test #4 of effects on η

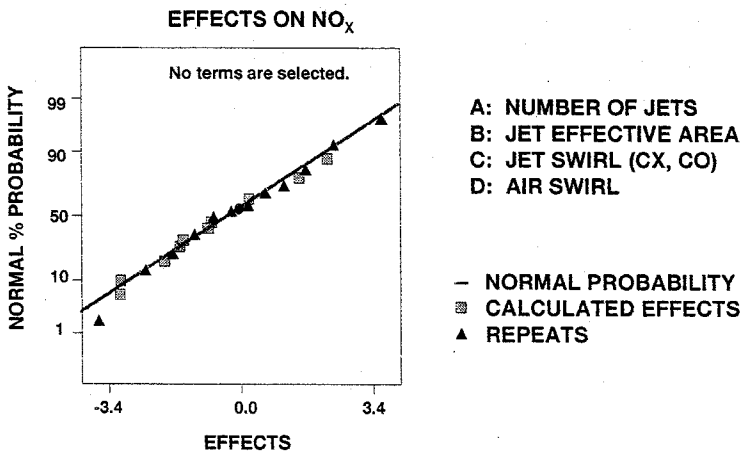

Figure 8.9: Results from test #5 of effects on NO_x

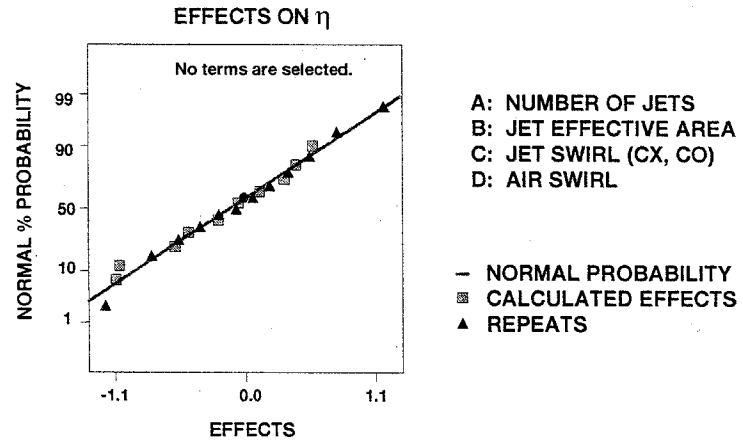

Figure 8.10: Results from test #5 of effects on η

Results from the series of DoEs indicate that the modularized *Kinedizer* burner is quite robust with respect to burner parameters and their effects on NO_x emissions. It also shows that the η of the high-temperature furnace is quite high. A question that remains from the analysis of these sets of data is whether the burner is so robust that it is insensitive to the changes in the burner geometry, whether the ranges of values for these parameters are too small to effect the responses or whether there is another factor (or combination of factors) which dominates the emissions at the stack. A series of diagnostics was used on the burner to determine whether or not there is enough of a difference in the ranges of values for the different parameters to make a difference in the mixing behavior. One quick way to determine qualitative differences is through a comparison between images of the reaction from different burner configurations.

8.2. Reaction Images

Results from the video images of the reactions with the low and high air swirl cases can be seen in the next two figures. The first image is of the low air swirl case. The reaction is long, thin and lazy, with separated "fingers" that can be seen from this view. The flame is actually longer than the image shows because the field of view for the camera is obscured by the refractory that surrounds the internal volume

of the furnace. The next image is of the high air swirl case. This reaction is shorter and bushier and more intense than the previous one.

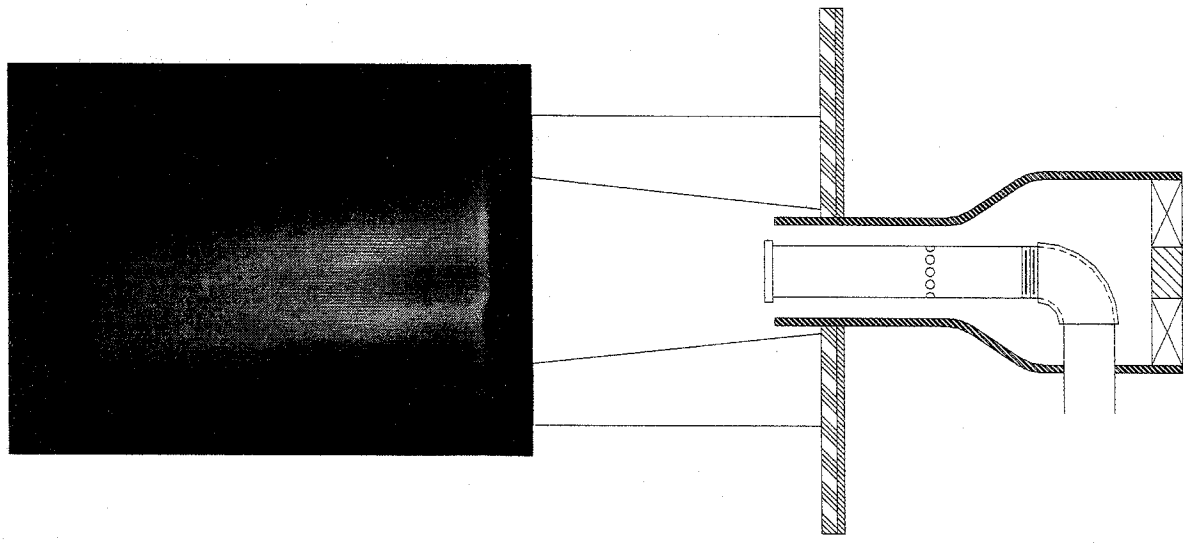

Figure 8.11: Reaction Image of Low Air Swirl Case

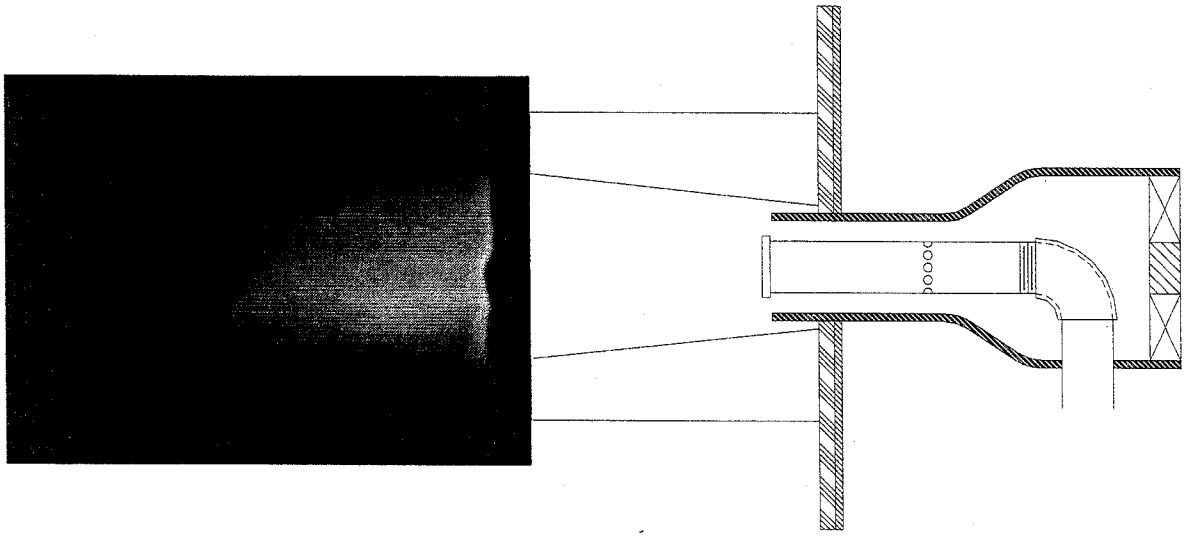

Figure 8.12: Reaction Image of High Air Swirl Case

These images show observable differences in the way the combustion reactions look. Therefore, it is appropriate to assume that the range of values for these two cases is wide enough to produce discernible differences in the aerodynamics of the two different reactions. It is also reasonable to assume that the shapes and sizes of the recirculation zones are different for these two cases. At the lower air swirl, lower azimuthal velocity and higher axial velocity are expected, which would allow a smaller recirculation zone. At the higher air swirl, higher azimuthal velocity and lower axial velocity are expected, which would give rise to a larger recirculation zone and a shorter, more intense flame. However, these are only

qualitative comparisons. To quantify the differences in air swirl, air velocity measurements must be taken, which leads to the next set of results.

8.3. Velocity Measurements

The LA measurements for non-reacting cases without the burner quarl give the following results. At the throat exit plane, both air swirl cases show very similar axial velocity readings. The velocity profiles are not unexpected. Along the center of the annulus, where the bluff body sits, the axial velocity is approximately zero because of the stagnation point induced in the wake of this obstacle in the flow. At the center of the annulus, however, the maximum axial velocity reaches 50 m/s. The surprise comes from the axial velocity plots at the plane one throat diameter downstream of the exit. The most surprising feature is that there are no negative velocities anywhere along this plane, especially along the centerline of the plane. This indicates that the recirculation zone has already closed, which means that the recirculation zone is less than 3 inches (7.6 cm) in length. If the recirculation zone were still open at this plane, then one would expect to see negative velocities along the centerline to show reverse flow of hot products being brought back into the primary combustion zone. Another interesting trait is that, overall, the higher swirl case results in lower axial velocity. This is most prominent along the centerline, where the high swirl case results in an axial velocity of 10 m/s, while axial velocity in the low swirl case is approximately twice as high – 20 m/s. The maximum axial velocity for the low swirl case is 35-40 m/s, while the maximum axial velocity for the high swirl case is 25-35 m/s. This is most probably the result of differences between the effective areas of the two swirlers. Since the effective areas of the two swirlers were not kept constant, the smaller effective area will lead to higher velocity for the same flow rate. The asymmetry of the profiles is also more noticeable at this plane.

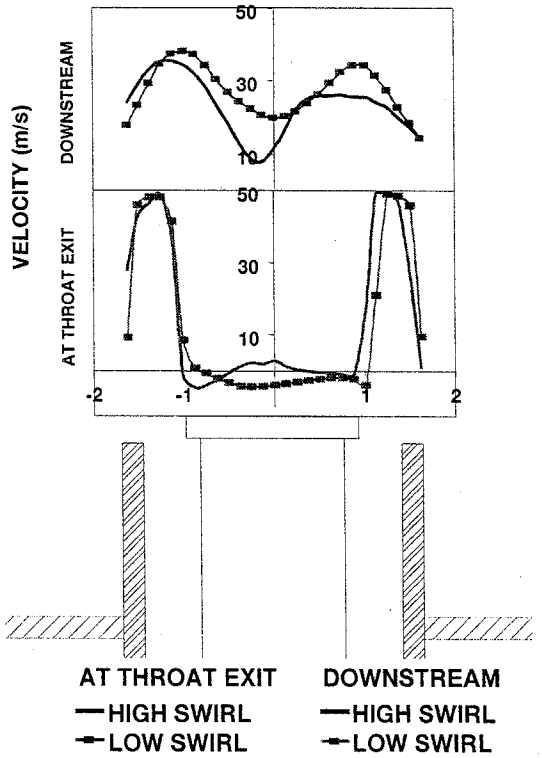

Figure 8.13: Axial Velocity Exiting the Burner at Two Planes and for Two Cases

Since the two-component velocity measurements were only taken along two orthogonal axes (X = 0 and Y = 0), all three components of velocity were obtained. The measurements taken along the X = 0 axis give the axial velocity (mentioned previously) and tangential velocity, i.e., a velocity that is tangent to the circle. The measurements taken along the Y = 0 axis provide both the axial velocity and the radial velocity. The next two figures show the plots of these data. Figure 8.14 plots the tangential velocity at both planes and for both cases. For the most part, these profiles are symmetric about the centerline. At the burner throat exit plane, the high swirl has a much greater tangential velocity than does the low swirl—25 m/s at the maximum for the former as opposed to 5 m/s at the maximum for the latter. As the air travels further away from the burner exit, the tangential velocity for the high swirl is still greater than that for the low swirl. The high swirl case has a maximum tangential velocity of 22 m/s and the low swirl case has one of 12 m/s. Figure 8.15 plots the radial velocity, also at both the exit and downstream planes and for high and low swirl cases. Overall, the radial velocities are less than the tangential velocities. At the burner throat exit plane, the high swirl case shows the greatest radial velocity along the centerline. At this plane, the radial velocity of the low swirl case along the centerline is negative.

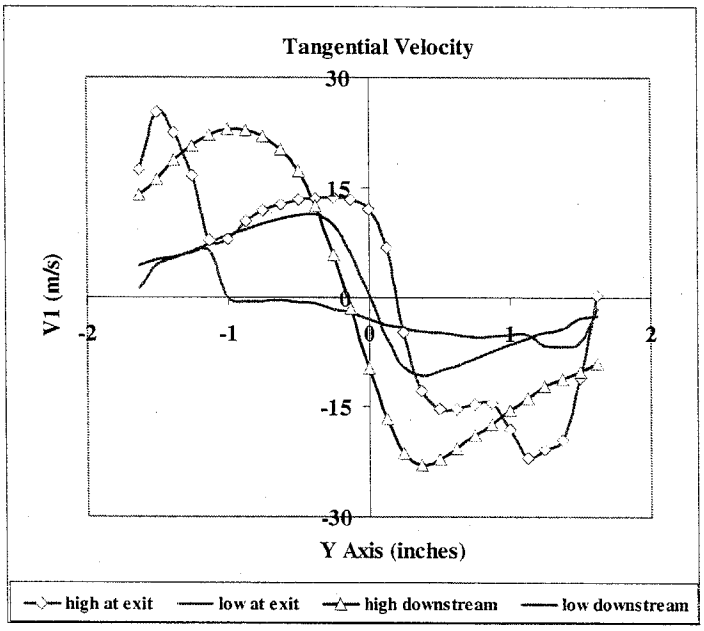

Figure 8.14: Plot of Tangential Velocity Profiles (Along X = 0 Axis)

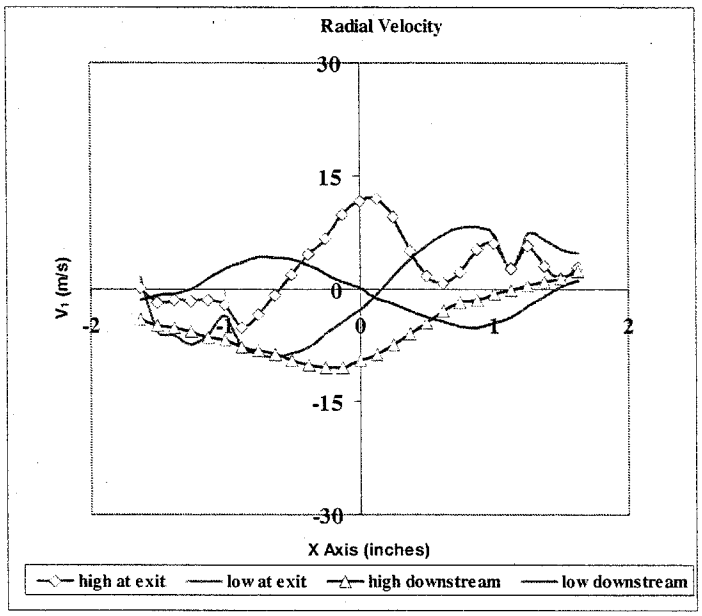

Figure 8.15: Plot of Radial Velocity Profiles (Along Y = 0 Axis)

These LA results quantify what was seen in the reaction images. Although the results were taken in non-reacting conditions without the burner quarl, the general trends for these velocities should remain the same. The plots agree with the conclusions drawn from the reaction images: noticeable differences in the aerodynamics of the burner were observed in going from one air swirler to the other. Another question that remains is whether or not the fuel injectors provide a wide enough range of values to produce different degrees of mixing.

8.4. Fuel Distribution

FID measurements of the non-reacting cases without the burner quarl also show appreciable differences in the fuel distribution of three fuel injectors. The first case has a fuel injector with 8 small counter-swirl jets and high air swirl. From the DoE results, the NO_x emission for this case is 60 ppm. Figure 8.16 is a contour plot of its fuel distribution. The average fuel concentration is 7.7 percent across the exit plane, with a 4.5 percent standard deviation. The maximum fuel concentration is 12.6 percent. Figure 8.17 is a contour plot of the fuel distribution for the second case, which includes a fuel injector with 4 large co-swirl jets with low air swirl. The NO_x emission for this case is 63 ppm. The average fuel concentration is 8.5 percent with a standard deviation of 6.1 percent and a maximum concentration in the grid of 18.6 percent. Figure 8.18 is a contour plot of the fuel distribution in the third case, where the fuel injector has 8 large radial holes and the air swirl is low. The NO_x emission from this configuration is 61 ppm. From the non-reacting FID measurements, however, the average fuel concentration at the exit of the burner is 8.2 percent with a standard deviation of 5.6 percent and a maximum of 16.7 percent. The results of the fuel distribution measurements are summarized in the following table:

Table 5-1. Summary of fuel distribution analysis

Case	NO_x (ppm)	Avg Conc (%)	St Dev (%)	Max Conc (%)
1	60	7.7	4.5	12.6
2	63	8.5	6.1	18.6
3	61	8.2	5.6	16.7

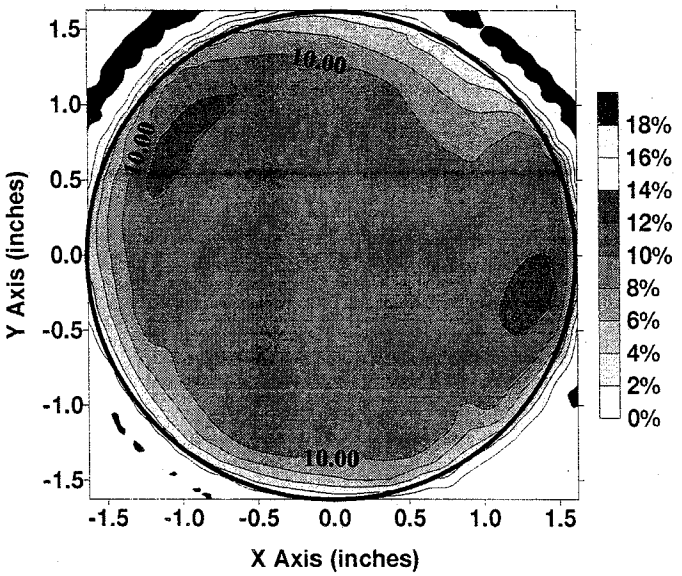

Figure 8.16: Fuel Distribution Contour for Case 1

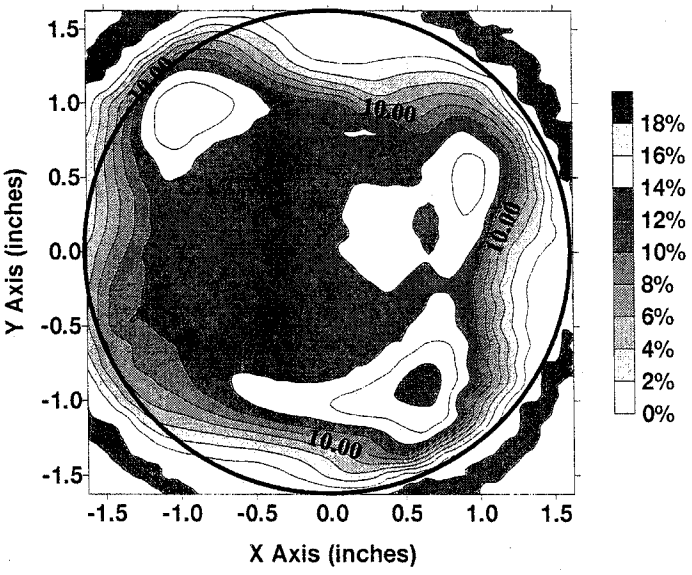

Figure 8.17: Fuel Distribution Contour for Case 2

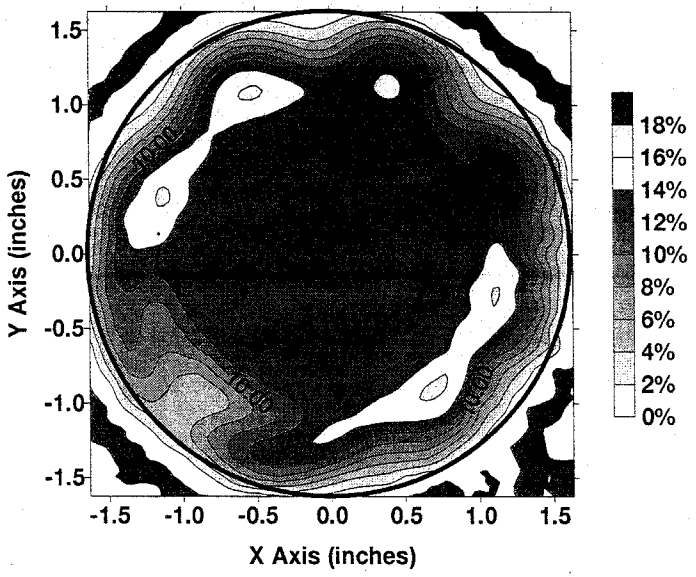

Figure 8.18: Fuel Distribution Contour for Case 3

The first case was expected to have the highest degree of mixing, which was borne out by the results. It shows the most uniform fuel distribution contour out of the three cases studied. It also has the lowest "maximum," meaning that its fuel rich pockets are more well-mixed than in the other two cases. The second case was anticipated to have the lowest degree of mixing out of these three cases. Once again, the results also support that hypothesis. The last case also did not reveal any surprises. Thus, these data show that there is sufficient variability in the fuel injection parameters to give distinct fuel distribution contours.

From the reaction photos, LA and FID measurements, differences in the reaction structure, aerodynamics and fuel distribution are evident. However, substantial variations in velocity profiles and fuel distribution do not contribute to much variation in NO_x.

8.5. Task 2B Summary

High-temperature combustion processes inherently produce very high levels of NO_x. The demands of certain processes include both high temperatures and high heat transfer rates to the charge, which cannot accommodate the application of many common methods of in-flame NO_x control because the effective methods succeed by lowering the peak reaction temperature. However more and more stringent regulations highlight the need for burners that are inherently low-NO_x producers. One solution is to design burners with geometric parameters to minimize NO_x production by optimizing the degree of fuel and air mixing.

A high-temperature furnace simulator was designed to be flexible enough to simulate many processes found in the field. After the simulator was constructed, an industrial burner was modularized to support many parametric configurations. Burner geometric parameters and their range of values were determined based on previous studies and with an industrial partner (Maxon Corporation). These geometric parameters include: tip geometry, fuel jet effective area, fuel jet injection location, air swirl, number of jets and jet swirl.

The operating conditions under which these and later tests were run simulate a high-temperature furnace application. These conditions include: 1.5 MM BTU/hr (440 kW) nominal firing rate, 3 percent furnace

O_2 content, 2000°F (1093 C) stack temperature, 0.1 to 0.3 inch H2O (0.004 psig to 0.01 psig) furnace pressure, and exhausting continuously out the rear stack.

A statistical tool for optimization called the Design of Experiments (DoE), also called multivariate studies or statistical experimental design, was applied to the system. Five DoE results show that the geometric parameters studied at the ranges that were set do not have an effect on the NO_x emissions and that the burner is robust at this operating condition with these parameters. To determine whether the ranges of the geometric parameters that were chosen differ enough to cause noticeable changes in the jet and air behavior, different diagnostic tools were applied to the burner. Reaction images from two different air swirl intensities reveal obvious differences in the length, size and intensity of the flames. Plots of the fuel distribution measurements of three different burner configurations under non-reacting conditions without the burner quarl also demonstrate the observable differences in the fuel and air mixing between these different cases. Velocity measurements of the combustion air under non-reacting conditions without the burner quarl also indicate visible differences between the air swirl produced by the two air swirlers.

9. HAZARDOUS AIR POLLUTANTS AND OZONE PRECURSORS

Measurement of air toxics was conducted to ensure that low NO_x operation was not obtained at the expense of other potentially more damaging emissions. Air toxics were measured for all three burner systems (generic, boiler, and high temperature) at different operating conditions. Details of this study are also included in Demayo (1997).

9.1. Goals and Objectives

The specific goals and objectives of this report are provided below:

- To characterize ozone precursor and air toxic emissions, specifically volatile organic compounds (VOCs), as well as total non-methane hydrocarbon emissions (TNMHCs), and fixed gases (specifically NO_x, CO, and CH_4) from the industrial, natural gas-fired stationary combustion systems operating under low-NO_x conditions,
- To determine the effect of (i) operating conditions near the lean blow-out limit, and (ii) different geometrical configurations on the formation of VOCs, TNMHCs, and fixed gases, and
- To identify whether operating conditions exist where emissions of all pollutants of concern (i.e., NO_x, CO, and VOCs) are low.

In order to achieve these goals, seven objectives were set forth:

- Determine the target compounds to measure.
- Design and construct a sampling system, based on EPA, CARB, and SCAQMD approved sampling methods.
- Identify the appropriate operating conditions to sample for the industrial burners.
- For each system, collect the VOC samples, as well as fixed gas (i.e., NO_x, CO, CO_2, O_2, and CH_4) emissions data.
- Send the samples to environmental laboratories for analysis.
- Evaluate the analytical results and attempt to identify trends and relationships between VOC emissions and (a) the various system operating conditions and geometrical configurations, and (b) other prominent compounds such as NO_x and CO.

9.2. Survey of Emissions from Natural Gas Combustion

Driven by the regulatory requirements of Title III of the CAAA and due to the ever-increasing number of natural gas-fired stationary sources, several studies have recently been conducted, looking at hazardous air pollutant (HAP) and ozone precursor (OP) emissions from natural gas combustion systems operating under fuel lean low-NO_x conditions. In this section, we briefly describe the types of sources tested and the resulting emissions. To simplify comparisons of emission concentrations, we report all levels corrected to 3% O_2.

In 1991, the ARB measured selected aromatic and halogenated VOC emissions from three natural gas-fired utility boilers (California ARB, 1991). Only benzene (1-2 ppbv) and toluene (2-3 ppbv) were consistently identified in the emissions from each of the sources. However, contamination of the sampling media prior to sampling may be responsible for the presence of toluene. NO_x emissions ranged from 87 - 241 ppmv, and CO from 0-56 ppmv.

In 1994, Carnot performed a series of air toxic emission tests on a series of gas turbines, including two utility turbines and seven industrial turbines, operating under lean conditions (Fangmeier et al., 1994a).

Only two of the sources were equipped with NO_x emission controls. At full load, benzene (1-30 ppbv), toluene (4 ppbv), and formaldehyde (3-7150 ppbv) were detected in the flue gas streams of most of the sources. In addition, the utility turbine emissions revealed trace levels of SVOCs (PAHs, PCDDs, and PCDFs), as well as very low levels of metals (i.e., Ba, Cr, Cu, Ni, Mn, and Pb). Possible sources of the metals include the fuel, the combustion air, sample contamination, and the stainless steel turbine surface, which contains Cr and Ni. NO_x varied between 200 - 600 ppmv for all sources, except those with NO_x controls which emitted levels between 90 - 120 ppmv. CO levels varied between 0 - 600 ppmv.

Again in 1994, Carnot conducted another series of HAP emission measurements on two natural gas-fired utility boilers, for varying amounts of excess air (2-10% O_2) (Fangmeier et al., 1994b). At maximum loads, benzene (1 ppbv), toluene (1-4 ppbv), formaldehyde (6-15 ppbv), trace levels of SVOCs (namely PAHs), and metals (such as Cr, Ni, V, and Cu) were detected. Possible metals sources are the fuel, the combustion air, and the boiler surfaces. NO_x levels ranged from 65-180 ppmv, and CO from 100-390 ppmv. Lastly, the excess air did not significantly impact benzene, toluene, and formaldehyde emissions.

Also in 1994, the Environmental and Energy Research Corporation undertook an extensive study to develop VOC and NO_x speciation profiles for natural gas combustion and oil refinery combustion sources (EERC, 1994). The natural gas sources tested included: a gas turbine equipped with selective catalytic reduction and a CO catalyst, a low-NO_x steam generator with exhaust gas recirculation, and a utility boiler not equipped with a NO_x pollution control device. Twenty-one of the 100 substances tested were detected. The principal VOC emissions consisted of formaldehyde (50-120 ppbv), acetaldehyde (20-70 ppbv) and acetone (10-80 ppbv) at all sources, as well as toluene (110-130 ppbv), m&p-xylenes (50-60 ppbv), hexane (330 ppbv) and phenol (180 ppbv) at some sources. Trace levels of heavier aldehydes and ketones were also detected at some of the sources. Detection limits for this study were on the order of 50 ppbv for most compounds. The gas turbine, steam generator, and utility boiler had NO_x emissions of 23, 23, and 116 ppmv, respectively.

The Combustion Research Facility at Sandia National Laboratories (Edwards et al., 1995) measured aromatic emissions (i.e., benzene, toluene, ethylbenzene and xylenes, also known as BTEX) for a research-grade, industrial-style diffusion flame burner in the Burner Engineering Research Laboratory (BERL) operating under well-controlled conditions, representative of refinery process heaters. The burner fuel consisted of refinery fuel gas, a process gas similar to natural gas, but containing higher amounts of C_2 - C_4 compounds, BTEX, and H_2. Tests under a range of firing conditions only yielded toluene (< 3 ppbv).

The company SCEC, located in Orange CA, has tested several natural gas-fired systems in Orange County, CA (SCEC, 1996). One source test of an internal combustion engine used for power generation looked specifically for aldehyde and halocarbon emissions. Results yielded formaldehyde (250 ppbv), acetaldehyde (35 ppbv), acrolein (4 ppbv), and, surprisingly, trace amounts (<20 ppbv) of 1,1,1-trichloroethane, perchloroethylene, and methylene chloride. Another HAP source test of two utility boilers revealed at high fire only aldehyde emissions, i.e., formaldehyde (300 ppbv) and acetaldehyde (30 ppbv).

The findings of this literature survey are summarized in Table 9.1.

Table 9.1. OP and HAP Emissions from Selected Fuel Lean Gas-Fired Combustion Systems.

COMPOUND	CONCENTRATION (ppbv @ 3% O_2)				
	Utility Boiler	Gas Turbine	Steam Generator	Internal Combustion Engine	BERL
Benzene	1-2 (ARB) 1 (Carnot)	1-30 (Carnot)	ND/NM[a]	ND/NM	ND/NM
Toluene	2-3 (ARB) 1-4 (Carnot)	4 (Carnot) 130 (EERC)	110 (EERC)	ND/NM	0-3 (Sandia CRF)
m & p-Xylenes	ND/NM	50 (EERC)	60 (EERC)	ND/NM	ND/NM
Formaldehyde	6-15 (Carnot) 60 (EERC) 300 (SCEC)	3-7150 (Carnot) 120 (EERC)	50 (EERC)	250 (SCEC)	ND/NM
Acetaldehyde	30 (EERC) 30 (SCEC)	70 (EERC)	20 (EERC)	35 (SCEC)	ND/NM
Acrolein	30 (EERC)	ND/NM	ND/NM	4 (SCEC)	ND/NM
Ketones and Heavier Aldehydes	0-10 (EERC)	ND/NM	ND/NM	ND/NM	ND/NM
Acetone	10 (EERC)	20 (EERC)	80 (EERC)	ND/NM	ND/NM
Halocarbons	ND/NM	ND/NM	ND/NM	0- 20 (SCEC)	ND/NM
Hexane	ND/NM	ND/NM	330 (EERC)	ND/NM	ND/NM
Phenol	ND/NM	ND/NM	180 (EERC)	ND/NM	ND/NM
SVOCs	Trace (Carnot)	Trace (Carnot)	ND/NM	ND/NM	ND/NM
Metals	Trace (Carnot)	Trace (Carnot)	ND/NM	ND/NM	ND/NM

[a] Not detected or not measured.

9.3. Selection of Target Compounds

The compounds of interest are the species which pose a health effect directly or through transformation in the atmosphere. As a result, the selected species considered were either ozone precursors (OPs) or hazardous air pollutants (HAPs). With over 60 OPs and 188 HAPs designated by the EPA, monitoring all these pollutants would require the use of a myriad of sample collection and analysis methods, the time and financial requirements of which were beyond the scope of this study. Hence, a target list of OPs and HAPs was selected based on two principal criteria, namely:

1) Potential for emission, based on theory, previous studies, and discussions with the ARB and SCAQMD, and

2) Sampling and analytical requirements.

The initial list of the volatile and semi-volatile organics included in the list of OPs and HAPs was narrowed down according to the discussions in the previous sections, which suggest possible emissions of lighter paraffins, olefins, and acetylenes (i.e., alkynes), aromatics (i.e., BTEX), aldehydes (i.e.,

formaldehyde, acetaldehyde, and acrolein), trace amounts of PAHs (i.e., anthracene, naphthalene), and even halocarbons. After further meetings with experts at the SCAQMD and given that this study is only a preliminary survey for potentially more detailed future studies, it was decided to measure only non-chlorinated VOCs, specifically all the VOCs included on the OP list, some of which also fall under the HAPs definition. Focusing on VOCs allows collection and analysis of almost all compounds using the same methods. Although the VVOCs (i.e., aldehydes) require different sampling and analysis methods, these were included due to their important contribution to overall OP and HAP emissions. The previous studies and the outcome of the meetings with agency officials indicate that SVOCs likely do not contribute significantly to the overall OP and HAP emission profile. As a result, and because SVOC sampling and analysis is much more complex and susceptible to field contamination, SVOCs were omitted from this study.

The target analytes are listed in Table 9.2. The chemicals are separated and classified into categories based on molecular structure, namely paraffins (i.e., alkanes and cycloalkanes), olefins (i.e., alkenes and cycloalkenes), alkynes, aromatics (also known as arenes), and aldehydes. The total number of compounds targeted in this study are 76 nonpolar VOCs and 2 carbonyls.

In addition to the OPs and HAPs, TNMHC and the principle "fixed gases" that constitute the matrix of natural gas combustion exhaust were also measured. The fixed gases consist of certain criteria pollutants, including NO_x, CO, and CO_2, and principle gases, including O_2 and CH_4.

9.4. Approach

To achieve the goals described in Section 9.1, the required tasks were as follows:

Task 1: Determine which compounds to measure, by conducting a survey of previous studies on OP and HAP emissions from natural gas combustion and discussing the topic with experts from the SCAQMD and the ARB.

Task 2: Design and construct a sampling system at the University of California Irvine Combustion Laboratory (UCICL), based on EPA, ARB, and SCAQMD approved sampling methods. Various sampling technique options were studied and the selection was based on discussions with the SCAQMD and the ARB staff, including on-site demonstrations and participation in the use of their source sampling systems.

Task 3: Decide which natural gas-fired sources to test. The actual systems selected include a scaled boiler burner, a model industrial low-NO_x burner, and a high temperature burner simulating VOC incineration and heating applications.

Task 4: Identify the appropriate operating conditions and geometrical configurations under which to sample, how many tests to conduct for each system, and how many samples to collect for each test. This decision was based on the on the particular design or application issue whose effect on OP and HAP emissions we wanted to study. Thus, for the low-NO_x burners, operating conditions such as excess air and fuel-air mixing were varied to simulate low-NO_x control strategy. For the high temperature burner, geometrical and operating parameters (e.g., stack position and furnace temperature) were changed to simulate the VOC incineration and process heating applications. This task also involved implementing a quality control protocol to ensure data reliability.

Task 5: For each system, collect the VOC samples using the VOC sampling train and measure the concentrations of the fixed gases (specifically NO_x, CO, CO_2, O_2, and CH_4) using an existing continuous emissions sampling system.

Task 6: Analyze the samples through independent environmental laboratories. Selection of the appropriate analysis laboratories was made based on the ability of the lab to conduct all the necessary analyses, reputation, convenience, and cost.

Table 9.2: Target Analytes

ALKANES (PARAFFINS)	ALKENES (OLEFINS)	ALKYNES	AROMATICS	ALDEHYDES
ethane (2)[a]	ethylene (2)	acetylene (2)	benzene (6)	formaldehyde (1)
propane (3)	propylene (3)	methylacetylene (3)	toluene (7)	acetaldehyde (2)
n-butane (4)	trichloroethylene (2)	dimethylacetylene (4)	ethylbenzene (8)	
isobutane (4)	isobutylene (4)	ethylacetylene (4)	m-xylene (8)	
2,2-dimethylpropane (5)	1-butene (4)		p-xylene (8)	
n-pentane (5)	1,3-butadiene (4)		o-xylene (8)	
isopentane (5)	trans-2-butene (4)		styrene (8)	
cyclopentane (5)	cis-2-butene (4)		cumene (9)	
n-hexane[b] (6)	1-pentene (5)		n-propylbenzene (9)	
2,2-dimethylbutane (6)	2-methyl-1-butene (5)		m-ethyltoluene (9)	
2,3-dimethylbutane (6)	isoprene (5)		o-ethyltoluene (9)	
2-methylpentane (6)	trans-2-pentene (5)		p-ethyltoluene (9)	
3-methylpentane (6)	cis-2-pentene (5)		1,3,5-trimethylbenzene (9)	
methylcyclopentane (6)	cyclopentene (5)		1,2,4-trimethylbenzene (9)	
cyclohexane (6)	1-hexene (6)		p-cymene (10)	
n-heptane (7)	trans-2-hexene (6)		1,4-diethylbenzene (10)	
2,3-dimethylpentane (7)	cis-2-hexene (6)		n-butylbenzene (10)	
2,4-dimethylpentane (7)	2-methyl-2-butene (6)			
2-methylhexane (7)	methyl tert-butyl ether (MTBE) (6)			
3-methylhexane (7)	4-methyl-1-pentene (6)			
methylcyclohexane (7)	2-methyl-2-pentene (6)			
n-octane (8)	1-heptene (7)			
isooctane (8)	1-octene (8)			
2,2,4-trimethylpentane (8)	1-nonene (9)			
2,3,4-trimethylpentane (8)	α-pinene (10)			
2,4-dimethylhexane (8)	β-pinene (10)			
2-methylheptane (8)				
n-nonane (9)				
n-decane (10)				

[a] The number in parenthesis refers to the number of carbon atoms in the compound.
[b] All highlighted compounds indicate compounds that are included in *both* the OP and HAP lists.

9.5. Experiment

9.5.1. VOC Sampling Train

The VOC sampling train consists of two main sections. The first section collects VOCs into a SUMMA canister, and the second adsorbs aldehydes onto DNPH cartridges. The equipment is mounted on a mobile cart, allowing the flexibility to conveniently position it according to the needs of each source test.

A dual-headed parallel diaphragm pump, located downstream of the DNPH cartridges and water dropout, draws the sample from the heated Teflon line at approximately 4 L/min, through a 6.4 mm (0.25") heated stainless steel tube. A heated 6.4 mm (0.25") Teflon tube branches off the main line into a pre-evacuated 6 L SUMMA passivated stainless steel canister into which all target OPs and HAPs, except aldehydes, are collected. The connecting lines as short as possible to minimize internal surface area and system residence time. The canisters, most of which were rented from Performance Analytical Inc., one from AtmAA Inc., the others of which were borrowed from the ARB, were equipped with mass flow controllers in order to integrate the sample collection over time at a constant flow rate. The integration period varied from one hour for the boiler burner source test to two hours for the generic burner and furnace tests.

The remaining sample stream is then divided into two parallel lines, each flowing through a Waters Sep-Pak XPoSure™ Aldehyde sampler (i.e., a DNPH cartridge) at approximately 2 L/min. This flow rate was selected based on Waters' specifications, to obtain maximal adsorption while preventing excessive flows that may wash away all the DNPH solution in the cartridges. The reason for sampling two cartridges simultaneously was to provide duplicates for quality control and reproducibility. In all source tests, the samples were collected over a span of two hours, the minimum time deemed necessary to ensure a result above a 0.1 ppbv detection limit.

Following the aldehyde sampler, the gas passed through a water drop out, consisting of a sealed Erlenmeyer flask in an ice bath, then through a rotometer regulating the sample flow and finally into a dry gas meter which records the total flow through the DNPH cartridges.

A series of K-type thermocouples (TCs) were mounted at strategic locations along the sampling train to monitor the temperatures of the sampling train inlet, SUMMA canister inlets, DNPH cartridge inlets, and the dry gas meter interior. The various inlets were heated to approximately 60°C (140°F) to prevent excessive condensation between the main sampling line and the VOC sampling media (i.e., the canisters and cartridges), a distance of approximately 1.2 m (4'), while maintaining the gas stream below the maximum operating temperatures of 100°C (212°F) of the DNPH cartridges.

Before and after each source test, the integrity of the sampling system was tested by conducting a leak check and ensuring, according to USEPA Method 5 (40 CFR 60, Appendix A), that the leakage rate was less than 60 mL/min. (0.02 scfm) at a vacuum of 380 mm Hg (15 in. Hg).

9.5.2. Sampling Conditions

For each industrial burner system, certain conditions were selected. These conditions are described in the following sections.

Generic Burner

To study the mechanisms responsible for OP and HAP formation and to relate the OP and HAP emissions to previous studies of the burner's performance, five test conditions, summarized in Table 9.3, were selected. Four of the runs used the superior performance counter-swirl injector with the burner operating at different combinations of EA and S'.

Run G1 *Low EA and low S'*: this run, characterized by high NO_x and low CO, was picked to determine the effect of low mixing and high temperatures on OP and HAP emissions.

Run G2 *Low EA and high S'*: because higher swirl increases mixing and results in increased quenching of the reaction, these conditions were selected to provide an indication of the effect of quenching on OP and HAP formation.

Run G3 *High EA and low S'*: because higher EA heightens the probability of oxidation, this run was chosen to verify the effect of lean burn on aldehyde formation. This case also represents a high performance condition for the counter-swirl nozzle (i.e., low NO_x and high combustion efficiency). Hence, G3 will help indicate the potential of OP and HAP releases at a potentially optimal operating condition.

Run G4 *High EA and high S'*: characterized by a larger recirculation zone, increased mixing, and high O_2 levels, these conditions were selected to reveal the compound effect of quenching and oxidation on OP and HAP formation.

The final test (Run G5) was conducted using the poorer performance co-swirl nozzle, as a "worst-case" scenario at high EA and high *S'*, near the stability limit. Similar to run G4, this test condition was picked to help identify the combined effects of quenching, oxidation, and instability, exacerbated by poor overall efficiency and high NO_x levels, on OP and HAP emissions.

Table 9.3: Generic Burner Test Conditions

Run Condition	Run G1A	Run G1B	Run G2	Run G3	Run G4	Run G5
Swirl Intensity (S')	0.73	0.73	0.92	0.66	0.76	0.50
Excess Air (%)	5	5	5	20	20	20
Injector Type	Counter-swirl	Counter-swirl	Counter-swirl	Counter-swirl	Counter-swirl	Co-swirl
Load (Btu/hr)	100 000	100 000	100 000	100 000	100 000	100 000
Swirl Air Flow scfm)	14.2	14.2	15.7	15.5	16.3	5.7
Axial Air Flow (scfm)	2.4	2.5	0.8	3.6	2.5	13.2
Fuel Flow (scfm)	1.63	1.63	1.63	1.63	1.63	1.63

Photographs of the burner during runs G1-G3 and G5 are shown in Figure 9.1, where the five test conditions are identified on a performance map. This map shows the performance of the burner over its stability limits when using the co-swirl and counter-swirl injectors. As indicated by the markers, most of the test cases lie in regions near the lean burn stability limits of the burner. In these regions, given the distributed nature of the reaction, there exists the possibility of "localized" flame out, i.e., fuel-air pockets that do not ignite or become extinguished and result in unburned fuel emissions. Thus, one of the challenges of the test runs was to maintain the reaction while on the edge of stability.

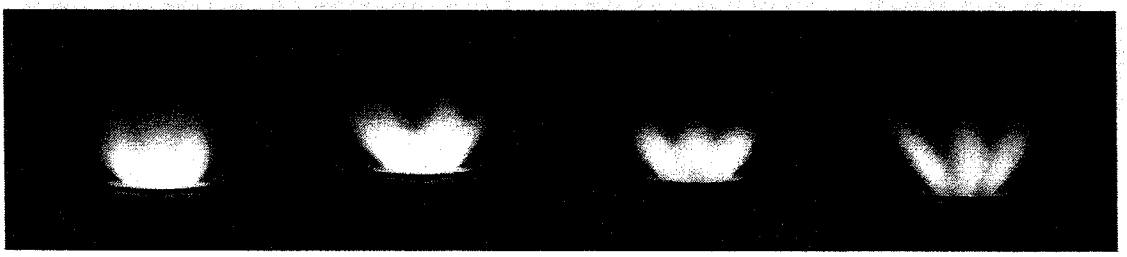

Figure 9.1: Photographs of Burner Reaction Zone Operating at Source Test Conditions

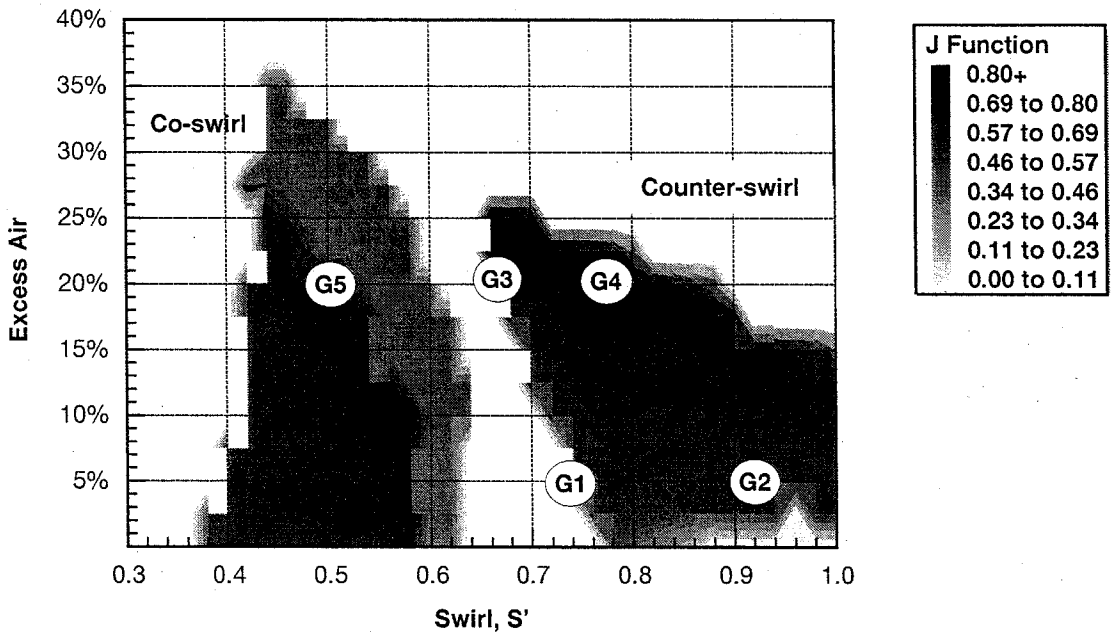

Figure 9.2: Generic Burner Performance Map
(Adapted from Miyasato and Samuelsen, 1995)

QLN Boiler Burner

The boiler burner was the first system to test. Three different operating conditions, ranging from extremely lean to stoichiometric operation, were selected. The conditions, listed in

Table 9.4, consisted of:

Run B1 *Extremely high excess air (EA)*: this condition, at the edge the burner lean blow-out limit, was chosen to investigate the effect of extremely lean operation on the formation of OPs and HAPs.

Run B2 *"Quasi-standard" EA:* this run was selected to determine OP and HAP emission levels at conditions of high performance (i.e., low NO_x levels and high combustion efficiency). At B2, the burner operates slightly leaner than the standard 3% O_2 operating region for most industrial boilers.

Run B3 *Stoichiometric*: this condition, at 0% EA, was selected as an "anchor" to test the integrity of the sampling system, since stoichiometric operation normally results in significant VOC emissions.

Table 9.4: Boiler Burner Test Conditions

Run Condition	Run B1	Run B2	Run B3
Excess Air (%)	75	45	0
Load (Btu/hr)			
1) Core	100 000	100 000	100 000
2) Radial	300 000	140 000	140 000
3) Outer	0	160 000	160 000
Base Air Flow (scfm)	76	62	62
Axial Air Flow (scfm)	32	28	1.0
Fuel Flow (scfm)	6.6	6.6	6.6
Radial Depth (in.)	0.625	0.625	0.625
Outer Depth (in.)	0.25	0.25	0.25
Throat depth (in.)	1.50	1.50	1.50
Outer Direction (°)	0	0	0
Fuel Split (%)			
1) 1ary Spuds	75	35	35
2) 2ary Spuds	0	40	40
3) Pilot	25	25	25

High Temperature Furnace

The furnace can emulate two important industrial applications:

1) *"Furnace Mode"* for industrial heating and kiln-simulation. This mode is attained by operating under adiabatic (i.e., insulated) high temperature (i.e., greater than 1100°C) conditions. Examples of high temperature heating applications include iron smelting, steel forging and reheating, carbonizing metals, aluminum production, glass making, and curing or drying mineral-based products such as bricks.

2) *"Incineration Mode"*. This mode is simulated by operating at low temperatures (i.e., 650 - 850°C) conditions, as is the case for certain important incinerator applications such as VOC incineration by regenerative thermal oxidation (RTO). RTO is a technique by which pollutant VOCs, (e.g., by-products of industrial processes such as petrochemical processing, metallic parts cleaning, manufacturing of organic chemicals, paints, solvents, and computer chips) are oxidized into CO_2 and other combustion by-products (e.g., Cl_2, HCl, and PCBs) depending on the chemical composition of the waste stream. When simulating RTO, ambient "auxiliary" air is injected downstream of the burner through ports installed in the furnace

walls at a maximal rate of 42800 L/min. (1500 scfm). In industry, RTO incinerators are also referred to as *afterburners*.

Four conditions, summarized in Table 9.5, were selected to test the furnace. Runs F1 and F2 simulated the VOC incineration mode, i.e., RTO conditions, but without the waste VOCs to be incinerated. The sampling was only for intrinsic or "background" OP and HAP emissions, resulting from the basic furnace system. These conditions, characterized by high O_2 levels and low temperatures (i.e., no insulation inside the furnace walls), have the propensity for OP and HAP formation due to oxidation and quenching. On the other hand, the injection of auxiliary air downstream through the furnace walls may increase mixing inside the furnace, thus improving combustion efficiency and helping to destroy potential OPs and HAPs. The sample was extracted from both the middle (run F1) and rear stacks (run F2) to test the uniformity of the flow fields inside the furnace. Samples exiting by the rear stack theoretically have longer residence times, which could affect the OP and HAP levels, depending on the degree of mixing, the O_2 flow fields, and the temperature distribution between the middle and rear stacks.

During runs F3 and F4, the furnace operated under adiabatic conditions, simulating the industrial heating applications. Compared to runs F1 and F2, at these conditions, temperatures were higher, O_2 levels lower, and mixing may have been decreased due to the absence of downstream auxiliary air. Thus, while higher temperatures tend to favor complete combustion and lower PIC and pollutant emissions, decreased mixing may result in an increase in OPs and HAPs. Once again, samples were taken from both the middle (run F3) and rear (run F4) stacks. In industry, batch processes tend to use the middle stack, while continuous processes would employ the rear exhaust configuration. In all cases, inlet air and fuel flows were set to operate the burner near 3% O_2.

Table 9.5: High Temperature Burner Test Conditions

Run Condition	Run F1	Run F2	Run F3	Run F4
Simulated Application (Heat Process)	RTO (diabatic)	RTO (diabatic)	High Temp. (adiabatic)	High Temp (adiabatic)
Stack	Middle	Rear	Middle	Rear
Load (MM Btu/hr)	2	2	2	2
Air Flow (scfm)	295	295	295	295
Gas Flow (scfm)	29	29	30	30
Burner Stoichiometry (% O_2)	~3	~3	~3	~3
Furnace P (in. H_2O)	0.1	0.1	0.1	0.1
Auxiliary Air (% O_2)	~17	~17	0	0
Aux. Air Injection P (in. H_2O)	0.3	0.3	0	0
Aux. Air Injection Flow (scfm)	1067	1067	0	0

9.6. Results

All concentrations were measured on a dry basis and were corrected to 3% O_2. Uncertainties of the reported values are approximately ±6% for O_2, ±2% for CO and CO_2, ±4% for NO_x, and ±0.5 ppm for CH_4. The total target VOCs were calculated as follows:

$$(\text{Target VOCs})_{\text{total}} = \sum_{i}^{N} (\text{Target VOC})_{i}$$

where i is given target VOC concentration in units of ppbC[1] and N is the total number of target VOCs detected. The non detectable (ND) levels for each of the species are provided in Appendix: Air toxics Data.

9.6.1. Generic Burner

Figure 9.3 through Figure 9.7 present the target VOC profiles for the generic burner source test. Test condition G1 yielded four reportable compounds, while G2 yielded 22, G3 four, G4 eight, and G5 fifteen. The co-swirl fuel injector case released the largest amount of VOCs (118 ppmC), while the low swirl, high EA (G3) condition emitted the least (172 ppbC). Although not on the list of target compounds, significant levels of ethanol were reported for most cases (444 ppbv for G1, 153 ppbv for G2, 0 for G3, 93 ppbv for G4, and 622 ppbv for G5). Low levels of aldehydes (i.e., mostly formaldehyde with trace levels of acetaldehyde) were detected for G1, G2, and G3, while the G4 and G5 samples contained high aldehyde concentrations.

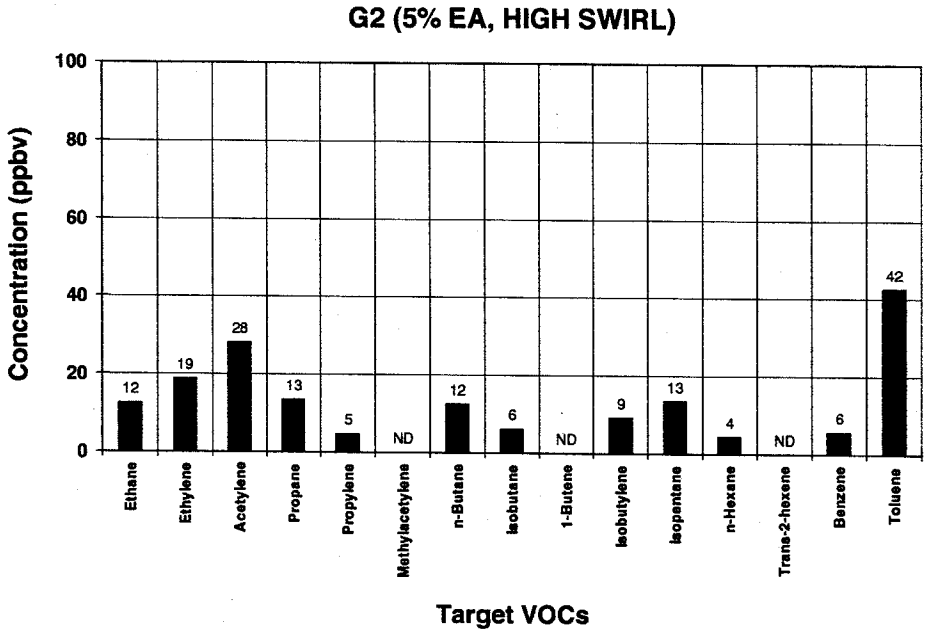

Figure 9.3: VOC Profile for Generic Burner Test G1

[1] ppbC = (volumetric concentration in ppbv) × (number of carbon atoms in compound)

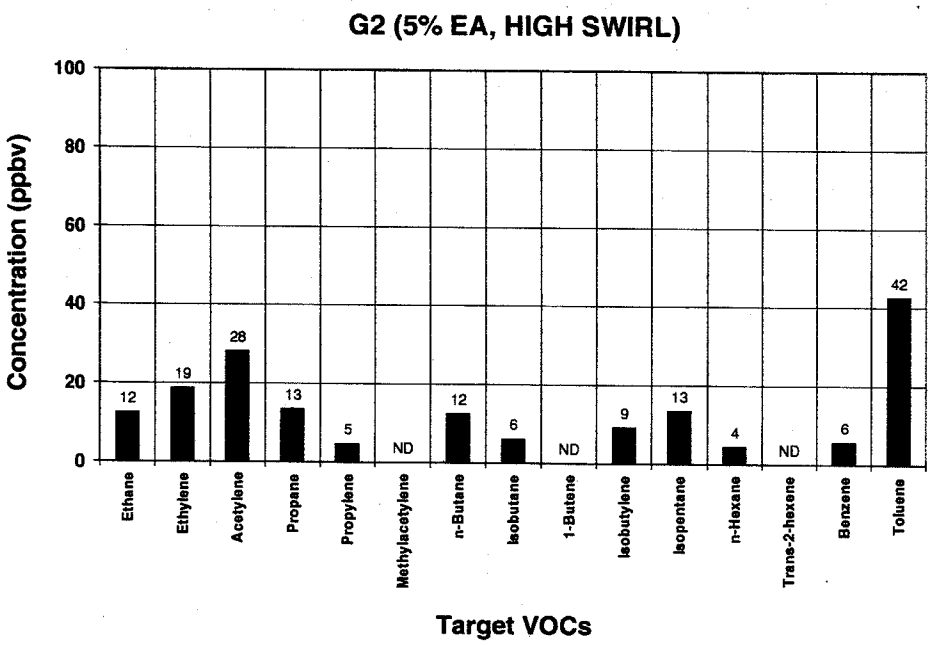

Concentrations (ppbv) of compounds not shown in the chart:

n-Pentane	8	3-Methylhexane	4
MTBE	6	n-Heptane	7
2-Methylpentane	3	Methylcyclohexane	17
3-Methylpentane	4	2,3,4-Trimethylpentane	5
Cyclohexane	6	m-Xylene	5

Figure 9.4: VOC Profile for Generic Burner Test G2

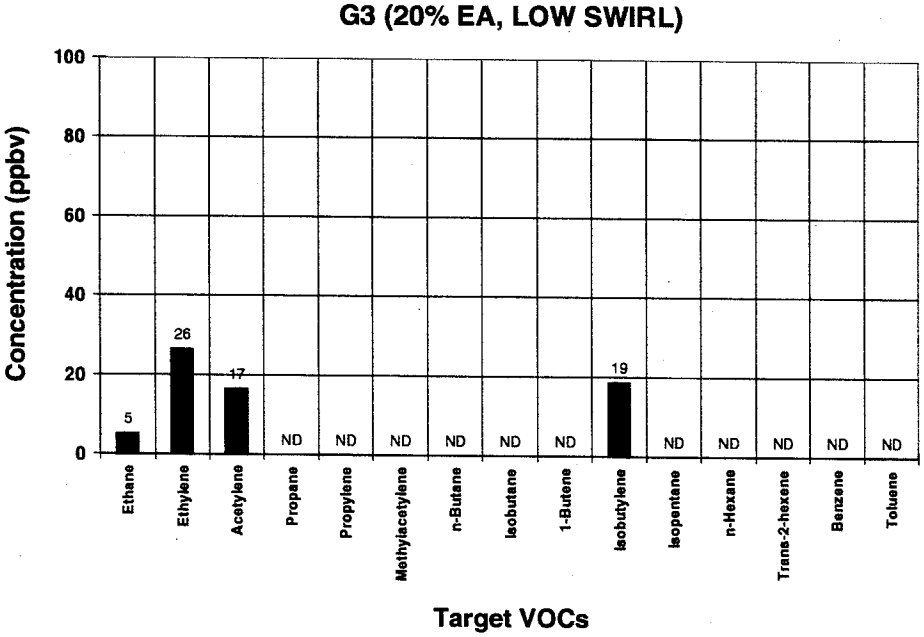

Figure 9.5: VOC Profile for Generic Burner Test G3

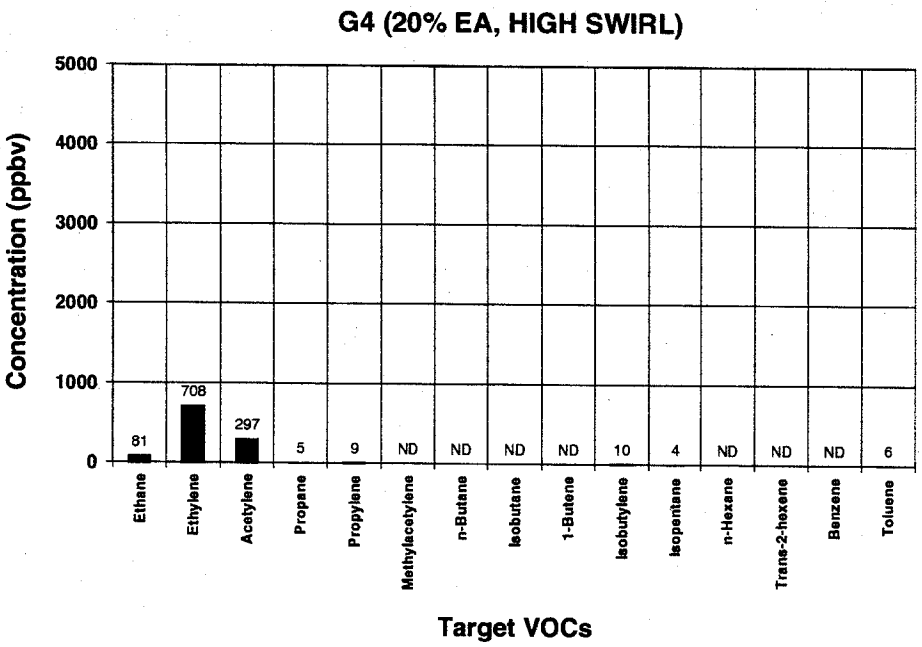

Figure 9.6: VOC Profile for Generic Burner Test G4

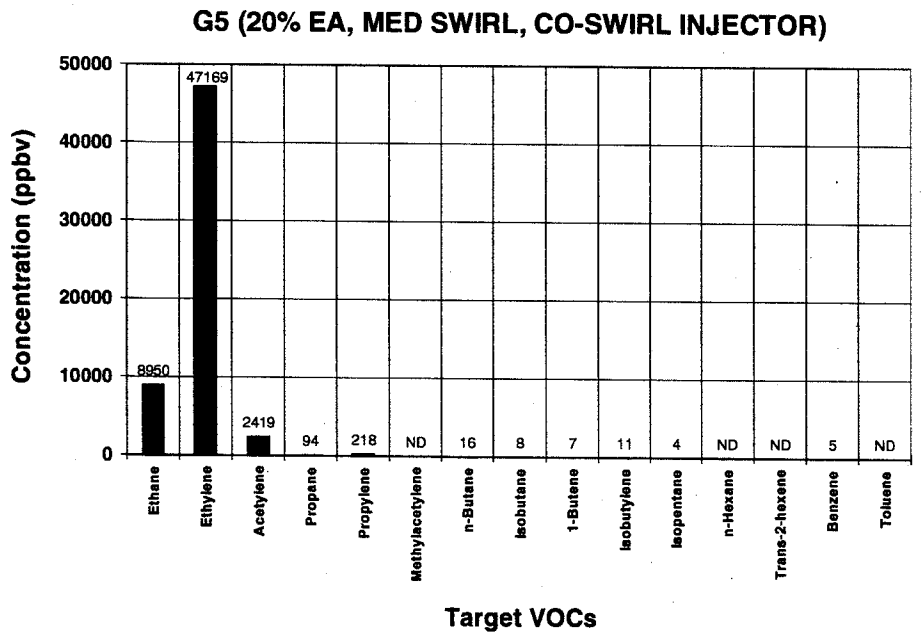

Concentrations (ppbv) of compounds not shown in the chart:

Propyne	7
1,3-Butadiene	8
2,2-Dimethylpropane	24
Styrene	13

Figure 9.7: VOC Profile for Generic Burner Test G5

9.6.2. *QLN* Boiler Burner

Figure 9.8 through Figure 9.10 show the target VOCs measured in the *QLN* burner test. The high EA case (B1) yielded five compounds with concentrations greater than the MRL. No target VOCs were found in the emissions from the 46% EA run (B2) and only benzene was found in the stoichiometric case (run B3). Low levels of aldehydes, mostly formaldehyde with trace levels of acetaldehyde, were detected for B1 and B2, while the B3 sample contained high aldehyde concentrations. The stoichiometric case released the largest amount of target VOCs (502 ppbC), and the 46% EA condition emitted the least (0 ppbC).

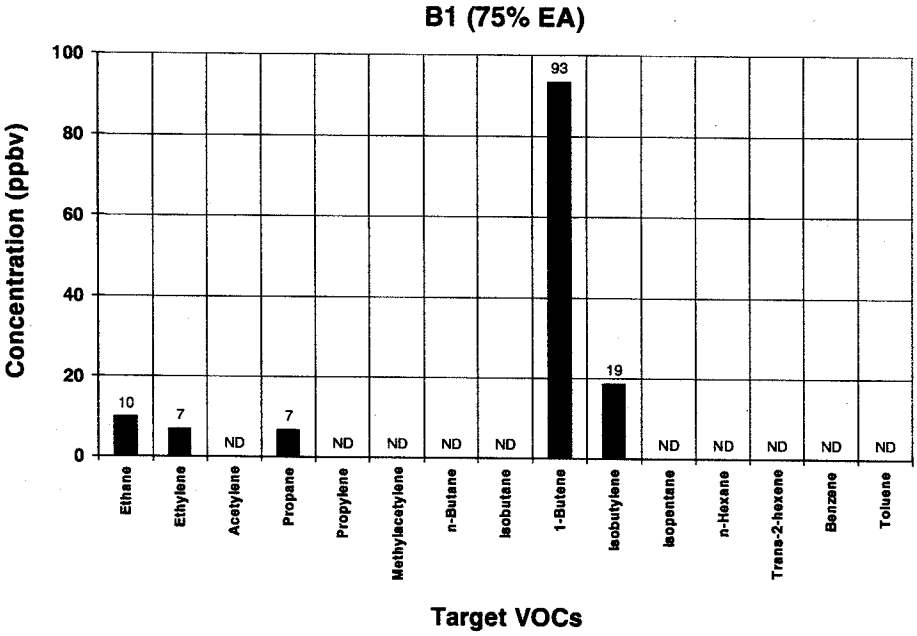

ND = Not detected

Figure 9.8: VOC Profile for Boiler Burner Test B1

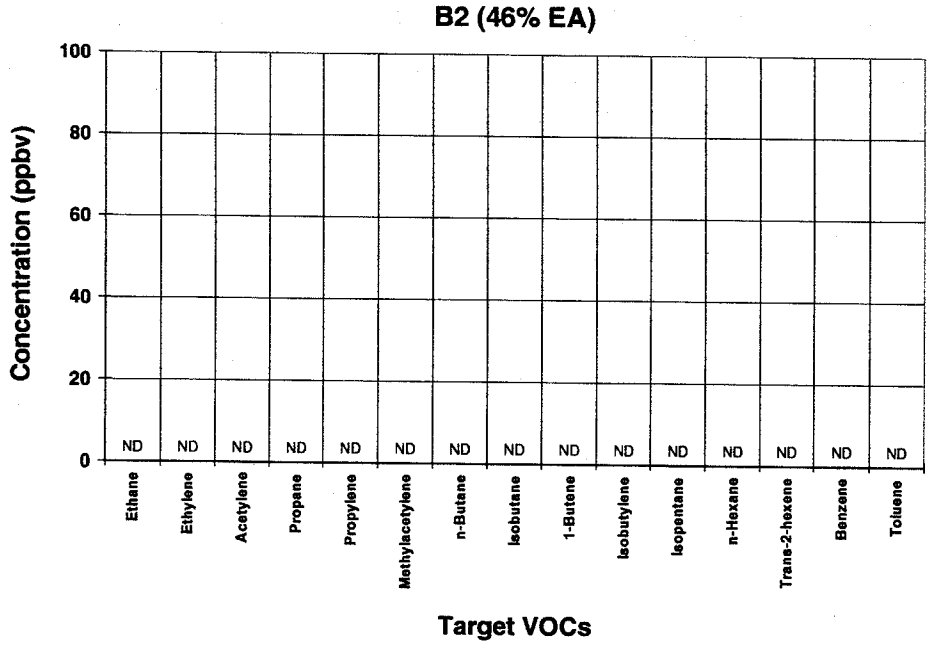

Figure 9.9: VOC Profile for Boiler Burner Test B2

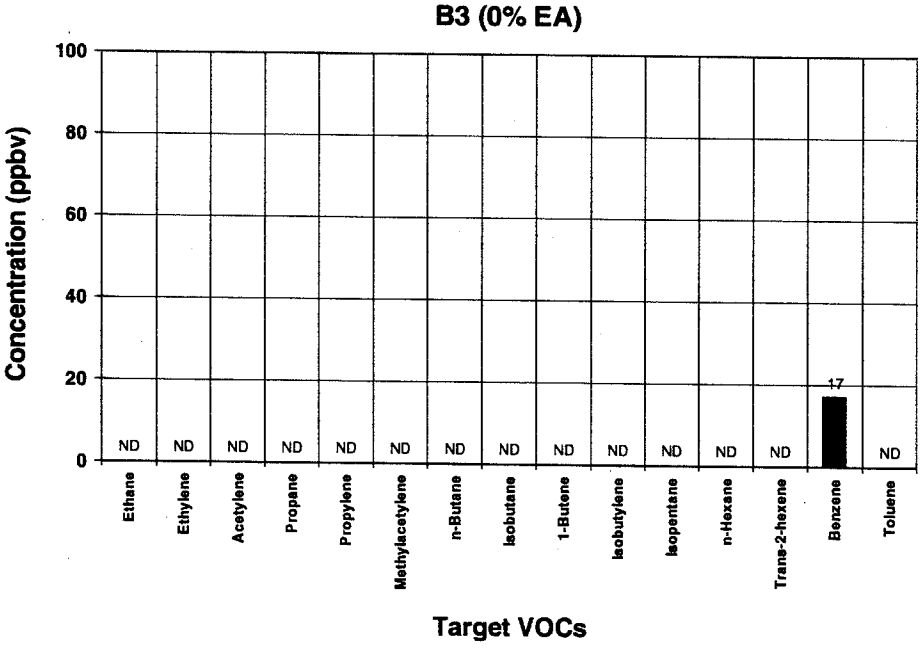

Figure 9.10: VOC Profile for Boiler Burner Test B3

9.6.3. High Temperature Furnace

Figure 9.11 through Figure 9.14 show the VOC profiles for furnace test. The VOC incineration mode tests resulted in the release of five and six reportable VOCs for the mid and rear stacks respectively.

Under furnace mode operation, six and three target VOCs for middle and rear stack positions were detected at levels greater than the MRL. High levels of aldehydes, mostly formaldehyde with trace levels of acetaldehyde, were detected for F1 and F2, while the F3 and F4 samples contained low aldehyde concentrations. The VOC incineration mode of operation emitted the largest amount of VOCs, with the middle stack (12 ppmC) releasing more than the rear stack (7 ppmC). Under furnace mode, the middle and rear stacks emitted respectively 190 ppbC and 23 ppbC of total target VOCs.

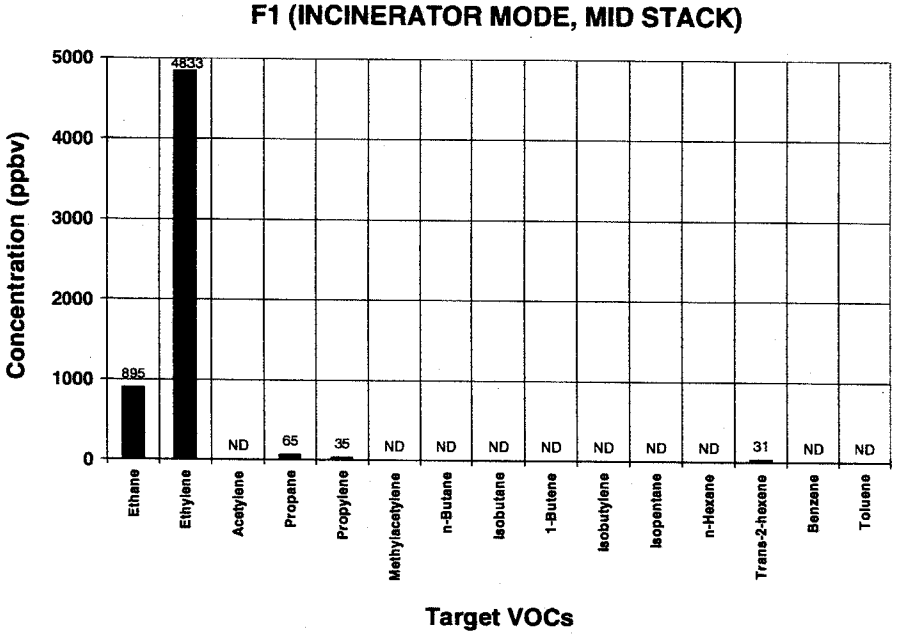

Figure 9.11: VOC Profile for High Temperature Burner Test F1

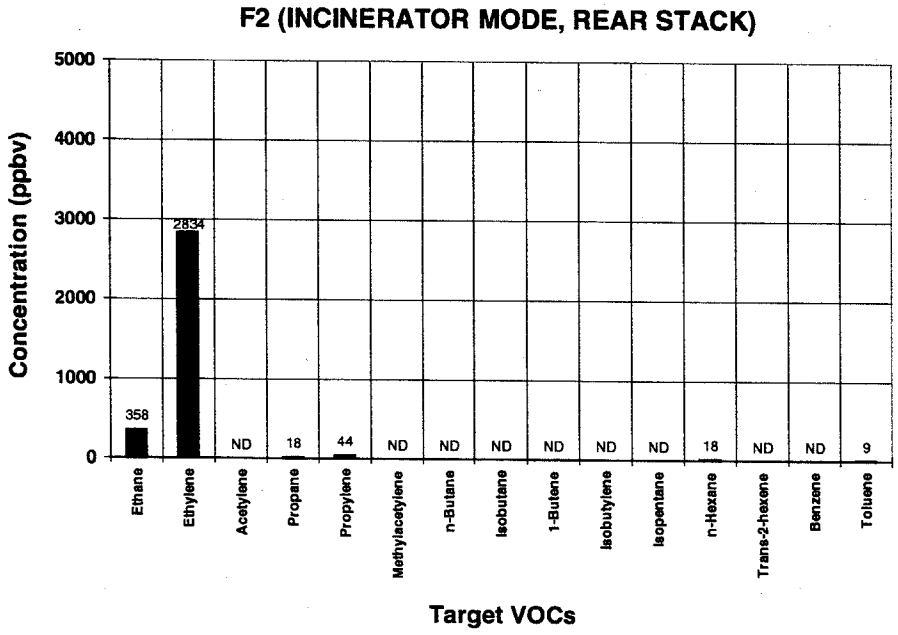

Figure 9.12: VOC Profile for High Temperature Burner Test F2

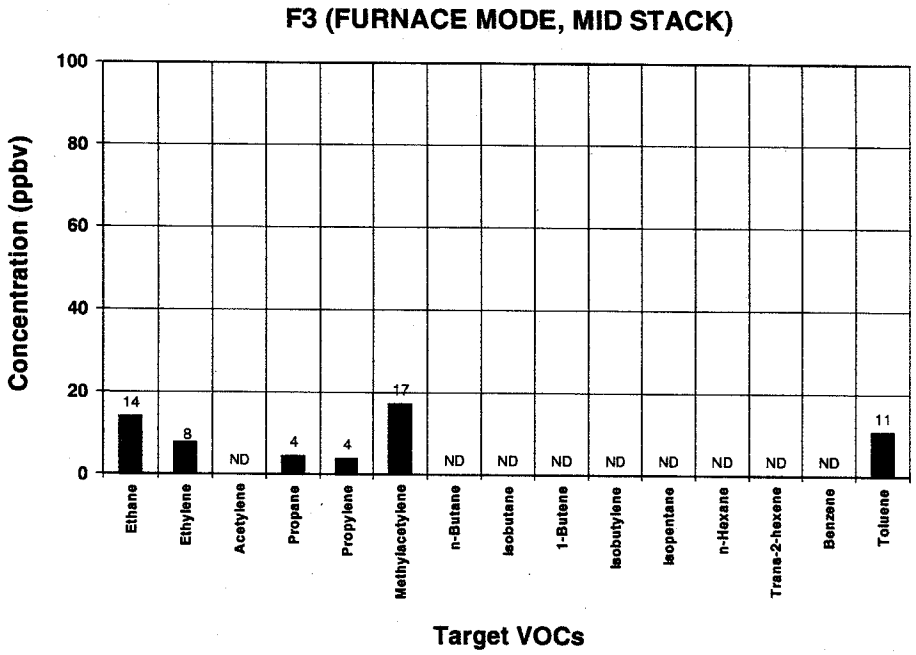

Figure 9.13: VOC Profile for High Temperature Burner Test F3

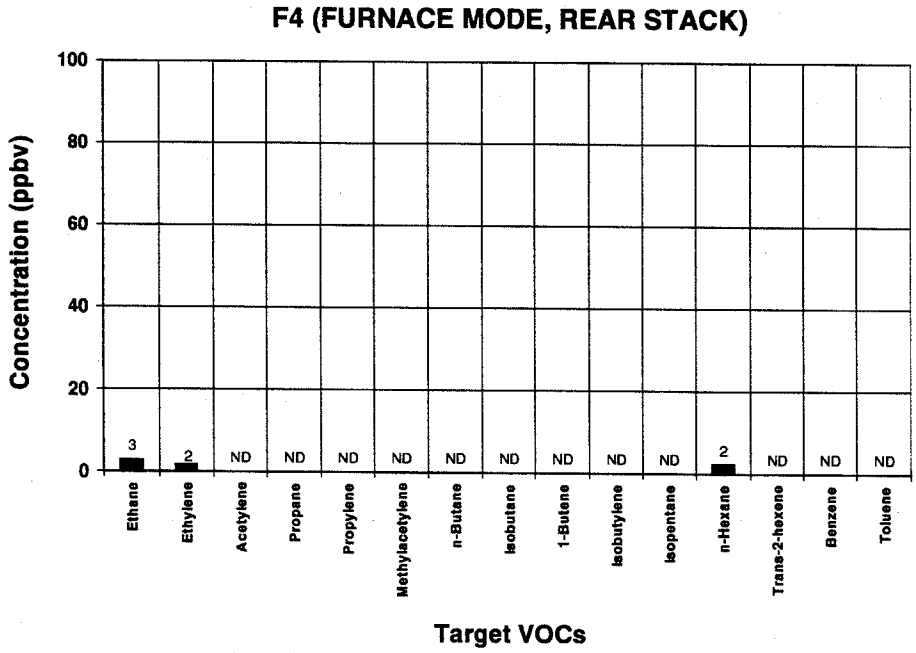

Figure 9.14: VOC Profile for High Temperature Burner Test F4

9.6.4. Natural Gas Supply

The natural gas analysis reveals that the gas supply consists of approximately 95.8% CH_4, 1.7% CO_2, 1.5% N_2, and 1% of TNMHCs (i.e., target and non-target VOCs). As shown in Figure 9.15, a total of 18 compounds were measured at reportable levels. Most of the detected VOCs consist of alkanes and cycloalkanes, as well as trace levels of toluene.

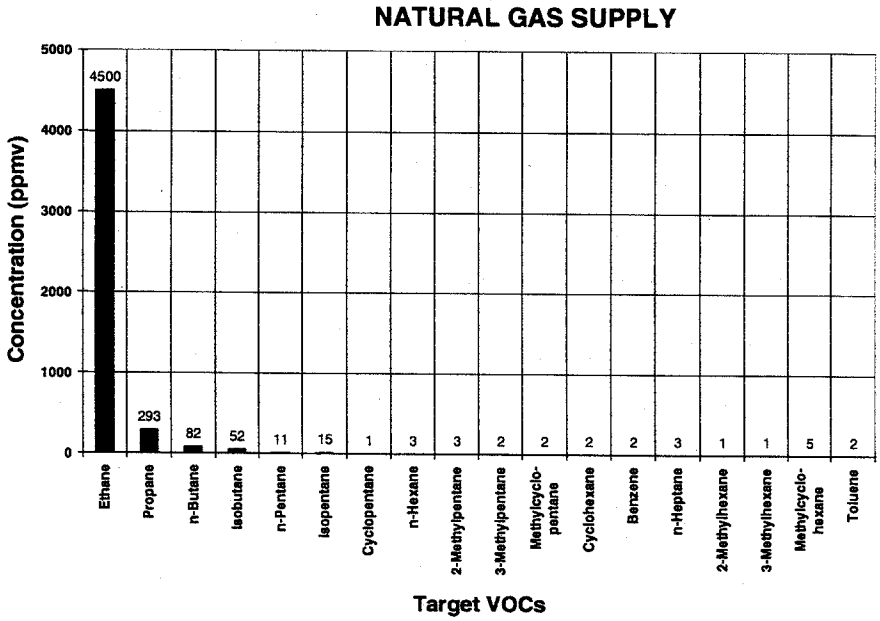

Figure 9.15: VOC Profile for Natural Gas Supply

9.6.5. Aldehydes

Due to the small concentrations of aldehydes in the exhaust emissions, the measured results can only be interpreted as qualitative. The normalized VOC and aldehyde emissions vs. CO emissions are shown in Figure 9.16 and Figure 9.17 for the generic burner and boiler burner, respectively.

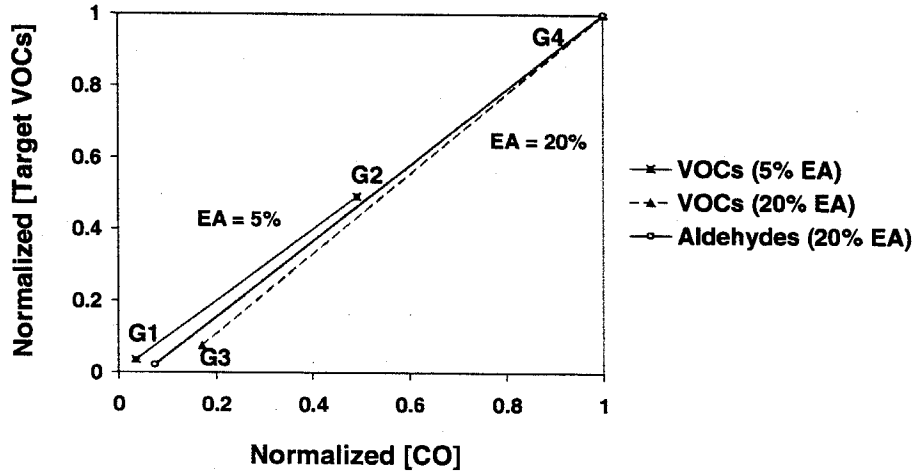

Figure 9.16: [Target VOCs] vs. [CO] for the Generic Burner

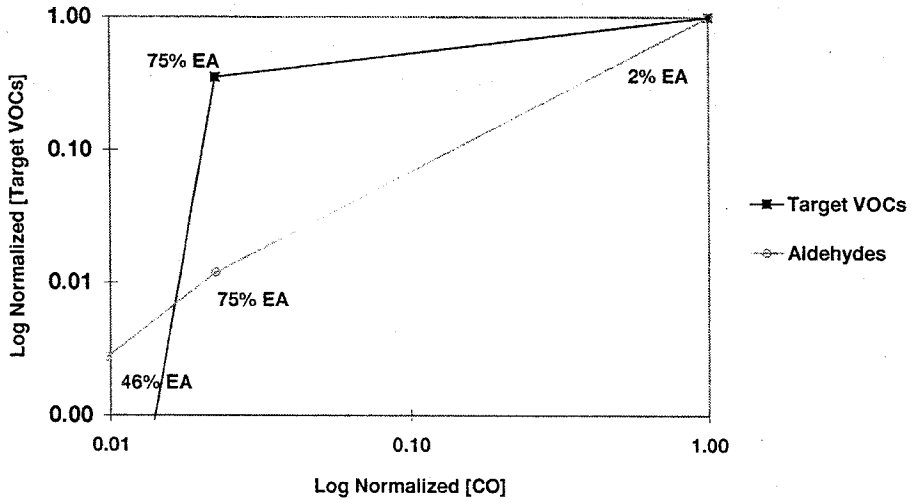

Figure 9.17: [Target VOCs] vs. [CO] for the Boiler Burner

Both burners indicate increases in VOCs and aldehydes with an increase in CO emissions. For the high excess air conditions, this can be attributed to quenching of the reaction, which can cause an increase in CO, aldehyde, and VOC emissions. For the low excess air case, the high VOC and aldehyde emissions for the boiler burner is attributed to rich pockets of the reaction and insufficient residence time at high temperatures. This type of scenario is further exemplified in the high temperature burner results for the mid-furnace stack emissions under incinerator mode operation (Figure 9.18).

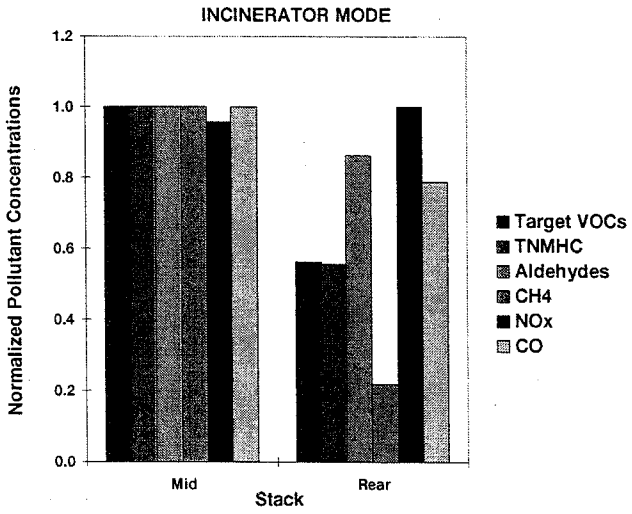

Figure 9.18: Normalized High Temperature Burner Pollutant Concentrations vs. Stack Position

In this figure, the emissions for all of the products of incomplete combustion and pollutants are higher in the mid-furnace stack case than for the rear-furnace stack case. Recall that for the incinerator mode of operation, a stream of air (simulating a VOC laden gas) is injected from the furnace walls below the flame. However, in this configuration, quenching is occurring and due to the short residence time, many of the products of incomplete combustion are escaping out the middle stack. For the rear stack, the

emissions are reduced, but there is still a large amount of aldehydes due to the quenching from the incinerator air stream.

The mechanisms for the aldehyde production are further investigated through the chemical kinetic modeling conducted at LLNL and presented in the following section.

9.6.6. Kinetic Modeling

The combustion of natural gas consists of the sequential deconstruction of the fuel molecule. Although it is generally unlikely that the small amounts of fuel components with more than 3 carbon atoms will play any significant role, especially under fuel-lean conditions, these non-methane components can affect ignition and other combustion properties of natural gas (Westbrook, 1979). As such, any reliable kinetic model for natural gas bust include the influences of the non-methane components. One current model with considerable validation is the GRI-Mech model (Smith, et al., 1999), which as been developed to model the oxidation of natural gas, and this model is quite generally adequate. The model used for this study, similar to GRI-Mech, has been used in recent modeling studies of hydrocabon oxidation (Curran, et al., 1998).

The main reactions of the most important constituent of natural gas, methane (CH_4), are the removal (abstraction) of a single H atom by an attacking radical species (e.g., O, OH, HO_2, H, etc.) to produce methyl (CH_3) radicals. These then often react with OH radicals to produce methoxy radicals (CH_3O) and H atoms, followed by the decomposition of the methoxy to yield formaldehyde (CH_2O), one of the most significant air toxic species and one which often has a comparatively high concentration in natural gas exhaust. Under optimal conditions, formaldehyde is rapidly consumed, primarily by removal of another H atom by another radical species, producing formyl (HCO) radicals which then decompose to produce carbon monoxide (CO), another air toxic species also commonly emitted from natural gas combustors. The final reaction step converts CO to CO_2, ending the sequence of reactions from fuel to product.

From this sequence, it should be clear that the most normal, straightforward oxidation of methane cannot avoid production of air toxic intermediates, which under optimal, desirable conditions are rapidly consumed, with the net result being only carbon dioxide. However, when something adverse occurs and the overall oxidation reaction is not permitted to complete itself, the residuals of incomplete combustion can consist of air toxic species.

Frequently, the adverse situation consists of having a combustion residence time that is too short to complete the full sequence of oxidation reaction steps. The residence time depends sensitively on the reaction temperatures, since the rates of most of the elementary reactions in the sequence are strongly dependent on temperature. Thus, when the reaction temperature is steadily reduced, for example by addition of diluents or excess air, then the required residence time becomes longer and often results in increased toxic emissions.

An illustration of the points above is shown in Figure 9.19, in which the starting conditions were natural gas and air, with 5% excess air. As stated in section 5.4.2 Chemical Kinetics, the simulation used incorporates a steady flow reactor with sufficient heat transfer to keep the chemical contents at a constant temperature. This type of model allows specification of characteristic time scales and investigation of the residence time affect on the reaction evolution. Models of this type have been widely used to describe and understand the kinetics of pollutant production and emissions from combustion systems (Pitz, et al., 1994; Seebold, et al., 1992; Pitz, et al., 1993). The conditions selected for the calculation were a constant temperature of 2000°F which was selected based on the detailed streamline measurements provided in section 6.2.1 Burner Exit Flowfield. The species concentrations evolve in time, and the major species in the computed results include the major air toxic species measured in the experiments, especially CO, formaldehyde (CH_2O) and acetaldehyde (CH_3CHO).

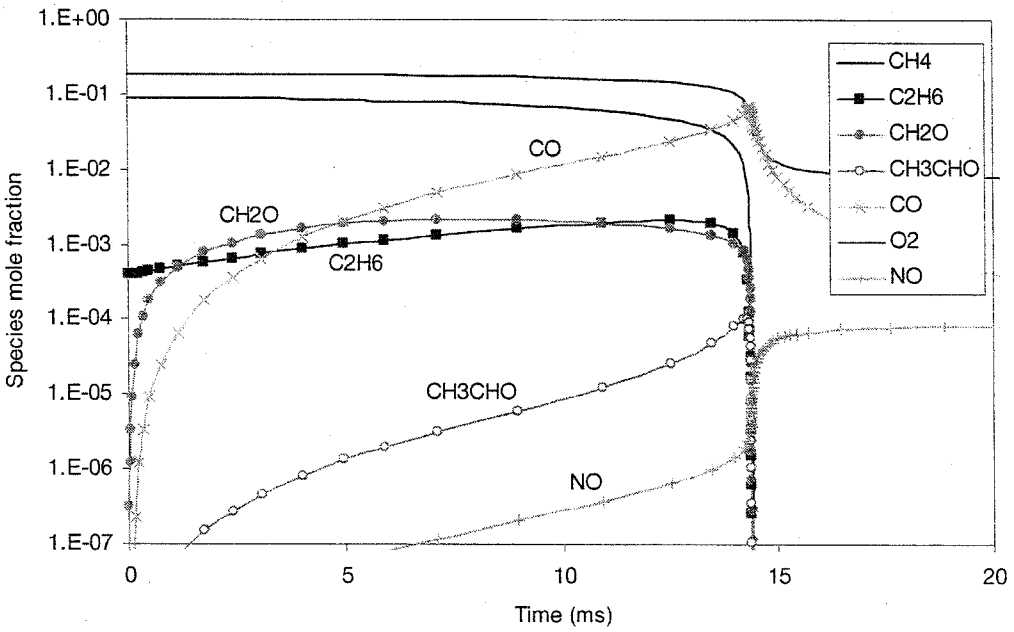

Figure 9.19: Chemical Kinetic Modeling Results at 5% Excess Air and 2000°F

This figure exemplifies the need for an adequate residence time for the reaction to complete. If the reaction is stopped (quenched) prior to the requisite time at high temperature, there is the potential for the intermediate species to be emitted, namely formaldehyde, acetaldehyde, carbon monoxide, and even ethane. A similar modeling result is presented in Figure 9.20, which also shows the combined effect of lower reaction temperature.

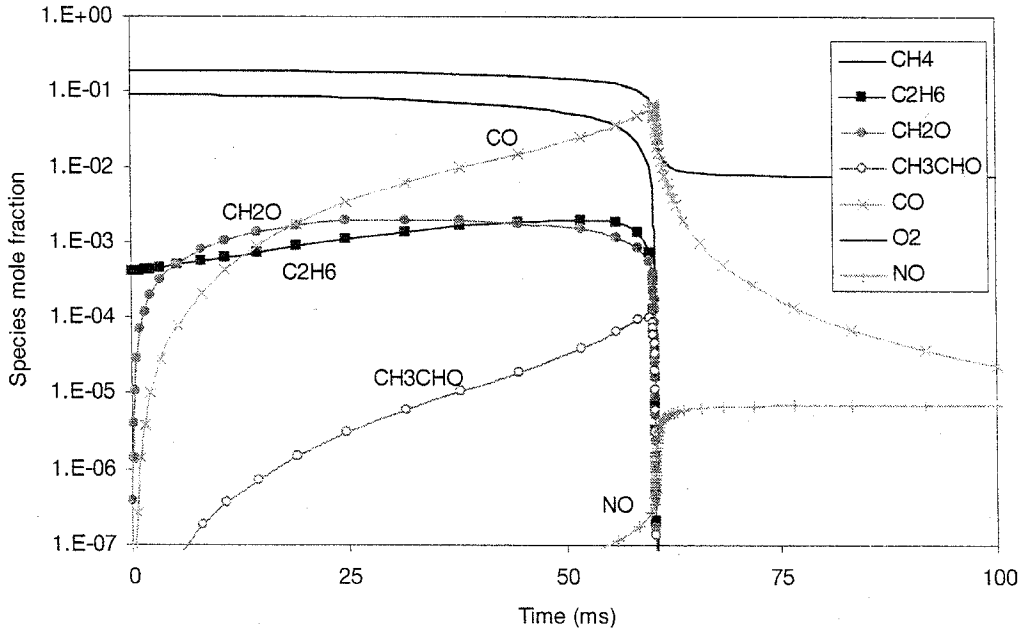

Figure 9.20: Chemical Kinetic Modeling Results at 5% Excess Air and 1800°F

The residence time required at this lower temperature is over four times longer, illustrating the characteristic of higher CO, aldehyde, and VOC emissions under conditions where temperatures are reduced, e.g., higher excess air levels, high amounts of internal FGR, or high velocity shear regions.

9.7. Summary

In this study, selected natural gas-fired systems at the UCI Combustion Laboratory, including a low-NO_x burner for boiler applications, a scaled low-NO_x generic industrial burner, a commercial, high temperature burner, and a gas turbine combustor, were evaluated for ozone precursor and air toxic emissions, specifically for 76 nonpolar VOCs and two polar aldehydes.

The three gas-fired units and the test conditions were chosen based on current, critical issues in the design and application of advanced natural gas combustion systems. Operating parameters (i.e., excess air and fuel-air mixing) of the low-NO_x burners were selected to reflect lean burn low-NO_x strategies with operation on the edge of stability. Geometric parameters on the furnace (i.e., operating temperature and stack position) were identified to simulate two important applications, i.e., VOC incineration and process heating.

To carry out the source tests, a sampling system was designed and constructed, based on EPA, CARB, and SCAQMD sampling methods. Major combustion by-products were analyzed in-house on the UCICL Continuous Emissions Sampling System. The VOCs were collected into passivated SUMMA canisters, while aldehydes were sampled onto DNPH cartridges. Both private and government laboratories analyzed the samples. Combining these measurements with numerical modeling of the reaction yields numerous observations that allow a better understanding of the nature of, causes of, and potential risk due to OP and HAP releases from natural gas combustion systems.

9.7.1. VOC Profiles

A comparison of the VOC profile of the natural gas supply with the VOCs measured from the various sources tested reveals that, depending on the test case, the combustion process results in total, partial, and even zero destruction of the target VOCs, as well as in the generation of new compounds. In general, the VOC emissions included mainly lighter (C_2 - C_6) alkanes, alkenes and alkynes, aromatics (i.e., benzene and toluene), and aldehydes (i.e., formaldehyde and acetaldehyde). Previous studies of natural gas-fired sources (see section 9.2 Survey of Emissions from Natural Gas Combustion) only found significant levels of aldehydes, as well as trace amounts of toluene and benzene. Of the other compounds included in the list of target compounds, only C_2 and C_3 compounds, hexane, and xylene were identified in previous studies.

In agreement with these studies, most concentrations of individual compounds were low (< 100 ppbv). However, certain "stressed", i.e., very lean conditions with cooler reactions such as for test runs B1, G4, G5, F1, and F2 generated high levels of some compounds, attaining a maximum of 93 ppbv (of 1-butene) for the boiler burner in run B1, 47 ppmv (of ethylene) for the generic burner in run G5, and 4.8 ppmv (also of ethylene) for the high temperature burner in run F1. The runs with the highest total target VOC emissions for each source are B3 (502 ppbC), G5 (118 ppmC), and F1 (12 ppmC).

Overall, the boiler burner emitted the least amount of total target VOCs (0 - 500 ppbC), followed by the generic burner with the counter-swirl fuel injector (80 - 2307 ppbC), and the high temperature burner (23 - 11910 ppbC). The emissions of NO_x were lowest for the both the boiler burner (19 - 25 ppm) and the generic burner with counter-swirl injector (16 - 51 ppm) and highest for the high temperature burner (73 - 82 ppm). The levels of CO displayed wide variations for all the burners: 30 - 3018 ppm for the boiler burner, 17 - 2298 ppm for the generic burner, and 15 - 573 ppm for the high temperature burner.

9.7.2. Boiler Burner

Only the 75% and 2% EA cases (B1 and B3) yielded reportable levels of target VOCs. In run B1, these compounds consisted of alkanes (i.e., ethane and propane) and alkenes (i.e., ethylene, isobutylene, and 1-butene). The presence of alkanes, the dominant hydrocarbon class in the natural gas supply (i.e., from ethane through isopentane), indicates the likelihood of unburned fuel packets in the emission gases. The alkenes in the emission gases may have resulted from the pyrolytic dehydrogenation of the corresponding alkanes. All of the higher aliphatics (> C_5) and most of the aromatics contained in the gas supply, with the exception of benzene (run B3), underwent complete destruction. Aldehydes were detected under all three test conditions, thus showing evidence of partial oxidation of the alkanes into carbonyls.

9.7.3. Generic Burner

In the case of the generic burner, as was found with the boiler burner results, the samples contain significant levels of alkanes (C_2 - C_5) suggesting evidence of unburned fuel. Only in the G2 case did trace amounts of heavier VOCs (C_7's, C_8's, xylene) appear, possibly due to excessive quenching that resulted from the high swirl intensity. Probably as a result of pyrolytic dehydrogenation of the dominant alkanes, substantial quantities of alkenes (especially ethylene, propylene, and isobutylene) and alkynes (especially acetylene) are formed, none of which were detected in the natural gas supply. As in the case of the boiler burner, the definite presence of aldehydes in all test cases suggests that alkanes are oxidized into carbonyls, particularly at the high EA test condition.

9.7.4. High Temperature Burner

Similar to the boiler and generic burner results, the samples from the high temperature burner test contained mainly alkanes (i.e., ethane, propane, and n-hexane), showing evidence of unburned gas. Alkenes (i.e., ethylene, propylene, and trans-2-hexene) and alkynes (i.e., methylacetylene), which may have formed by pyrolytic dehydrogenation, were also present. Aromatics were only detected in two cases (F2 and F3). Aldehydes were only detected in reportable quantities for the VOC incineration mode runs (F1 and F2), probably due to the high O_2 levels and high quenching rates in these runs, which create conditions favorable to the oxidation of alkanes into aldehydes.

9.7.5. HAPs and OPs Conclusions

In the case of all four systems, the test conditions produced emission profiles, ranging from complete combustion to various stages of partial combustion. The analytical speciation results of exhaust stream products yield evidence of:

- Complete destruction of most target VOCs, especially of heavier compounds (> C_5)
- Unburned fuel (i.e., mainly C_1 - C_5 alkanes with traces of aromatics)
- Pyrolytic dehydrogenation of alkanes into alkenes (especially ethylene, propylene, 1-butene, and isobutylene) and alkynes (especially acetylene),
- Synthesis of aromatics, namely benzene and toluene, and
- Oxidation of aliphatics into aldehydes, mainly formaldehyde and acetaldehyde, and even into ethanol as found in the generic burner results.

In agreement with the findings of previous studies, most of the target VOCs detected in this project were present in low concentrations (< 100 ppbv). However, certain "stressed" test conditions, i.e., the very lean, turbulent, or cooler reactions, generated high levels of some compounds, especially ethylene (~5 ppmv for the high temperature burner test and ~50 ppmv for the generic burner test). In addition to high

emission levels, certain stressed conditions also produced a large number of target VOC emissions. For example, in one run during the generic burner test (G2) 22 compounds were detected. These results show that certain stressed runs generate high amounts of a limited number of target VOCs, while others release numerous target VOCs but at lower concentrations. The general trend and cause for these "stressed" conditions were verified using chemical kinetic modeling of the reaction at different temperatures.

Overall, the boiler burner emitted the least amount of target VOCs (~0 - 500 ppbC), followed by the generic burner equipped with the counter-swirl fuel injector (~100 - 2300 ppbC), and lastly, by the high temperature burner (~20 - 11900 ppbC).

10. TASK 3 – SUPPORT TO PRACTICAL APPLICATIONS

Support to the industrial burner demonstrations is evidenced in two significant outcomes of this program. Each of the interactions with the burner manufacturers has evolved into a commercial development. The two different systems are described in the following sections.

10.1. Maxon Interaction

The first is the commercial launch of a burner system by Maxon Corporation called the *SmartFire* system which the UCICL helped in the initial demonstration testing. This burner system uses a feed-forward control algorithm to maintain the burner fuel and air flows within pre-ordained parameters for pollution control. The system schematic is shown in Figure 10.1. The emissions monitoring is done beforehand such that setpoints for the fuel and air are determined for the specific application. This scenario is exactly what is done at UCI for active control program testing. A performance map is generated (e.g., Figure 6.30) for experimental reasons such that we know if the active control program actually reaches an optimum. Maxon has taken this strategy and preprogrammed their *SmartFire* burner to go automatically to these areas of high performance based on the performance maps.

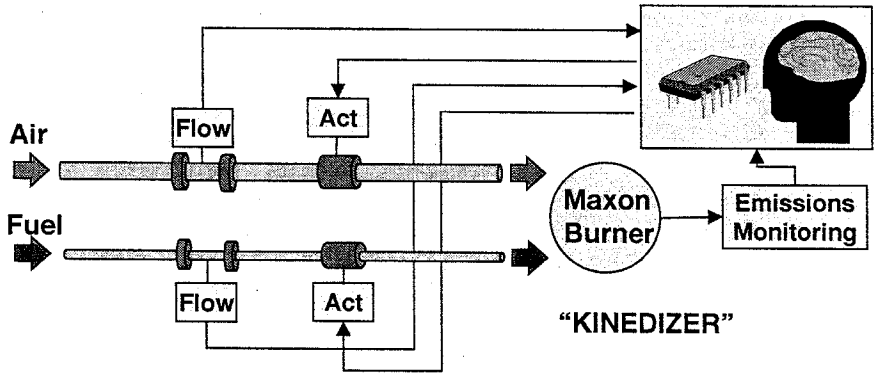

Figure 10.1: Maxon *SmartFire* System

Conceptually straightforward yet advanced in terms of burner control, the *SmartFire* system has been a success for Maxon. A potential drawback of this type of system is that the control cannot compensate for changes in the system such as hardware degradation, fuel composition, or humidity, etc. Hence the need for *active* control instead of "feedforward" or "lookup table" control.

10.2. Coen Interaction

The burner design utilized for the UCICL experiments was the *QLN*, a current commercial burner design offered by Coen. This burner uses partial fuel-air premixing and fuel staging to reduce NO_x emissions. A rendering of the Coen burner from their sales literature is shown in Figure 10.2. The measurements conducted on the scaled model of this burner, including emissions and design of experiments, helped Coen conduct internal CFD modeling of the burner to establish possible emissions gains that could be made. Images of the modeling are shown in Figure 10.3 for temperature and NO_x distributions based on the UCICL data.

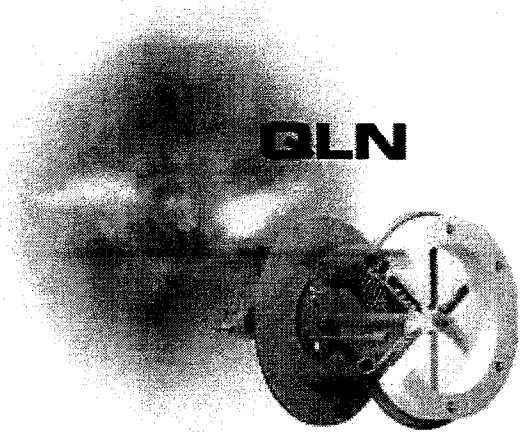

Figure 10.2: Coen *QLN* Low NO_x Burner

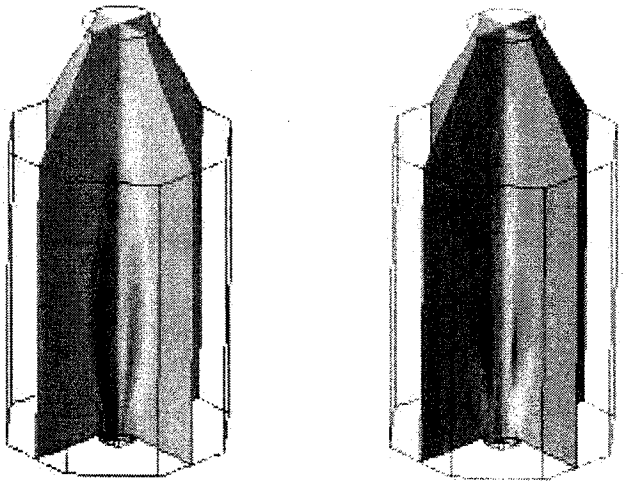

Figure 10.3: Coen *QLN* Modeling of UCICL Optical Furnace

Based on these models and the verification using the detailed data provided, Coen can better predict and design future burners. An outcome of this process has been Coen's determination that this model staged burner could not achieve the ultra-low NO_x levels desired. As a result, different burner designs are being pursued for this market. The *QLN*, however, still plays a major role in the low NO_x burner market. Furthermore, work and collaboration are continuing with Coen toward the application of active control on their low NO_x burners.

11. SUMMARY

The major findings for each task are outlined in the following sections.

11.1. Task 1: Support Research and Technology Development

The support research and technology development task examined the pollutant formation mechanisms in a generic, model industrial burner. Fuel and air mixing processes were examined in detail to determine their effect on the burner performance. Stack emissions measurements were collected to determine global emissions. From these data, specific conditions of good and bad performance were identified for detailed measurements. These measurements included velocity, temperature, and species distributions inside the burner flowfield as well as inside the burner throat; computational fluid dynamic modeling was also used as a tool to aid in the fuel-air mixing studies. The two dominating factors affecting NO_x and CO emissions were found to be initial fuel and air mixing and the extent of internal flue gas recirculation. Both factors were found to be optimized for the counter-swirl fuel injector at 20% excess air and S'=0.66. Furthermore, the optimal condition occurred very near the stability limit, indicating the need for active control of the combustion process to maintain the burner at high performance without blowoff. A final major finding was that a perfectly premixed system was not the optimal solution since the high performance region was reduced compared to the counter-swirl performance.

Using this mechanistic understanding, the active control methodology was further developed. Since the fuel and air mixing were demonstrated to affect and control the performance, the fuel and air delivery were modified to be computer/algorithm controlled. The active control program was modified in several areas to take advantage of improved computer processing advancements and make future upgrades and changes more user friendly. These modifications included adoption of new data acquisition software and hardware, a modular coding environment, adoption of a new cost function, and application to a real industrial burner design (Coen *QLN*). The modified active control program was successfully demonstrated on the model Coen *QLN* burner. The active control methodology and mechanistic understanding garnered during the Task 1 phase set the groundwork for the industrial burner testing that followed in Task 2.

11.2. Task 2: Industrial Burner Simulator Development

Two different burner investigations were conducted to aid in the development of industrial boiler burners and high temperature burners. The boiler burner investigations were conducted on the Coen *QLN* design and the high temperature burner investigations were on the Maxon *Kinedizer* design. Both burner investigations relied on the statistical design of experiments (DoE) methodology to determine the factors most affecting the emissions. Based on the Task 1 findings, fuel and air mixing and internal flue gas recirculation aspects were targeted. For both burner designs, stack emissions were the responses measured using the DoE; promising designs were then selected for detailed measurements.

11.2.1. *QLN* Boiler Burner

A specific geometric configuration was identified as the optimum for the *QLN* burner. This condition has a longer throat depth (1.50 inches) and 5% fuel staging at 15% excess air. Detailed measurements were conducted for this optimized condition and a poor performing configuration which had a slightly shorter throat depth (1.125 inches), less fuel staging, and the same excess air. Laser anemometry measurements determined that optimized configuration exhibited much greater central recirculation, inducing higher amounts of internal FGR and thereby providing better NO_x control. In-situ species measurements and

subsequent local equivalence ratio calculations also determined that the optimized configuration provided leaner local equivalence ratios further upstream than the poor condition, indicating faster fuel and air mixing.

11.2.2. *Kinedizer* High Temperature Burner

For the high temperature burner investigations, similar fuel injection iterations as with the generic burner were fabricated to determine their effect on NO_x and CO emissions. A DoE matrix was constructed and the data were collected. For this burner system, however, no clear factors (fuel delivery or swirl intensity) were found to produce statistically significant effects on NO_x or CO despite visual differences in the reaction shape. In order to understand the flowfields better and gain insight into the robust nature of this burner design, non-reacting laser anemometry and fuel distribution measurements were taken at the burner throat. Despite differences in the fuel distribution, the velocity profiles and NO_x emissions showed little variation. It is suspected that the long, insulated refractory quarl expansion allows sufficient time and high temperatures to override any mixing gains normally attributed to low NO_x. Furthermore, since the furnace enclosure is so large in comparison to the boiler burner enclosure, significant internal flue gas recirculation does not occur, again limiting the effect of this parameter on NO_x control.

11.2.3. HAPs and OPs Measurements

In order to ensure that low NO_x or high performance operation was not produced at the expense of increased air toxics emissions, measurements of hazardous air pollutants (HAPs) and ozone precursors (OPs) were conducted for the generic model burner, boiler burner, and high temperature burner. Due to the very small concentrations involved and large number of air toxics, a new sampling system was designed and a subset of species targeted based on EPA, SCAQMD, and CARB guidelines. The results for the different systems indicate potential for high HAPs and OPs emissions, especially under high excess air conditions, with high quenching rates; this finding was further verified through chemical kinetic modeling. Overall, the boiler burner emitted the least amount of total target VOCs (0 - 500 ppbC), followed by the generic burner with the counter-swirl fuel injector (80 - 2307 ppbC). The high temperature burner released the highest amount of VOCs (23 - 11910 ppbC) when operating at incineration mode (middle stack and high excess air).

11.3. Task 3: Support to Practical Applications

The UCICL worked with the industrial partners on two commercial product developments, specifically the initial testing and design concept for the Maxon *SmartFire* system, and the detailed measurements for predictive modeling for the Coen *QLN* burner. Both interactions provided measurements and design inputs necessary for the industrial manufacturers to make product decisions for current and new hardware. Work and interaction with both industrial partners are planned to continue and incorporate the active control methodology to commercial burner systems.

11.4. Major Products and Contributions

The major products and contributions for the program are outlined below. Each task produced several key findings which allowed further research and interaction.

Task 1

- Developed a better understanding of NO_x and CO formation processes in industrial burners.
- Developed the methodology for conducting such complex investigations.
- Established that perfectly premixed systems may not be the best performing in terms of emissions and stability and that fuel and air mixing can control emissions performance.
- Upgraded the active control methodology with better software, data acquisition hardware, programming structure, and improved cost function.
- Demonstrated the upgraded active control system on an industrial burner (Coen *QLN*).

Task 2

- Determined controlling parameters affecting NO_x and CO for a boiler burner and high temperature burner.
- Demonstrated effectiveness of statistical tool called design of experiments (DoE) for optimizing industrial burner hardware configurations.
- Provided data for burner manufacturers to use in present/future burner designs (see Task 3).

Task 3

- Provided input for design and testing of two commercial burner systems: Maxon SmartFire system and the Coen *QLN* burner.
- Established interaction and protocols for working with industrial partners with goal of commercializing research findings.

A final major product of this program has been the research support for five graduate students. Four students received their Master of Science degrees and one student completed his Doctor of Philosophy degree through funding provided in part by this program.

12. REFERENCES

A. F. Ali A-Shaikhly, G. E. Andrews, and C. O. Aniagolu, "Jet Shear Layer Turbulent Diffusion Flames for Ultralow NOx Emissions." *Journal of Engineering for Gas Turbines and Power/Transactions of the ASME*, vol. 114, 1992. pp. 55-62.

K. M. Bentley and S. F. Jelinek, "NO_x Control Technology for Boilers Fired with Natural Gas or Oil." *Tappi Journal*, v(April), 1989. pp. 123–128.

G. E. P. Box, W. G. Hunter, and J. S. Hunter, *Statistics for Experimenters. An Introduction to Design, Data Analysis, and Model Building.* Wiley Series in Probability and Mathematical Statistics. John Wiley and Sons, 1978.

D. S. Brouwer, "Characterization and Design Optimization of a Scaled, UltraLow-NOx Burner." University of California, Irvine, Master of Science Thesis, 1996.

California Air Resources Board, "Draft of 1995 Emission Inventory." http://www.arb.ca.gov, CARB, 1997

California Air Resources Board, *Emissions Tests on Natural Gas-Fired Utility Boilers at Three Power Plants.* Engineering Evaluation Branch, Monitoring and Laboratory Division, Sacramento, CA. 1991

A. Chang, "Optimization of a Natural Gas-Fired Burner through the Application of Statistical Experimental Design and Analysis." University of California, Irvine. Master of Science Thesis, 1998.

H. J. Curran, P. Gaffuri, W. J. Pitz, C. K. Westbrook, "A Comprehensive Modeling Study of n-Heptane Oxidation." *Combustion and Flame*, v.114, 1998. pp. 149–177

T. N. Demayo, "Air Toxic and Ozone Precursor Emissions From Natural Gas-Fired Stationary Sources." University of California, Irvine. Master of Science Thesis, 1997.

F. Durst, A. Melling, and J. H. Whitelaw, *Principles and Practive of Laser-Doppler Anemometry.* Academic Press, New York, NY, 1976.

A. C. Eckbreth, *Laser Diagnostics for Combustion Temperature and Species.* Energy and Engineering Science Series, ed. A. K. G. a. D. G. Lilley. Abacus Press, Cambridge, MA, 1988.

C. Edwards, "Investigation of Spray Flame Structure in a Near-Axisymmetric, Optical Access Research Furnace," in *Collected Papers in Heat Transfer*, K. T. Yang, Editor. 1988, ASME, Chicago, Illinois. pp. 99–110.

C. Edwards, and P. J. Goix. "Effect of Fuel Gas Composition and Excess Air on VOC Emissions and Flame Structure of a Small-Scale Industrial Burner." *1995 International Symposium of the American Flame Research Committe*, California, USA. 1995.

Energy and Environmental Research Corporation (EERC). *NO_x and VOC Species Profiles for Gas Fired Stationary Combustion Sources.* Vol. 1. Report prepared for the California Air Resources Board by EERC. Irvine, CA, 1994.

B. Fangmeier, R. Himes, M. McDannel, R. Lott, and B. Toole-O'Neil. "A Summary of Air Toxic Emissions from Natural Gas-Fired Combustion Turbines." *AFRC/JFRC Pacific Rim International Conference on Environmental Control of Combustion Processes*. Maui, Hawaii, October 1994a.

B. Fangmeier, M. McDannel, and B. Toole-O'Neil. "Hazardous Air Pollutant Emissions from Natural Gas-Fired Utility Boilers." Carnot/EPRI internal report. Carnot, Tustin, CA. 1994b

D. Feikema, R. H. Chen, and J. F. Driscoll, "Enhancement of Flame Blowout Limits by the Use of Swirl." *Combustion and Flame*, v80, 1990. pp. 183–195.

Federal Register, Code of Federal Regulations, Title 40: Protection of Environment, Part 60 - Standards of Performance for New Stationary Sources. Vol. 60. Office of the Federal Register, Washington, D. C., 1996.

J. P. Gore and N. J. Zhan, "NOx Emission and Major Species Concentrations in Partially Premixed Laminar Methane/Air Co-flow Jet Flames." *Combustion and Flame*, v105, 1996. pp. 414–427.

J. P. Holman, *Experimental Methods of Engineers*. 4th Edition ed. McGraw-Hill, New York, NY, 1984.

R. K. Hanson, J. M. Seitzman, and P. H. Paul, "Planar Laser-Fluorescence Imaging of Combustion Gases." *Applied Physics B.*, v50, 1990. pp. 441–454.

T. K. Kim, B. J. Alder, N. M. Laurendeau, and J. P. Gore, "Exhaust and In-situ Measurements of Nitric Oxide for Laminar Partially Premixed C2H6–Air Flames: Effect of Premixing Level at Constant Fuel Flowrate." *Combustion Science and Technology*, v110–111, 1995. pp. 361–378.

A. Lozano, B. Yip, and R. K. Hanson, "Acetone: A Tracer for Concentration Measurements in Gaseous Flows by Planar Laser-Induced Fluorescence." *Experiments in Fluids*, v13, 1992. pp. 369-376.

J. R. Maughan, R. E. Warren, A. K. Tolpadi, and T. P. Roloff, "Effect of Initial Fuel Distribution and Subsequent Mixing on Emissions From lean, Premixed Flames." *ASME International Gas Turbine and Aeroengine Congress and Exposition*, Cologne, Germany. 1992.

M. M. Miyasato, "The Influence of Fuel and Air Mixing on NOx Production in a Model Natural Gas Burner." University of California, Irvine, Master of Science Thesis, 1993.

M. M. Miyasato, "The Effect of Rapid Jet Mixing on Emissions in a Model Industrial, Natural Gas Burner." University of California, Irvine, Doctor of Philosophy Dissertation, 1998.

S. V. Patankar, Numerical Heat Transfer and Fluid Flow. *Series in Computational Methods in Mechanics and Thermal Sciences*. McGraw-Hill, New York, NY, 1980.

W. J. Pitz, C. K. Westbrook, A. E. Lutz, and R. J. Kee, "Chemical Kinetic Pathways for the Emission of Trace By-Products in Combustion Processes." *Western States Section Meeting of the Combustion Institute*, Salt Lake City, UT. March 1993

W. J. Pitz, C. K. Westbrook, A. E. Lutz, R. J. Kee, S. Senkan, and J. G. Seebold, "Numerical Modeling Capabilities for the Simulation of Toxic By-Products Formation in Combustion Processes." *Combustion Science and Technology*, v.101, 1994. pp.383-396.

SCAQMD, "Emissions of Oxides of Nitrogen from Industrial, Institutional, and Commercial Boilers, Steam Generators, and Process Heaters." South Coast Air Quality Management District, Rule 1146, 1988.

SCAQMD, BACT Determinations, http://www.aqmd.gov/bact/AQMD_BACT_Determinations.htm, 2000.

SCEC. Personal communication. Orange, CA, 1996.

J. G. Seebold, R. J. Kee, A. E. Lutz, W. J. Pitz, C. K. Westrbook, and S. Senkan, "Emissions of Volatile Organic Compounds from Stationary Combustion Sources: Numerical Modeling Capabilities." *1992 American Flame Research Committee Symposium Proceedings*, Cambridge MA, October 1992.

G. P. Smith, D. M. Golden, M. Frenklach, N. W. Moriarty, B. Eiteneer, G. Goldenberg, C T. Bowman, R. Hanson, S. Song, W. C. Gardiner, V. Lissianski, Z. Qin, http://www.me.berkeley.edu/gri_mech, 1999.

D. St. John, "Active Optimization of a Natural Gas Fired Research Burner for the Control of Nitrogen Oxides." University of California, Irvine. Master of Science Thesis, 1994.

D. St. John and G. S. Samuelsen, "Active, Optimal Control of a Model, Natural Gas–Fired Industrial Burner." *Twenty-fifth Symposium (International) on Combustion*, The Combustion Institute, 1994. pp. 307–316.

W. H. Stevenson, "A Historical Review of Laser Velocimetry." *Laser Velocimetry and Particle Sizing*, Hemisphere Publishing, 1978. pp. 1–12.

R. E. Thompson, G. H. Shiomoto, and L. J. Muzio, "Utility Boiler Tuning: Importance and Implementation through Advanced Diagnostics." *Western States Section Meeting of the Combustion Institute*, 1999 Fall Meeting, U. C. Irvine.

S. R. Turns, F. H. Myhr, R. V. Bandaru, and E. R. Maund, "Oxides of Nitrogen Emissions from Turbulent Jet Flames: Part II – Fuel Dilution and Parial Premixing Effects." *Combustion and Flame*, v93, 1993. pp. 255–269.

C. K. Weakley, "Emissions Behavior of High-Temperature Industrial Burners in a Controlled Simulation of a Practical Furnace Environment." University of California, Irvine. Master of Science Thesis, 1997.

C. K. Westbrook, Personal Communication, 2000.

C. K. Westbrook, "An Analytical Study of the Shock Tube Ignition of Mixtures of Methane and Ethane." *Combustion Science and Technology*, v. 20, 1979. pp. 5–17.

13. APPENDIX: AIR TOXICS DATA

For each system tested, the first table includes operating data, fixed gas emission concentrations, system performance (*J*) values, total target VOCs, total aldehyde levels, and TNMHC concentrations. The second table lists the target VOCs that were reported (i.e., detected at levels greater than the Minimum Reporting Limit). As a result, compounds that were not reported are either not listed or, in the case where the compound occurs for one or a few runs but not others, the corresponding cell in the table is left blank.

Table 13.1 VOC Concentrations (in ppbC @ 3% O2) for *QLN* Burner

	Test Run	B1		B2		B3		MRL B1		MRL B2		MRL B3	
	(Excess Air)	(75%)		(46%)		(2%)							
Carbon Atoms	Target Compounds Detected	PA (a)	SCAQMD (b)	PA	SCAQMD	PA	SCAQMD	PA	SCAQMD	PA	SCAQMD	PA	SCAQMD
2	ethylene	13.7						9.3	2.3	7.5	1.9	5.2	1.3
2	ethane	19.6						9.3	2.3	7.5	1.9	5.2	1.3
2	trichloroethylene	NM (c)	7.2	NM	3.2	NM		NA	2.3	NA	1.9	NA	1.3
3	propane	20.1						14.0	2.3	11.2	1.9	7.8	1.3
4	isobutylene	74.7						18.7	2.3	14.9	1.9	10.4	1.3
4	1-butene	373.6						18.7	2.3	14.9	1.9	10.4	1.3
4	cis-2-butene						2.1	18.7	2.3	14.9	1.9	10.4	1.3
5	n-pentane		3.9		2.5			23.3	2.3	18.6	1.9	13.0	1.3
6	4-methyl-1-pentene		13.1		6.0		6.7	28.0	2.3	22.4	1.9	15.6	1.3
6	2-methylpentane		3.7		3.0		2.6	28.0	2.3	22.4	1.9	15.6	1.3
6	3-methylpentane		2.8		2.2		1.6	28.0	2.3	22.4	1.9	15.6	1.3
6	n-hexane		3.7		2.2		1.6	28.0	2.3	22.4	1.9	15.6	1.3
6	methylcyclopentane		12.1		6.0		2.1	28.0	2.3	22.4	1.9	15.6	1.3
6	benzene		11.2		3.7	176.4	101.7	28.0	2.3	22.4	1.9	15.6	1.3
6	cyclohexane		6.5		3.0			28.0	2.3	22.4	1.9	15.6	1.3
8	isooctane (2,2,4-trimethylpentane)		13.7		7.0			37.4	2.3	29.8	1.9	20.8	1.3
7	n-heptane		3.3		2.6			32.7	2.3	26.1	1.9	18.2	1.3
7	methylcyclohexane		16.3		8.7			32.7	2.3	26.1	1.9	18.2	1.3
7	toluene		6.5		8.7		8.5	49.0	2.3	39.2	1.9	27.2	1.3
8	m-xylene		2.5		7.0		4.8	56.0	2.3	44.8	1.9	31.1	1.3
10	n-decane				5.0			186.8	4.7	149.2	3.7	103.8	2.6
11	n-undecane (NM)	NA		NA	5.5	NA		NA	4.7	NA	3.7	NA	2.6
	Total Target VOCs	501.7	106.6	0.0	65.8	176.4	131.6						

[a] Samples analyzed by Performance Analytical Inc..

[b] Samples analyzed by the SCAQMD.

[c] Not measured.

Table 13.2: VOC Concentrations (in ppbC @ 3% O_2) for Generic Burner

Carbon Atoms	Target Compounds Detected	G1	G2	G3	G4	G5	MRL Max	MRL Min
2	ethylene	21.6	37.3	53.0	1416.5	94337.8	7.3	6.2
2	acetylene (ethyne)		56.0	33.1	594.0	4837.8	14.5	12.4
2	ethane	12.8	24.9	10.6	162.2	17900.0	7.3	6.2
2	propylene (propene)		9.3		17.4	435.4	7.3	6.2
3	propane		40.4		15.4	283.0	10.9	9.3
3	methylacetylene (propyne)					21.0	10.9	9.3
4	isobutane		24.5			31.0	14.5	12.4
4	isobutylene	20.8	36.5	75.0	39.3	43.5	14.5	12.4
4	1-butene					26.1	14.5	12.4
4	1,3-butadiene					31.9	14.5	12.4
4	n-butane		49.8			62.9	14.5	12.4
5	2,2-dimethylpropane					121.0	18.1	15.6
5	isopentane		67.4		17.7	18.1	18.1	15.6
5	n-pentane		42.0				18.1	15.6
5	methyl tert-butyl ether (MTBE)		29.5				18.1	15.6
6	2-methylpentane		19.9				21.8	18.7
6	3-methylpentane		21.8				21.8	18.7
6	n-hexane		26.1				21.8	18.7
6	benzene		33.6			29.8	21.8	18.7
6	cyclohexane		38.6				21.8	18.7
7	3-methylhexane		30.5				25.4	21.8
7	n-heptane		52.2				25.4	21.8
7	methylcyclohexane		116.1				25.4	21.8
7	toluene	25.7	297.5		44.8		38.1	32.7
8	2,3,4-trimethylpentane		39.0				43.5	37.3
8	m-xylene		42.3				43.5	37.3
8	styrene (vinyl benzene)					106.4	58.1	49.8
	Total Target VOCs	80.9	1134.9	171.7	2307.2	118285.9		

Table 13.3: VOC Concentrations (in ppbC @ 3% O_2) for Furnace

	Operational Mode	Incinerator				Furnace			
	Stack Position	Mid	Rear			Mid	Rear		
Carbon Atoms	Target Compounds Detected	F1	F2	MRL F1	MRL F2	F3	F4	MRL F3	MRL F4
2	ethylene	9666.0	5668.3	53.7	29.8	15.4	(3.6) (a)	6.4	6.0
2.0	ethane	1790.0	716.0	53.7	29.8	27.8	(5.8)	6.4	6.0
2.0	propylene	69.8	88.5	53.7	29.8	7.7		6.4	6.0
3.0	propane	196.0	55.2	80.6	44.8	13.1		9.6	9.1
3.0	methylacetylene			80.6	44.8	51.3		9.6	9.1
6.0	n-hexane		107.4	161.1	89.5			19.2	18.1
6.0	trans-2-hexene	188.0		161.1	89.5			19.2	18.1
6.0	benzene		56.7	161.1	89.5			19.2	18.1
7	toluene			281.9	156.6	74.8		33.6	31.7
	Total Target VOCs	11909.8	6692.1			190.0	23.3		

[a] Concentrations in parentheses are less than the MRL but are reported because of the likelihood of real emissions based on the fact that these compounds were detected in all the other test cases.

Table 13.4: VOC Concentrations (in ppmC) in Natural Gas Supply

Carbon Atoms	Target Compounds Detected	Concentration (ppmC)	MRL NG
2	Ethane	9000	1.5
3	Propane	880	2.25
4	Isobutane	207	3
4	n-Butane	328	3
5	Isopentane	76	3.75
5	n-Pentane	55	3.75
5	Cyclopentane	4.2	3.75
6	2-Methylpentane	17.5	4.5
6	3-Methylpentane	12	4.5
6	n-Hexane	19.8	4.5
6	Methylcyclopentane	12.6	4.5
6	Benzene	11.9	4.5
6	Cyclohexane	12.6	4.5
7	2-Methylhexane	9.6	5.25
7	3-Methylhexane	9.8	5.25
7	n-Heptane	22.4	5.25
7	Methylcyclohexane	31.5	5.25
7	Toluene	16.8	7.98